WBS: 1.2.2
QA: L

Civilian Radioactive Waste Management System
Management & Operating Contractor

WASTE PACKAGE PROBABILISTIC CRITICALITY ANALYSIS: SUMMARY REPORT OF EVALUATIONS IN 1997

Document Identifier: BBA000000-01717-5705-00015 REV 00

September 16, 1997

Prepared for:

U.S. Department of Energy
Yucca Mountain Site Characterization Project Office
P.O. Box 30307
Las Vegas, NV 89036-0307

Prepared By:
Civilian Radioactive Waste Management System
Management & Operating Contractor
1180 Town Center Drive
Las Vegas, NV 89134

Under Contract Number
DE-AC01-91RW00134

Civilian Radioactive Waste Management System
Management & Operating Contractor

WASTE PACKAGE PROBABILISTIC CRITICALITY ANALYSIS: SUMMARY REPORT OF EVALUATIONS IN 1997

Prepared By: Peter Gottlieb Date: 9/16/97
P. Gottlieb, Manager
Degraded Mode and Risk Analysis

Prepared By: J.W. Davis Date: 9/16/97
J.W. Davis
Degraded Mode and Risk Analysis

Prepared By: John Massari Date: 9/16/97
J. Massari
Degraded Mode and Risk Analysis

Prepared By: Paul L. Cloke Date: 9/16/97
P. Cloke
Degraded Mode and Risk Analysis

Checked By: L. E. Booth Date: 9/16/97
L. E. Booth, Systems Engineering
MGDS Safety Assurance

Approved By: Copy for H.A. Benton Date: 9/16/97
H. A. Benton, Manager
Waste Package Development

Approved By: A. M. Segrest Date: 9/16/97
A. M. Segrest, Manager
Mined Geologic Disposal System

Table of Contents

List of Tables

List of Figures

1. Introduction

1.1 Background

The emplacement of nuclear waste in the proposed geologic repository must satisfy relevant regulatory requirements with respect to criticality, 10CFR60.131(h) (Ref. 25). The waste packages for the various waste forms will be designed to preclude criticality (typically by the inclusion of neutron absorbers) even if the waste package becomes filled with water. Criticality may, however, be possible if the contents of the waste package become degraded in such a way that the fissile material can be separated from the neutron absorbers, while sufficient moderator is retained. Several of the most likely degradation scenarios have been discussed in previous studies. Those studies reported in fiscal year (FY) 1995 and 1996 have been summarized in *Degraded Waste Package Criticality: Summary Report of Evaluations Through 1996* (Ref. 1), together with the overall methodology which guided the individual studies.

Five additional studies have been reported in FY 1997: (1) *Criticality Evaluation of Degraded Internal Configurations for the PWR AUCF Waste Package Designs*, (2) *Third Waste Package Probabilistic Criticality Analysis: Methodology for Basket Degradation with Application to Commercial Spent Nuclear Fuel*, (3) *Analyses of Geochemistry Influenced by Waste Packages in a Geologic Repository*, (4) *Criticality Consequence Analysis Involving Intact PWR SNF in a Degraded 21 PWR Assembly Waste Package*, and (5) *Degraded Mode Criticality Analysis of Immobilized Plutonium Waste Forms in a Geologic Repository* (Refs. 2-6, respectively). These studies have analyzed additional configurations and further refined the overall degraded mode criticality evaluation methodology. The last of these studies has extended the application of the methodology to the immobilized plutonium waste form.

1.2 Objective

The purpose of this document is to summarize the degraded waste package disposal criticality evaluations which were reported in FY 1997 (Refs. 2-6), and to explain how those evaluations have served to further develop various aspects of the overall methodology for such evaluations.

The objective of this document is to show how the individual studies reported in FY 1997 fit into the overall criticality evaluation methodology, and to use the results of these studies to demonstrate that the probability of occurrence of criticality is very small, and that the consequences of such a criticality (if it were to occur) would be so small as to be unnoticeable from outside the repository.

1.3 Scope

The scope of this document includes the most likely of the possible criticality configurations resulting from the degradation of the waste package internals (waste form and basket containing it) for the appropriate waste packages containing the following waste forms: (1) commercial pressurized water reactor (PWR) spent nuclear fuel (SNF), (2) immobilized weapons plutonium, and (3) mixed oxide (MOX) PWR SNF. The commercial PWR SNF analysis covers the entire range of burnup and enrichment parameters expected for that waste type. The other two waste forms have not been finally specified, but the current formulations have been analyzed for

internal criticality (Refs. 6 and 7, respectively). Evaluations with these two plutonium waste forms are summarized in this document for external criticality only; the complete description of these analyses forms a major part of Reference 4. The immobilized plutonium is important for external criticality because of its very high effective enrichment. The MOX is important for external criticality because it provides a different source term than the ordinary commercial SNF.

This document covers scenarios and configurations for both internal and external criticality. The probabilistic analysis and the consequence analysis are focused primarily on the internal criticality, because any realistic external scenarios and configurations identified thus far do not provide sufficient accumulation of fissile material (together with low enough amounts of neutron absorber) to support criticality.

1.4 Relation to Previous and Future Work

The degraded mode criticality evaluations which have been completed to date are listed in Table 1.4-1, together with the the most important result of each, and the document in which it is summarized.

Table 1.4-1. Summary of previous degraded mode criticality studies

Ref.	Title	Principal result	Summary Reference
8	Initial Waste Package Probabilistic Criticality Analysis, April 1995	Internal criticality is very unlikely for certain conservative conditions.	1
9	Second Waste Package Probabilistic Criticality Analysis, March 1996	Internal criticality is very unlikely over the range of uncertainty in key parameters. Maximum steady state power of 2.2 kW.	1
10	Probabilistic External Criticality Evaluation, May 1996	External criticality (far-field) is extremely unlikely, even under worst case assumptions.	1
11	Probabilistic Criticality Consequence Evaluation, August 1996	A criticality lasting 10,000 years in a commercial SNF waste package will produce only a small increase in radionuclide inventory. External criticality steady state power limited to 1.5 to 5 kW.	1

Table 1.4-1. Summary of previous degraded mode criticality studies

Ref.	Title	Principal result	Summary Reference
6	Degraded Mode Criticality Analysis of Immobilized Plutonium Waste Forms in a Geologic Repository, March 1997	Under worst case conditions the neutron absorber built into the waste form can be removed from the package, but internal criticality can still be avoided by limiting Pu loading (at a practical level).	None
7	Evaluation of MOX Spent Fuel from Existing Reactors for Repository Disposal, Oct 1996	The risk of MOX internal criticality is no more severe than commercial PWR SNF.	None
2	Criticality Evaluations for Degraded Internal Configurations, Sept 1997	The degraded absorber plate basket k_{eff} for the spectrum of commercial SNF characteristics can be represented by a regression as a function of the degradation state and the SNF burnup, enrichment, and age. The B_4C control rod waste package can preclude internal criticality in the worst case commercial SNF for the worst case degraded basket.	This document
3	3rd Waste Package Probabilistic Criticality Analysis, Sept 1997	At least 85% of the commercial PWR SNF for the absorber plate WP will be of too low reactivity to support criticality in the worst case degraded internal configuration (flooded fully degraded basket with all boron removed; see Fig. 7.5-1).	This document
4	Analysis of Geochemistry Influenced by Waste Packages in a Geologic Repository, Sept 1997	Geochemical interactions of WP outflow cannot accumulate potentially critical mass in any of the known YM geologic formations.	This document
5	Criticality Consequence Analysis Involving Intact PWR SNF in a Degraded 21 PWR Assembly Waste Package, Sept 1997	Transient analysis of worst case internal criticality for commercial SNF shows much smaller consequences than the previous steady state analysis.	This document

Last year's consequence analyses (Refs. 9 and 11) evaluated a conservative steady-state criticality event lasting 10,000 years. The power was limited by a balance of the evaporation and infiltration rates in a waste package to 2.2 kW, and by the boiling point of water external to the package to 5 kW. The only consequences of these events were a small increase in radionuclide inventory. An analysis by LANL (Ref. 34), which started with an improbable autocatalytic configuration at a super-prompt-critical state, concluded that a nuclear fission transient with explosive yields (nuclear explosion) in the hundreds of tons range of TNT is not possible, that negligible kinetic energy will be created, and the repository natural barriers would not be compromised. The current analysis is focused on evaluating under what conditions a prompt-critical state can be achieved along with evaluating the associated consequences for an event limited by physical constraints. The configuration for this analysis is defined by the physical processes and degradation stages that the SNF and waste package can undergo.

Further refinements of the overall degraded mode criticality methodology will be reflected in the *Disposal Criticality Analysis Methodology Topical Report* to be published in 1998. Further analyses to broaden the scope of the demonstrations of "no degraded mode criticality", according to both deterministic and probabilistic criteria, will be given in the September 1998 summary report on this subject.

1.5 Quality Assurance

The Quality Assurance (QA) program applies to this document. The work summarized in this document is part of the preliminary waste package (WP) design analyses that will eventually support the License Application Design phase. This activity, when appropriately confirmed, can impact the proper functioning of the Mined Geologic Disposal System (MGDS) waste package; the waste package has been identified as an MGDS *Q-List* item important to safety and waste isolation (Ref. 35, pp. 4, 15). The waste package is on the *Q-List* by direct inclusion by the Department of Energy (DOE), without conducting a QAP-2-3 *Classification of Permanent Items* evaluation. The Waste Package Development Department responsible manager has evaluated this activity in accordance with QAP-2-0, *Conduct of Activities*. The *Perform Probabilistic Waste Package Design Analyses* activity evaluation (Ref. 23) , has determined that work associated with the probability and consequences of criticality is subject to *Quality Assurance Requirements and Description* (Ref. 24) requirements. As specified in NLP-3-18, *Documentation of QA controls on Drawings, Specifications, Design Analyses, and Technical Documents*, this activity is subject to QA controls. Guidance for the development and review of this document is provided in the *Technical Document Preparation Plan for the Supporting Analysis Results Summary Reports for the Disposal Criticality Analysis Methodology Reports* (TDPP; Ref. 22).

All inputs and assumptions which are identified in this document are for preliminary design and shall be treated as unqualified data; these inputs and assumptions will require subsequent qualification (or superseding inputs) as the waste package design proceeds. This document will not directly support any construction, fabrication or procurement activity and therefore is not required to be procedurally controlled as TBV (to be verified). In addition, the inputs associated

with this document are not required to be procedurally controlled as TBV. However, use of any data from this document for input into documents supporting procurement, fabrication, or construction is required to be controlled as TBV in accordance with the appropriate procedures.

The assumptions for this document are those given in the assumptions sections (4.3) of each of the supporting QAP-3-9 analyses (Refs. 2 through 5). In some of the topic areas, the assumptions may differ between individual supporting QAP-3-9 documents; in those cases the controlling document is clearly identified.

The correspondence between the QAP-3-5 Section 5.2.C Items and the sections of this document is as follows:

Item	Description	Location
1.	Title page requirements (a - h)	On the cover sheets of the report.
2.	History of Change page	After title page(s), if required (revised).
3.	Table of Contents, Lists etc.	After title page(s) and History of Change page.
4.	Objective and scope	In Sections 1.2 and 1.3.
5.	Discussion of QA Controls	In Section 1.5.
6.	Identification of inputs	In Section 3.
7.	Identification of assumptions	Section 1.7 references associated QAP-3-9 documents which have the assumptions listed.
8.	Location of unqualified inputs	In Section 3.
9.	References	In Section 10.
10.	Technical approach	In Section 2.
11.	Identification of interfaces	N/A
12.	Presentation of information	In Sections 3 through 8.
13.	Computer software controls	In Section 1.6.
14.	Conclusions	In Section 9.

The correspondence between the items in the TDPP (Ref. 22) annotated outline and the sections of this document is as follows:

Item	Description	Section
1.0	Introduction	Same
1.1	Background	Same
1.2	Objective	Same
1.3	Scope	Same
1.4	Quality Assurance	1.5
2.0	Analysis Model	2, 6, 7, 8
3.0	Systems Analyzed	1.3, 3, 5
4.0	Analysis Results	5, 6, 7, 8
5.0	References	10

1.6 Computer Software

No computer software was used in the preparation of this document. Information on the various software packages and computer codes discussed in the text can be found in the supporting QAP-3-9 analyses in which they were used (Refs. 2 through 5).

2. Methodology and Procedures

The criticality evaluation methodology consists of the following steps: (1) Determination of initial parameters, (2) Scenario generation, (3) Initial application of configuration generator to develop ranges of configuration parameters, (4) Intensive criticality evaluation of configurations and development of regressions, (5) Final application of configuration generator to support probabilistic criticality evaluation over the range of uncertainty in the environmental and material parameters and statistical criticality evaluation over the range of waste form parameters, and (6) Evaluation of consequences for the most reactive configurations. These steps are described in the following subsections.

2.1 Determination of Initial Parameters

The criticality evaluation methodology begins with the determination of the values, or range of values, for the important parameters of waste package material performance and of the repository environment. The values of these parameters are taken to be consistent with those given in the *Controlled Design Assumptions Document* (CDA, Ref. 13) and those used for the performance assessment documents (TSPA-95, Ref. 14, and TSPA-VA, not yet released). Probability distributions will be used for some of these parameters; if guidance is not provided for such distributions, they will be justified in the appropriate waste package document (Ref. 2 through 5).

2.2 Scenario Generation

The scenarios which can lead to criticality consist of degradation, mobilization, transport, and accumulation of fissile material (required for external criticality). The relationship among these processes, and the way in which they support the three types of criticality (internal, external near-field, and external far-field) is indicated in Figure 2.2-1. All such scenarios must begin with the breach of the waste package, and the most likely mechanism for such a breach is corrosion of the waste package barriers by water. The barrier lifetimes (or ranges and probability distributions) are taken to be consistent with the CDA and the latest TSPA (Refs. 13 and 14). The following steps are used to develop the remainder of the scenarios:

- Use of chemical modeling together with experimental corrosion rate data to determine the following for waste package internals (waste form and basket): the degradation rates, the degradation products, and possible mobilization rates of individual degradation products.

- Use of chemical modeling to estimate the chemical components of solutions flowing out of the waste package, to support the determination of the amount of neutronically significant material being removed from the waste package, and the amount of material available for accumulation external to the waste package.

- Use of geochemical modeling to determine the quantity and chemical composition of accumulations of solids (minerals) containing neutronically active elements, both inside and outside the waste package (from solutions inside, and flowing out of, the waste package, respectively).

Figure 2.2-1. Overview of Postclosure Criticality Scenarios

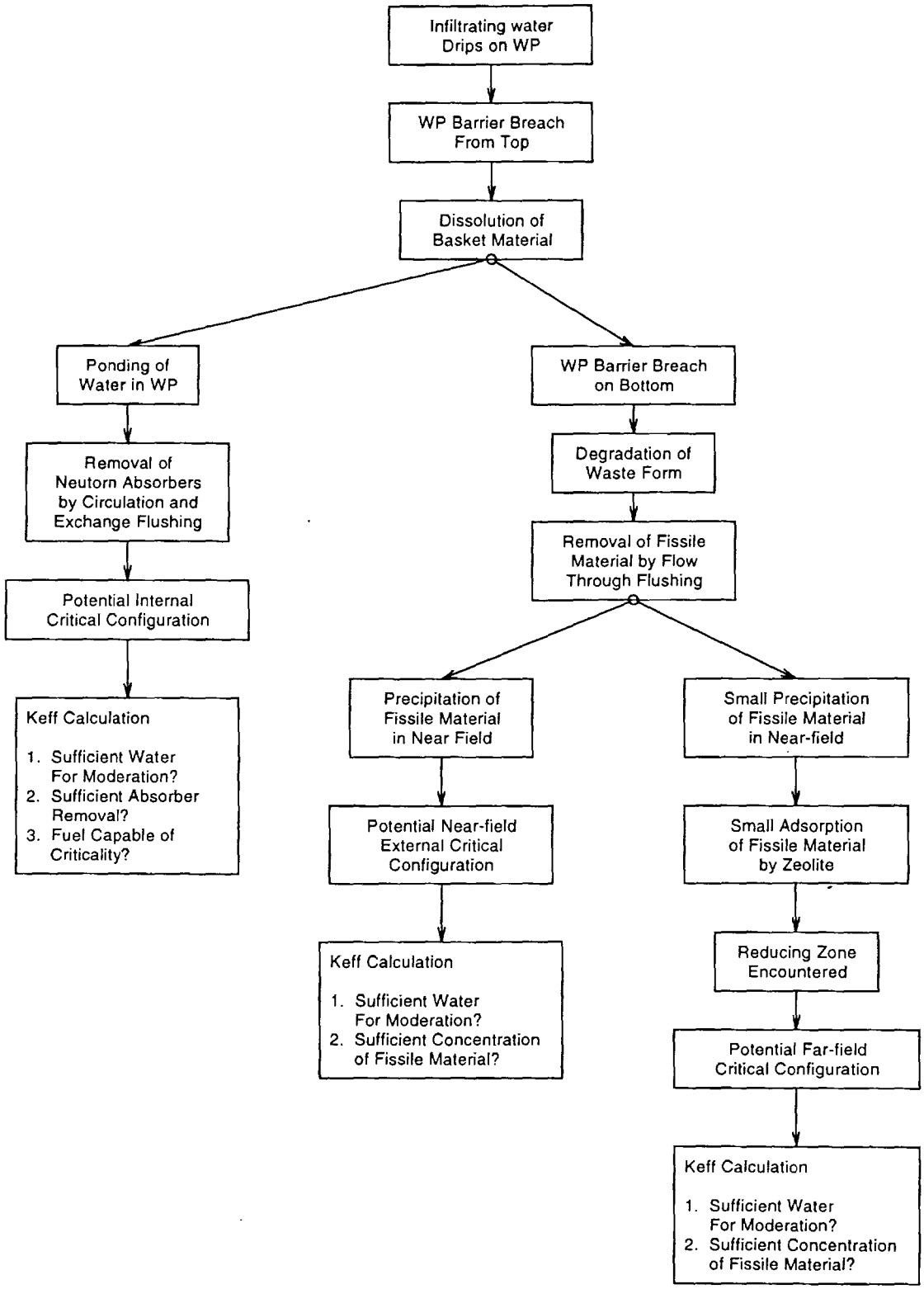

Figure 2.2-1. Overview of Postclosure Criticality Scenarios

The last of these steps is partly guided by an examination of those possible mechanisms of formation for the major uranium ore deposits which could occur in the geology of Yucca Mountain. This step is implemented by addressing the following changes in solution chemistry which are known to frequently result in significant precipitation:

1. Change of pH.
2. Change in oxidation potential (Eh).
3. Change in dissolved gases.
4. Changes in other components within the solution.
5. Change in temperature and/or pressure.
6. Change in phases which the solution contacts. Generally this will in turn cause a change within the solution which could involve immobile solid phases, e.g., invert, host rock, minerals in fractures or veins. The change could involve suspended phases, e.g., colloidal clay particles.

The most extensive application of the scenario generation methodology thus far has been in Reference 4, where it was used in an attempt to identify potential configurations for external criticality.

2.3 Initial Configuration Generation

The results of individual geochemical analyses which make up the scenario generation process are linked together by the configuration generator code which tracks the chemical components as they flow from the output of one process to the input of another. The configuration generator code is described in Section 7.1 below, and more fully in Reference 3. Configurations having the potential for criticality are identified and characterized in terms of concentrations of neutronicly significant species. For the criticality evaluations summarized in this document, the configuration generator is applied to internal criticality only, because the scenario generation analyses, as reported in Reference 4, have not yet identified any external locations with significant criticality potential.

2.4 Criticality Evaluations

Calculations of k_{eff} are performed for the potentially critical configurations and the range of parameters identified with the configuration generator exercises described in the previous paragraphs. The calculation of the PWR spent fuel isotopics used in the criticality evaluations was performed with the SAS2H and ORIGEN-S code sequences, which are part of the SCALE 4.3 code system (Ref. 18). The Monte Carlo N-Particle computer program, MCNP4A (Ref. 17), is used to calculate k_{eff} for the criticality evaluations. The results of the criticality analyses are used to develop a regression for k_{eff} as a function of neutronicaly significant parameters (fuel burnup, initial enrichment, decay time, amount and distribution of iron oxide corrosion products, amount of boron remaining in the form of plate or in solution). The criticality calculations and the derivation of the k_{eff} regression are summarized in Section 6.

2.5 Final Configuration Generation and Probabilistic Evaluation

For those configurations which are confirmed as critical by the criticality analyses, the configuration generator code is re-applied, incorporating the appropriate k_{eff} regression to determine the earliest time of criticality occurrence and sensitivity to various parameters of waste package design, waste package materials, and repository environment. For commercial PWR SNF, the augmented configuration generator was also used for statistical criticality evaluation of the entire database of expected reactor discharges.

2.6 Criticality Consequences

Criticality consequences are measured principally by the following parameters: (1) increased radionuclide inventory, (2) pressure pulse, (3) water/steam release. These are determined by the reactivity insertion rate, the total reactivity insertion, and the thermodynamic properties of the system. A bounding estimate of the increase in radionuclide inventory can be made from a steady-state analysis in which the water in-flow and out-flow are balanced (actual behavior would likely oscillate between subcritcal and supercritical) as was done in References 9 and 11. In order to demonstrate that the steady-state radionuclide inventory increase is conservative, and to estimate the other parameters of criticality consequence, a transient analysis of the evolution of the reaction parameters must be performed in which the neutronic and thermohydraulic responses are coupled through feedback, and physically relevant reactivity insertion mechanisms (limits) are investigated.

The transient behavior of an internal waste package criticality is modeled in a manner analogous to transient phenomena in a nuclear reactor core. The light water reactor (LWR) transient analysis code, RELAP5/MOD3 (Ref. 21), is used to calculate the time evolution of the power level and other characteristics of a criticality involving PWR SNF. Reactivity tables based on changes in k_{eff} from a baseline configuration, as a function of changes in reactor parameters (principally temperature, density, and water volume) are included in the RELAP5 input. MCNP4A (Ref. 17) is used to calculate a baseline k_{eff} for criticality safety evaluations and to determine the change in reactivity from one configuration to another, as a function of the changing parameters which describe the configurations. MCNP4A does not have an associated cross section library with sufficient temperature dependent data to calculate the reactivity changes associated with fuel and moderator temperature changes required for this analysis. SCALE4.3 (Ref. 18) and its SAS2H sequence do have the necessary cross sections. SAS2H employs a one-dimensional (1-D) assembly-cell discrete-ordinates technique for calculation of the multiplication factor (k_{eff}) for a configuration. A correction for three dimensions can be made through use of buckling terms. Initially, infinite MCNP cases were run with which to compare the results from infinite SAS2H cases in order to develop the appropriate SAS2H model to match MCNP results. Corrections were then made to the SAS2H model to account for finite dimensions using the appropriate buckling terms for inclusion in the models based on the baseline MCNP finite case. The resulting SAS2H model incorporating the buckling terms are then used for calculating temperature and density reactivity effects. The reactivity changes calculated by MCNP4A and SAS2H are used as input to RELAP5 to track the transient behavior of a criticality. The SAS2H sequence in the SCALE4.3 code package is used to calculate the changes to the radioisotopic inventory as a result of the analyzed criticality events.

3. Initial Conditions

3.1 Waste Package and Waste Form Descriptions

3.1.1 Commercial PWR Waste Package

The intact PWR waste package geometry parameters important in analysis are listed Table 4.1-2 in Reference 2. Figure 3.1-1 depicts the 21 Pressurized Water Reactor (PWR) Advanced Uncanistered Fuel (AUCF) absorber plate WP, its internals, and the material specifications; this information is from (Ref. 15). This is considered unqualified TBV information, as other WPD QAP-3-9 analyses being performed in parallel may result in design changes not reflected in this analysis.

3.1.2 PWR SNF Composition

A commercial spent fuel waste package will consist of 21 PWR assemblies of spent fuel held in a basket and placed inside a corrosion barrier. The design for the corrosion barrier itself specifies a corrosion allowance outer barrier material and a corrosion resistant inner barrier material. For modeling of the chemical behavior of this system, the chemical compositions of each of these materials, their masses, their surface areas, and their corrosion or degradation rates are required. Tables 4.1.1.1-1 to 4.1.1.1-3 in Reference 4 show the data used that are specific to commercial SNF.

The configuration for a MOX waste package differs from that for commercial nuclear fuel only with regard to the fuel itself. The degradation rate is included in Table 4.1.1.1-3 of Reference 4. A representative composition of the fuel is given in Table 4.1.1.2-1 of Reference 4.

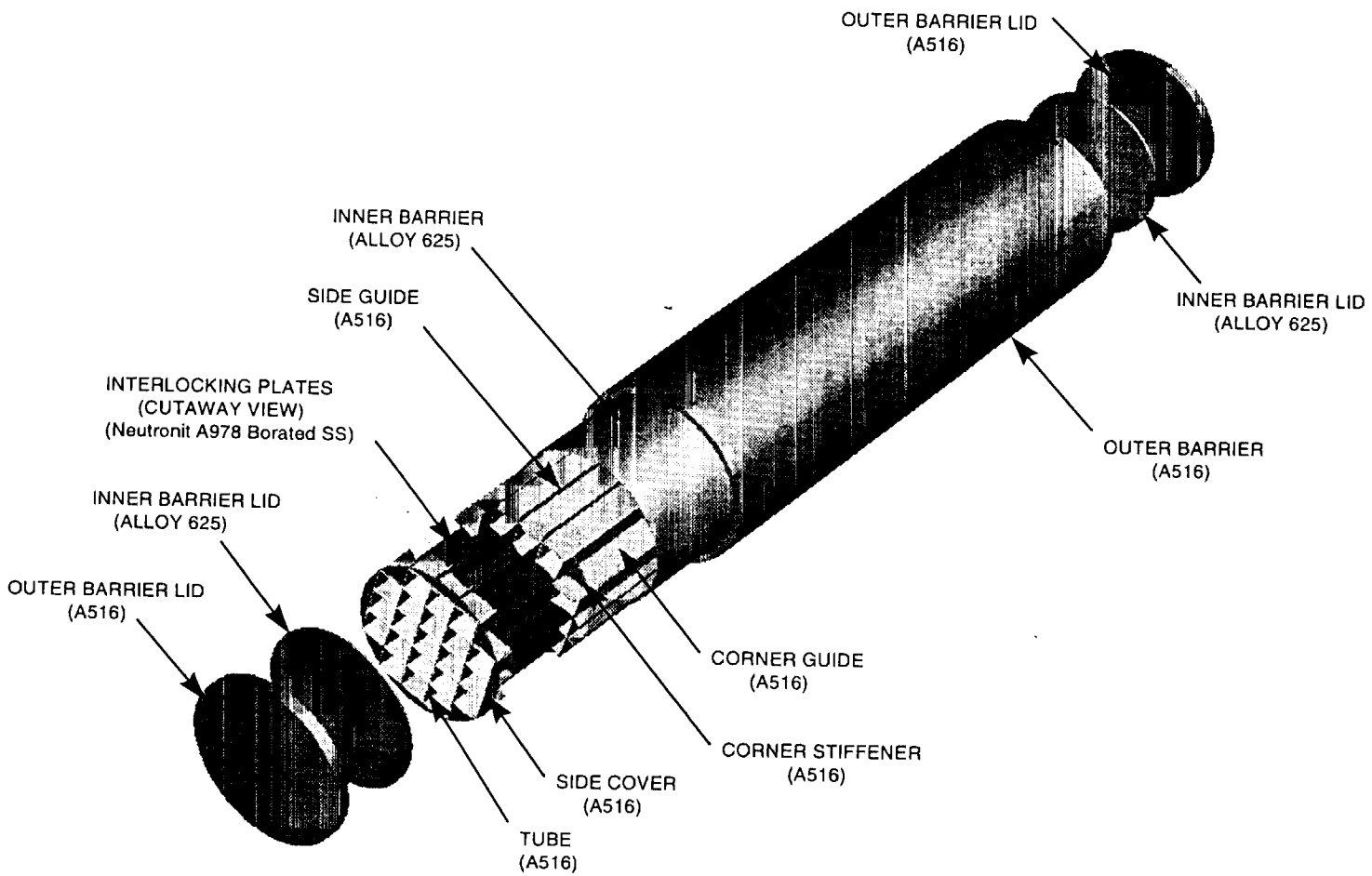

Figure 3.1-1. Advanced Uncanistered Fuel Waste Package with Internals Shown

3.1.3 Immobilized Pu Waste Package

The waste package for immobilized Pu will be similar to the Civilian Radioactive Waste Management System (CRWMS) current design for the defense high-level waste (DHLW) waste package. The waste package is nominally loaded with four canisters. The waste package design may be enlarged somewhat to accommodate five canisters in the interest of greater efficiency, but such a design is not considered as part of this study. The cross section of a four canister package is given in Figure 3.1-2 (Ref. 6). The nominal Pu loading per waste package is specified by four Pu loaded canisters per waste package.

The waste package for the immobilized Pu consists primarily of a corrosion allowance outer barrier and a corrosion resistant inner barrier. The corrosion allowance outer barrier will likely be 5 cm thick C71500 Cu-Ni or 10 cm thick A516 carbon steel, as is used in the CRWMS current design for the commercial spent nuclear fuel waste package (Ref. 6). The inner barrier will be corrosion resistant, high nickel, Alloy 825 or Alloy 625, 2 cm thick (Ref. 6).

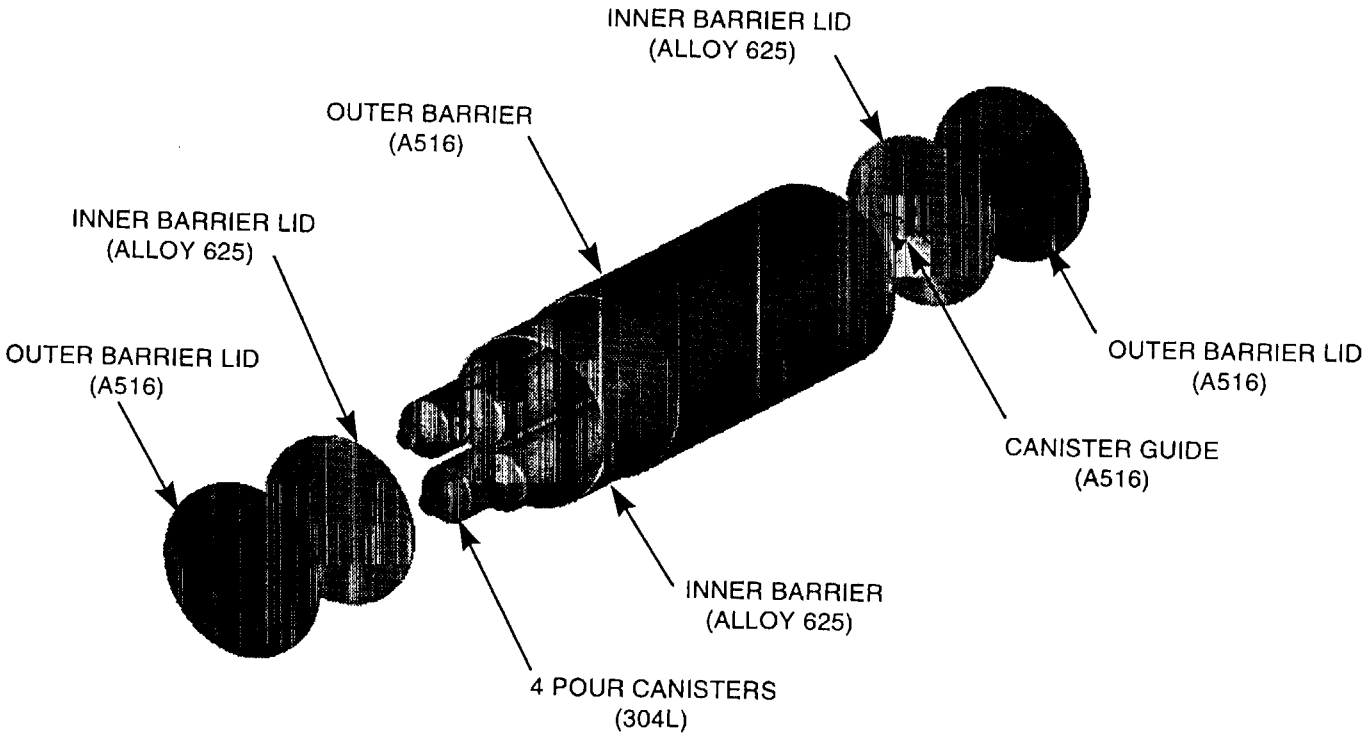

Figure 3.1-2. Immobilized Pu/DHLW Waste Package

3.1.4 Immobilized Pu waste form

The La-BS glass composition is listed in Table A-1 of Reference 6. The final composition is still subject to some change.

3.2 Material Performance Parameters

3.2.1 Metal performance parameters

The following metals are considered directly in computer models for waste package degradation: Alloy 625 (a candidate for the inner corrosion resistant barrier), A516 carbon steel (used for outer barrier and basket tubes, guides, and supports), 304L stainless steel (used for containment of glass waste forms and for some other purposes), borated stainless steel (used in basket structures for spent nuclear fuel), and 316 stainless steel (used for end-fittings for commercial spent nuclear fuel). Tables 4.1.5-1 and 4.1.5-2 in Reference 4 show data for the metals.

3.2.2 Glass performance parameters

High-level waste (HLW) glass and Immobilized Pu reaction rates are listed in Table 4.1.1.3-3 of Reference 4.

3.3 Environmental Parameters

3.3.1 Infiltration rate

For the internal criticality evaluations, the present day net infiltration rate is taken to be 5 mm/yr, which is close to the results (6.2 mm/yr)of the most authoritative current Yucca Mountain hydrological model (Ref. 5.35 and assumption 4.3.7). In contrast, the current CDA (Ref. 5.13; see assumption 4.3.7) specifies long-term (up to 20,000 years) WP drip rates of 0.5 m^3/yr (fully mediated; equivalent to 50 mm/yr), with 20 m^3/yr flows occurring once every 40 years (focused flow). This yields an average long term infiltration rate of ≈ 100 mm/yr. Accounting for the maximum factor of 5 due to spatial variations in flux across the repository footprint (see assumption 4.3.7), yields an upper bound of 500 mm/yr for this analysis. This range (0.1 mm/yr to 500 mm/yr) was used for sensitivity analysis of the commercial PWR SNF in Reference 3, the most significant of which are included in Section 7.3.4.

For the external criticality scenario generation, the infiltration rates were taken to be 1 mm/yr and 10 mm/yr. These are somewhat below the CDA range, but were used for the following reasons:

- The lower infiltration rate is conservative for criticality evaluations (not dose performance) under most circumstances because it leads to more extreme pH (high or low).

- The accumulation of fissile material, resulting from pH change during the limited time when

pH and aqueous fissile concentration is high, is relatively insensitive to infiltration rate (Ref. 4, Section 7.4.2.2.1.

3.3.2 Water Chemistry

It was assumed that the water composition entering the waste package would be the same as for water from well J-13 (Ref. 4, Assumption 4.3.1). This water has been analyzed repeatedly over a span of at least two decades, as explained in Reference 4 (and the References cited therein). The average composition is reproduced in Table 3.3.2-1 (Ref. 4, Table 4.1.4-1).

Table 3.3.2-1 Analyzed Composition of J-13 Well Water

J-13 water	Molality	Mole Fr.
Na	1.9922E-03	1.1963E-05
Si	1.0169E-03	6.1064E-06
Ca	3.2437E-04	1.9478E-06
K	1.2891E-04	7.7410E-07
C	1.4474E-04	8.6916E-07
F	1.1475E-04	6.8907E-07
Cl	2.1533E-04	1.2930E-06
N	1.42E-04	8.5270E-07
Mg	8.27E-05	4.9660E-07
S	1.9154E-04	1.1502E-06
B	1.2388E-05	7.4389E-08
P	1.2711E-06	7.6329E-09
H	111.0167	6.6665E-01
O	55.5084	3.3332E-01
Total	166.529467	1

3.3.3 Other environmental parameters

The following parameter ranges were used for calculations of the external criticality results in Ref. 4. They represent the time ranges over which the reactions leading to external criticality can occur. (Ref. 6, Table 4.3-1).

Parameter	Max	Min
Temperature (°C)	66 (5,000 yrs)	26 (100,000 yrs)
pH of J-13 water	7.4	6.9
Partial Pressure CO_2 , J-13	$10^{-2.6}$ bar	$10^{-4.6}$ bar

3.3.4 Ranges of Design Parameters

The following ranges are used for the sensitivity analyses presented in Section 7.3. Further

discussion of their basis is given in Reference 3.

- Threshold k_{eff}: 0.91 to 1.0 (Ref. 3, Sections 7.4-1 and -2). The low end of the range is equal to the value which would be found by subtracting the current assumed bias and uncertainty (0.04) from the 0.95 limit from 10CFR60.131(h) (Ref. 25). This is very conservative because the extensive benchmark comparisons of MCNP calculations with benchmark commercial reactor criticals currently in progress are expected to lower the bias and uncertainty to no more than 0.02 (as explained in References 2 and 3). The high end of the range is the actual physical threshold k_{eff} which would be required to produce a criticality. Any lower threshold represents some significant degree of conservatism.

- Thickness of borated stainless steel plates used for criticality control: 7-10 mm. The lower end of the range is the current design value for the 21 PWR absorber plate waste package. The high end represents the largest thickness which has thus far been considered for a waste package (Ref. 2).

4. Scenarios: Degradation, Transport, and Accumulation

4.1 Internal Criticality: Commercial PWR SNF

The commercial SNF waste package criticality control measures are designed to prevent criticality when intact and when degraded. Since the commercial SNF exhibits a broad range of reactivities, the waste package criticality control measures are grouped into separate designs to cover this range of reactivities in three segments, as defined in Reference 16. For the least reactive SNF, little or no neutron absorber is necessary to prevent criticality; sufficient criticality control is provided by the moderator exclusion and the neutron absorbing capabilities of the carbon steel which forms the basket structural support. For the moderately reactive commercial SNF, a stronger neutron absorber is required; this function is provided by borated stainless steel plates which are inserted into the waste package basket structure between adjacent assemblies, where their neutron absorption can be the most effective. For that small fraction of the commercial SNF which is the most reactive, a third design is required. This third design provides very robust (resistant to corrosion) neutron absorption by means of control rods (placed within the assembly guide tubes) made of zircaloy clad boron carbide (B_4C).

However, the effectiveness of the criticality control measures will be reduced by eventual degradation of the neutron absorber material. Of the three general waste package designs for PWR commercial SNF, the one with borated stainless steel plates (to be used for the moderately reactive fuel) is most appropriate for extensive analysis at the present time for the following reasons: (1) it covers most of the commercial SNF for which criticality could be a possibility; (2) it is the one most susceptible to aqueous degradation; and (3) it is the only one for which there is presently an established design.

The waste package degradation scenarios summarized in this report are similar to those used for the previous summary report (Ref. 1), but are characterized in greater detail and over a greater range of the principal parameters, in order to support the detailed evaluation of the entire spectrum of commercial PWR SNF. As with these previous analyses, the degradation scenarios leading to criticality begin with breach of the waste package barriers by aqueous corrosion, followed by corrosion of the carbon steel of the basket structure, and then the degradation of the borated stainless steel plates. The expected successive stages of degradation are shown in Figure 4.1-1. In that figure, the time sequence begins in the upper left and progresses to the lower right by rows. The grey shaded amorphous area indicates the increasing amount of iron oxide.

It is well known that the corrosion rate of the zircaloy cladding of the SNF is much slower than the corrosion rates of the two principal materials which make up the basket, carbon steel and borated stainless steel (Refs. 2 and 3, Section 4). Therefore, the basket materials will degrade while the SNF is still mostly intact. What is not known is the exact disposition of the basket material after it has degraded. The iron oxide is very insoluble and will tend to precipitate, but the distribution of the precipitate could range from: (1) collecting equally on all the available surfaces, to (2) settling into the configuration with the lowest gravitational energy, limited only by the maximum density of hydrated iron oxide. The parameters for these two alternatives, called the uniform and settled distributions, respectively, are described in some detail in Reference 2.

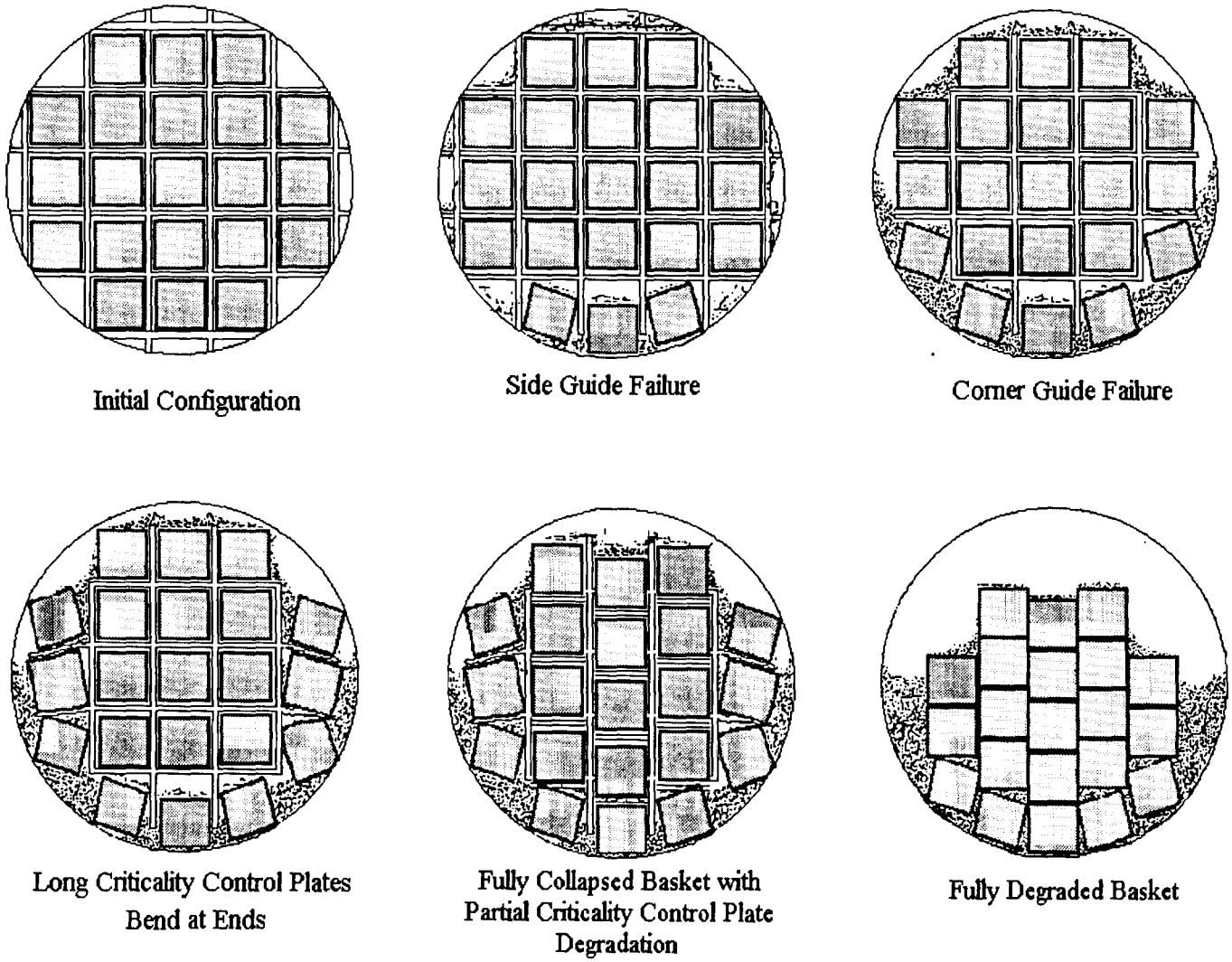

Figure 4.1-1. Illustration of Degraded 21 PWR WP Internal Configurations with Intact Fuel

4.2 External Criticality: Near-Field

The most quantitative external criticality applications of the scenario generation methodology have been to the development of external criticality source terms (concentration of fissile and other significant species in the water flowing out of the waste package), and the consideration of precipitation mechanisms. These are described in detail in Reference 4, and are summarized in the following subsections.

4.2.1 Source terms

Immobilized Pu source term

For the immobilized plutonium waste form, the degradation of the codisposal canister internals begins with the alteration of the HLW glass. This may be followed by the dissolution of the waste form in the presence of water (either vapor or liquid). To calculate the properties (concentrations) of the waste package solution and outflow, EQ6 was run as a sequence of cases using an intermediate program to convert the output of one case to the input for the next case, with suitable dilution of the solution components to account for infiltration to (or through) the waste package. The results show that the pH increases as the alkaline glass degradation products are formed. For about 600 years the simulated effluent from the package will have a pH of about 10. For these pH conditions, the solubilities of U and Pu are three orders of magnitude higher than at pH neutral. The solution predicted by EQ3/6 contains 6,111 ppm total U and 78.3 ppm Pu. The percentage of ^{235}U will be about 3.31% of the total uranium. The ^{235}U is a result of the decay of ^{239}Pu taken at 5,000 years. It is assumed that the ^{235}U from the La-BS glass will mix with the ^{238}U from the HLW glass before any U or Pu solids precipitate or are otherwise immobilized within the waste package. This assumption has been used for the calculations of Ref. 4 and Ref 6.

After the complete dissolution of the HLW glass, the alkaline ions are expected to be removed by the flushing action of the infiltrating water (which may take between 2 and 1,000 years, depending on the infiltration rate) so the effluent is expected to become neutral (pH=7). It is conservatively assumed that the neutral condition lasts about 1,200 years, after which the effluent pH is lowered to approximately 5 by the complete oxidation of the chromium released by the corrosion of the stainless steel used for the canisters. This acid phase may last as long as there remains stainless steel to corrode, perhaps for another 8,000 years. During the entire degradation period the solution remains oxidizing. Solutions with these three pH conditions were used as feed solutions for reactions with the environment external to the waste package.

Fissile concentrations in solutions from immobilized Pu for neutral and low pH are given in Reference 4, but not repeated here, because the resulting external accumulations are much smaller than for the high pH.

Commercial SNF

The solution composition was modeled by EQ6 as the contents of the waste package were dissolved. The degradation of package contents by J-13 water was modeled with the assumption that the chromium oxidizes to chromate so that the pH drops to 3.9 and an ionic strength of 0.295 molal. The solution contained 1,416 ppm U and 0.002 ppm Pu, based on a typical commercial PWR SNF which contained approximately 1.43 wt % ^{235}U and 0.56 wt% ^{239}Pu (Ref. 4).

MOX SNF

The modeling for MOX was similar to that for commercial SNF, except that the ^{239}Pu concentration was 4.5 wt% of the total heavy metal (uranium plus plutonium) and there was no ^{235}U initially. The solution characteristics predicted by EQ3/6 were pH= 4.09, ionic strength = 0.173 molal, 782.6 ppm U , and 0.0013 ppm Pu (Ref. 4).

4.2.2 Accumulation: mechanisms and locations

A simulation of this reaction using EQ6 shows that when the solution first enters the invert, its composition changes slowly as it reacts with the tuff producing small quantities of alteration minerals, but neither uranium nor plutonium solids are produced. The alteration of the tuff principally consists of a recrystallization of the tuff to a mixture of quartz and feldspar. As the solution flows deeper into the invert and finally into the host rock below, there is further reaction and change of solution composition. At this time, a small quantity of solid $Na_4UO_2(CO_3)_3$ is simulated to form, primarily due to dissolution of additional sodium from the tuff. The small decrease in pH causes a concomitant shift in the proportions of carbonate and bicarbonate ions in solution and consequent destabilization of the plutonyl carbonate aqueous complex primarily responsible for the solubility of plutonium. Thus, PuO_2 also precipitates.

The EQ6 program computes the quantity of various minerals precipitating from the solution as a function of time. The results generally show one mineral dominating the precipitation at a time, but that the dominant species changes with time. The transition times at which the dominant species change can be mapped into distances along the flowpath by simply multiplying by the flow velocity. For this purpose the flow velocity is taken to be the infiltration rate.

Using this time-to-distance mapping, the flow path was discretized into finite lengths or "cells". The boundaries of these cells are points where there is a significant shift in the mineralogy of the deposit. The first cell extends from the invert entry point to where the uranium and plutonium species begin to precipitate (approximately 2 cm below the upper surface of the invert). The second cell extends to the point where a new mineral, borax, is added to the precipitating solid (approximately 5 cm below the invert surface). The third cell extends to where another new mineral, Albite (low temperature type) is added to the solid composition (approximately 19 cm below the invert surface. Cell 4 extends to a somewhat arbitrary point where no significant additional uranium plus plutonium solids are forming (approximately 1 meter below the invert surface, which is actually partly in the rock). Cell 5 is entirely in the rock and extends to the point where the water is in equilibrium with the rock and no further reactions will take place (approximately 18 meters). It should be noted that cell 5 is entirely in the far-field, which appears to violate the categorization of this report. However, it will be seen in Section 5.2 that

the accumulation in the far-field from this mechanism will be so dilute as to be insignificant.

4.3 External Criticality: Natural Analogs for the Far-Field

Natural analogs provide an interim technique to exclude (rule out) configurations which are inconsistent with the Yucca Mountain geology. The least unlikely will ultimately be analyzed by a geochemical code to provide stronger demonstration for license application.

In order to provide the basis for a natural analog study of uranium deposition in the far-field, the thesis is proposed that epigenetic (i.e., mineralization deposited much later than the host rock) uranium ore deposits documented in the literature should provide some understanding as to the environmental conditions/setting necessary for significant uranium mineral deposition in the far-field. Not only will the epigenetic ore deposits document potential environmental conditions, but they will also define the mechanisms of precipitation that would be necessary to accumulate enough fissile material to produce a critical assemblage. The additional assumption is that this depositional process will operate over geologic time and ^{239}Pu will have sufficient time to decay to ^{235}U. In this section we do not evaluate the transport and deposition of plutonium. These assumptions are discussed further in Reference 4, together with the following general requirements for epigenetic ore deposition:

1. A source of uranium,
2. Oxidation, mobilization and transportation of the uranium,
3. Sufficient permeability in the host rock,
4. Reducing capacity (or sorptive capacity) in the host rock, and
5. Stable, sustained groundwater flow.

Epigenetic uranium mineral deposits vary in size and grade, depending on geology, but one fact remains; he need for a reducing environment (or vanadium) for the primary mineral(s) to precipitate. The evidence for this conclusion is presented in Reference 4, Section 7.3.2, and references given therein. Therefore, without sufficient reducing potential in the depositional environment, the precipitation of uranium by reduction of uranyl ions cannot occur, and only minor amounts would precipitate in cases of low reducing potentials or small reducing capacity. Once there is sufficient reducing capacity within the host rock, uranium will accumulate in sufficient quantities to form ore grade deposits if other conditions necessary for mineral deposition are present, e.g., sufficient porosity, favorable host rock, stable groundwater flow, etc.

The uranium deposits at Oklo, Gabon and Pena Blanca, Mexico have often been cited as natural analogs to Yucca Mountain. However, these two deposits did not utilize epigenetic processes to accumulate the uranium ore. The Oklo deposit falls under the quartz-pebble-conglomerate type deposit and the Pena Blanca deposit is classified as a hydrothermal type deposit, as explained in Reference 4, Section 7.3.2, and the references cited therein. Therefore, neither of these two deposits apply to this study. Therefore, below is a brief description of the three types of deposits that do seem to apply to epigenetic ore deposition at Yucca Mountain.

Unconformity

The key to the formation of these deposits, and thus to their geologic characteristic, is the interplay of dissolved U^{+6} ions reacting with a reducing environment. The general mechanism seems to be a leaching of uranium into oxidizing groundwaters and flowing in a permeable sandstone/conglomerate above an unconformity. The reductant consists of methane or other hydrocarbon charged fluids moving upward along faults from the basement rock and through the unconformable contact boundary (Ref. 4, Figure 7.3.2-2).

Sandstone

Generally there are two major types of epigenetic sandstone uranium deposits; those associated with organic material as a reducing agent and those deposited without organic material (includes mineral deposits formed by sorption).

Common organic reducing environments seem to be fluvial organic debris and/or buried logs (Ref. 4, Figure 7.3.2-5); however, lignite or petroleum bearing sands or shales can also be the location for deposition. Common inorganic redox environments tend to be associated with reduced iron or sulfide based minerals (Ref. 4, Figure 7.3.2-4). An alternate mechanism for formation of a few of these types of deposits can be attributed to sorption onto zeolites and clays.

Calcrete

These epigenetic deposits occur in areas of internal drainage where evaporation exceeds rainfall. The general locations for these types of deposits occur along the lower ends of alluvial valleys, at playa lakes, and at desiccated calcrete terraces. One possible mechanism for precipitation is related to evaporitic processes by which potassium is concentrated, uranyl ion activity is increased, as carbonate complexes are weakened by common ion effects, and as pH decreases. This is a somewhat unique process which requires interaction with vanadium. The precipitation occurs as groundwater is constricted by barriers and caused to move upward to some slight concentration of vanadium where V^{+4} is oxidized to V^{+5} thus allowing the precipitation of the oxidized uranium mineral carnotite, as described in Reference 4, Section 7.3.2 and references cited therein. This precipitation mechanism is unlikely to occur at Yucca Mountain because of the lack of vanadium in the environment. An alternate mechanism of precipitation (one that should operate in the arid environment of the Yucca Mountain region) is that of upward diffusion of uranyl ions into the unsaturated soil were evaporation can concentrate the uranyl complexes, thus allowing precipitation to occur, as described in Reference 4, Section 7.3.2 and references cited therein. The only ore that has been found deposited in this type of depositional environment is carnotite [requires vanadium to precipitate–the chemical formula for carnotite is $K_2(UO_2)_2(VO_4)\cdot 3H_2O$] and is located in regolith, fluvial detritus, or in fractures and voids in the calcretes.

5. Potentially Critical Configurations: Definition and Screening

5.1 Internal Criticality: Commercial PWR SNF

This section summarizes the configurations evaluated in the criticality analysis based on the discussion of scenarios presented in Section 4.1. The configurations which will be evaluated in this analysis are represented by the final two pictures in Figure 4.1-1. Since the intermediate configurations still retain the majority of the borated stainless steel, and the fully collapsed basket configuration has been previously shown to be more reactive than the intact basket configuration, with or without the boron (Ref. 30, Vol. III, p. 6.3-139), they were not evaluated. Furthermore, reduced moderator density has already been shown to be less reactive (Ref. 30, Vol. III, p. 6.3-139) and thus was not considered. Similarly, all configurations are assumed to be in a waste package filled with water, since moderation is a required condition for criticality in commercial SNF with an enrichment of less than 5 wt% (Ref. 31). The effects of water level were also evaluated. Finally, it should be noted that while Figure 4.1-1 (and the subsequent MCNP models) shows the waste package oriented such that the basket grid is perpendicular/parallel to the direction of gravity, the results are not expected to be affected by other orientations. In the uniform oxide cases, orientation with respect to gravity does not affect the distribution of the oxide, and in the settled cases, it will not alter the fraction of assemblies covered by oxide (as represented by rows of rods or assemblies covered).

The specific configurations evaluated in the criticality analysis (Ref. 2) for intact assemblies were as follows:

1) Collapsed Basket with Partial Thickness Borated Stainless Steel (B-SS) Remaining

    a) Uniformly distributed oxide occupying 30-40 vol% of the assembly void space (30% = carbon steel tube degradation only, 40% = carbon steel tube and all B-SS degradation), depending on the amount of B-SS plate remaining, with the remainder as water, and
    b) Settled oxide covering the bottom 8 to 10 rows of an assembly (8 rows = carbon steel tube degradation only, 10 rows = carbon steel tube and all B-SS degradation), depending on the amount of B-SS plate remaining. The oxide occupies 58% of the covered void, with the remainder being water.

2) Fully Degraded/Oxidized Basket

    a) Uniformly distributed oxide occupying 30, 33, or 40 vol% of the waste package void space (33% base vol%, with 30 vol% evaluated to consider the maximum estimated 3 vol% loss due to flushing, and 40 vol% evaluated to consider concentration of most oxides in the fuel region), and
    b) Settled oxide covering the bottom 3, 3.5, 4, and 4.5 rows of assemblies (3.5 is the base case for the current amount of basket material). The oxide occupies 58% of the covered void, with the remainder being water.

In general, the fully degraded basket configurations were evaluated without consideration for any remaining boron, because the boride particles from the borated stainless steel are not expected to last for more than a few hundred years (see Ref. 2), even though they may have a corrosion rate similar to that of the stainless steel matrix. This is due to their extremely small size. However, the boron from the degraded particles may still remain in solution for some time, or become adsorbed onto the iron oxide (0.67% retained in the oxide at the peak adsorption rate from Ref. 32), so the effects of these mechanisms on degraded waste package k_{eff} were also evaluated.

The following geometries involving full degradation of the basket structure and various degrees of rod consolidation were also evaluated for the limiting fuels to address the effects of degraded or crushed fuel assemblies:

1) Various amounts of assembly crushing (i.e., reduced fuel rod pitch) in the vertical direction, and both the vertical and horizontal directions for the fully degraded basket, and

2) Fuel rods piled at the bottom of the fully degraded basket waste package (simulates complete spacer grid degradation).

Discussion of the criticality evaluations performed for the above configurations are provided in Section 6.

5.2 External Criticality: Near-Field

The near field configurations are all characterized by a decrease in concentration of fissile material with depth. The maximum values of accumulations are summarized in Table 5.2-1 for the waste forms considered thus far. In all cases the fluid in the environment is presumed to have pH=7, and the source of precipitation is connected with the difference between that pH and the high or low pH outflow from the waste package, with the high pH producing a much stronger effect. For the high pH cases, most of the fissile precipitate is plutonium (despite the fact that the uranium concentration is much higher); for the low pH cases, most of the fissile precipitate is uranium. This difference in behavior is the result of the difference in slopes of the solubility curves for uranium and plutonium as a function of pH.

All cases in Table 5.2-1 are for infiltration rates of 1 mm/yr, except cases 1 and 3 which are for 10 mm/yr. These higher infiltration rates result in a larger total amount of fissile deposition than the similar 1 mm/yr cases (cases 2 and 4, respectively), but most of this total is diluted over a large volume. The amount in the more concentrated zone (given in parentheses, and corresponding to cells 1-3 in the notation described in Section 4.2 above) is similar in the two sets of cases, which demonstrates the relative insensitivity to infiltration rate. The expression N/A has been used to indicate that a time period is not relevant for those cases which were not run because they are completely dominated by cases already shown to have negligible fissile accumulation. Additional details of the individual cases are given in Reference 4 and are discussed briefly below.

Table 5.2-1. Summary of fissile accumulation possibilities beneath waste packages of the indicated waste forms

Waste form	pH	Invert medium	Accumulation duration (yrs)	Max accumulation of fissile (g)*
1. Immobilized Pu	10	Tuff	300	1,780 (350)†
2. Immobilized Pu	10	Tuff	600	356 (36)†
3. Immobilized Pu	10	Tuff	3,000	17,800 (3,500)†
4. Immobilized Pu	10	Tuff	6,000	1,440 (145)†
5. Immobilized Pu	7	Tuff	600	Nil
6. Immobilized Pu	5	Tuff	8,000	0.0016
7. Immobilized Pu	10	Concrete	600	0.03
8. Immobilized Pu	7	Concrete	N/A	Less than case 5
9. Immobilized Pu	5	Concrete	8,000	2.9×10^{-6}
10. Commercial SNF	7	Tuff	N/A	Less than case 5
11. Commercial SNF	4	Tuff	600	60
12. Commercial SNF	7	Concrete	N/A	Less than case 5
13. Commercial SNF	5	Concrete	N/A	Less than case 9
14. MOX	7	Tuff	N/A	Less than case 5
15. MOX	4	Tuff	500	3.85
16. MOX	7	Concrete	N/A	Less than case 5
17. MOX	5	Concrete	N/A	Less than case 9

* Maximum accumulation in a volume equal to the waste package footprint area times the pathlength: 5.5 m^2 for the immobilized Pu emplacement and 6.8 m^2 for the commercial SNF waste package.

† The values in parentheses are distributed over less than 3 meters path length, the other values are distributed over tens of meters, which greatly reduces the potential for criticality.

Cases 1 and 2 represent the most likely durations of high pH, for infiltration rates of 10 mm/yr and 1 mm/yr, respectively. Cases 3 and 4 have this duration extended by a factor of 10, as a conservative worst case. Even these cases do not produce amounts sufficient for criticality, the maximum being case 3 with 3.5 kg spread over a volume 3 meters deep and 5.5 square meters in cross section, which amounts to a concentration of approximately 0.2 kg/m^3. To examine this worst case in further detail, the peak concentration at the surface is shown in Reference 4 to be 2.65 g/mm. It is also shown in Reference 4 that the concentration cannot go much higher because by the time this much Pu has precipitated, the voidspace is nearly filled with other competing

precipitates. The worst case conceivable would be for this concentration to be extended uniformly vertically downward (although the EQ6 runs do not indicate a mechanism for achieving this concentration); when spread over the 5.5 square meter footprint area, it would give a plutonium concentration of 0.48 kg/m^3, which is far below any critical density.

5.3 External Criticality: Far-Field

Over 60% of the total fissile material is in a region (Cells 4 and 5) where the fissile material per mm of depth is less than 0.2 g/mm and the % voids filled with fissile material is less than 0.01%. Therefore, this case does not present a scenario which would support a criticality.

Table 5.3-1. Summary of geologic reducing zone occurrence requirements, and expectation at Yucca Mountain

Formation type	Reducing media	Expectation at Yucca Mountain
Unconformity	Hydrothermal fluid	Requires volcanic activity; highly unlikely
	Other methane source	Incredibly low probability
Sandstone	Organic logs	Very unlikely*
	Petroleum	None observed, nor likely to be
Calcrete	Vanadium	None observed

* This case has been shown to have very low probability for low enriched uranium (LEU) commercial SNF even with the log occurrence frequency of the Colorado Plateau which was the richest uranium ore deposit in the United States (Ref. 10).

6. Evaluations of Internal Criticality: Commercial PWR SNF

6.1 Commercial PWR SNF Isotopics

This section identifies the different fuel isotopic sets which were used in the criticality analysis of degraded waste package configurations. The 21 PWR absorber plate waste package is currently planned to be used for fuel assemblies with k_∞ between 1.0 and 1.13 (Ref. 16, p. 30). Based on the database of historical and projected waste streams (Ref. 27), and a non-linear regression developed by Oak Ridge National Laboratory (Ref. 28) to estimate k_∞ as a function of assembly burnup, enrichment, and age, Reference 2 projected that there are 99,608 PWR assemblies within this range. Figure 6.1-1 shows the burnup/enrichment distribution of the population of assemblies with $k_\infty \geq 1.0$, with the burnup/enrichment combinations yielding $k_\infty = 1.13$ indicated by a solid line. Burnup/enrichment pairs were selected for analysis such that the population of fuel to be placed in the absorber plate waste package was covered. Burnup/enrichment pairs which bound the population of fuel to be placed in the control rod waste package (high enrichment with low burnup) were also identified. For both waste package types, the burnup/enrichment pairs evaluated are given in Table 6.1-1.

Table 6.1-1. Burnup/enrichment pairs evaluated in criticality analysis

Waste Package Type	Burnup/Enrichment Pairs Evaluated
Absorber Plate	9 GWd/MTU, 1.7%; 27 GWd/MTU, 3.9%; 34 GWd/MTU, 4.9%; 3 GWd/MTU, 0.8%; 23.5 GWd/MTU, 3%; 35 GWd/MTU, 4.5%; 12 GWd/MTU, 1.5%; 28 GWd/MTU, 3.25%; 39 GWd/MTU, 4.6%; 32.5 GWd/MTU, 3.5%; 44 GWd/MTU, 4.9%; 38.5 GWd/MTU, 3.85%; 48 GWd/MTU, 4.9%
Control Rod	3 GWd/MTU, 4.3%; 13 GWd/MTU, 4.7%

The calculation of the PWR spent fuel isotopics was performed with the SAS2H code sequence, which is a part of the SCALE 4.3 code system. The basic SAS2H model used to perform the depletion and decay are identical to those defined in Reference 29, with only those portions relating to the burnup and enrichment of the assembly changed as indicated in Reference 2. The decay out to 1 million years was run as a separate case from the SAS2H burnup calculation. The decay case is a stand-alone ORIGEN-S problem which utilizes the output from SAS2H and decays to a number of specified times. The grams/assembly per time step from the combined SAS2H/ORIGEN-S output was used to calculate the number density of each principal isotope at the times of interest for each burnup/enrichment pair. These number densities were used as input to the fuel region for MCNP criticality calculations.

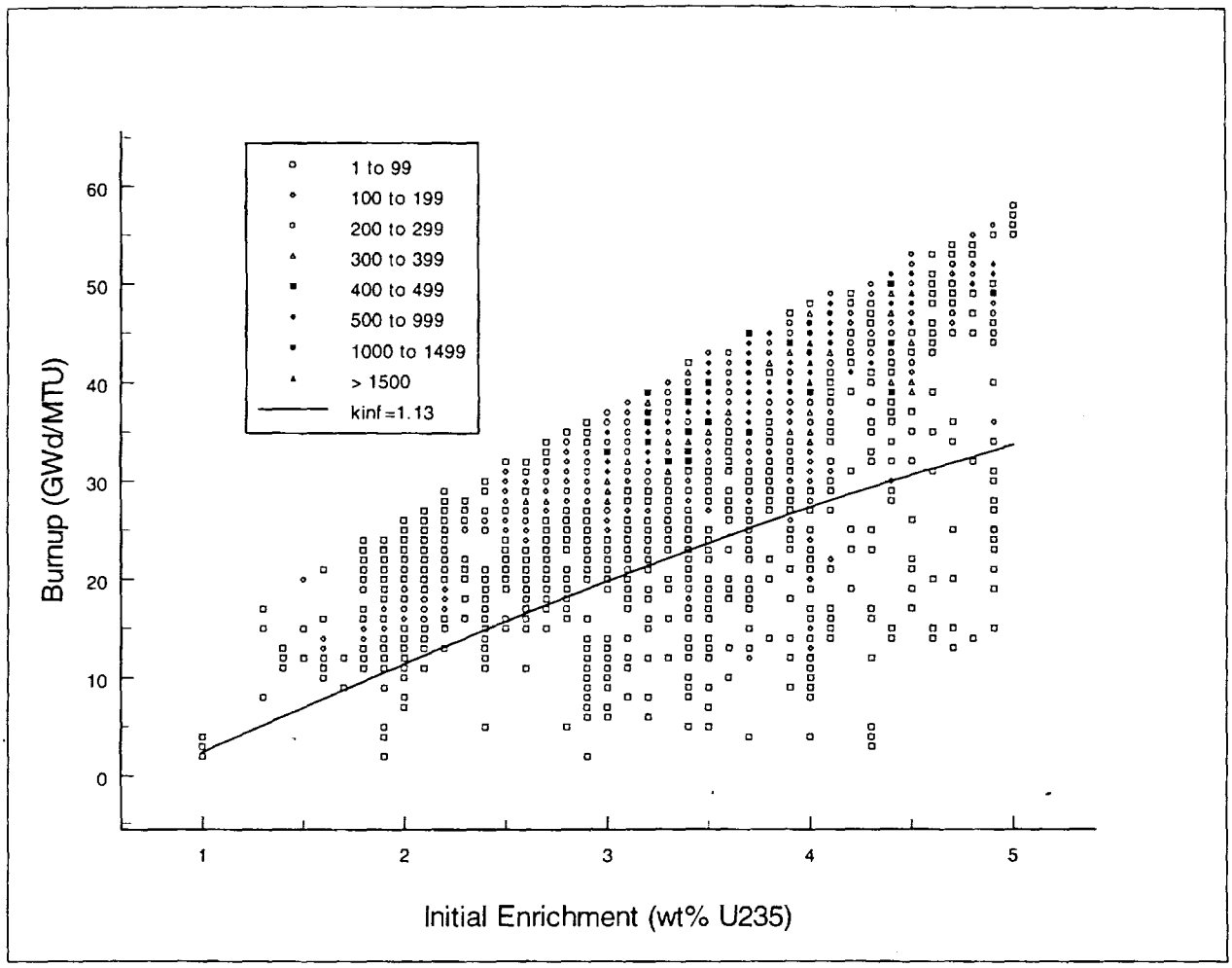

Figure 6.1-1. Distribution of historical and projected PWR fuel assemblies with $k_\infty \geq 1.0$ (burnup/enrichment pairs yielding $k_\infty = 1.13$ shown by solid line)

6.2 Parametric criticality analysis

This section presents the results of MCNP4A criticality analyses, performed in Reference 2, for the degraded configurations outlined in Section 5.1.

6.2.1 Partially Degraded Basket with Intact Fuel

The purpose of this section is to describe the MCNP cases performed in Reference 2 to evaluate the possible partially degraded basket configurations. Both the uniformly distributed oxide and the settled oxide configurations were evaluated for 7 plate thicknesses. For the uniformly distributed configurations, iron oxide concentrations of 30 vol%, 35 vol%, and 40 vol% were evaluated for several burnup/enrichment pairs. Figure 6.2.1-1 shows the results for the 4.9%/34 GWd/MTU burnup/enrichment pair at 30 vol% and 40 vol% uniform oxide. For the settled scenarios, 58 vol% iron oxide fully covering the bottom 8, 9, and 10 rows of fuel rods in an assembly were evaluated for several burnup/enrichment pairs. Figure 6.2.1-2 shows the results for the 4.9%/34 GWd/MTU burnup/enrichment pair with the bottom 8 and 10 rows of fuel rods covered by 58 vol% oxide. For most cases, each burnup/enrichment pair was only evaluated for the 14,000 year decay time, as this has been the time of peak postclosure k_{eff} in previous analyses of a collapsed basket with some boron remaining (Ref. 30, Vol. III, p. 6.3-142).

The degraded 21 PWR absorber plate waste package was modeled in MCNP by explicitly modeling ¼ of the package and then using two reflective planes to represent the entire package. The composition and dimensions of the containment barriers are modeled explicitly. The details of the outer barrier's skirt were not modeled in detail, since the skirt would not affect the criticality results appreciably (less than the standard deviation in the Monte Carlo method). The fuel assemblies are modeled as part of a lattice array, with the lattice positioned such that it represents a basket structure which has uniformly collapsed towards the bottom of the waste package. The assemblies were not modeled as resting on the bottom of the waste package because some oxide from corrosion of the side guides may be there to support them, and the approximate cylindrical geometry is more reactive than that which would occur if all assemblies were touching the bottom. Each fuel assembly is treated as a heterogeneous system with the fuel rods, control rod guide tubes, and instrument guide tubes modeled explicitly. Fuel rods are modeled with water in the gap region, and guide and instrument tubes are also filled with water only (no oxide). The remaining borated stainless steel plate is modeled at the edge of the assembly lattice cell.

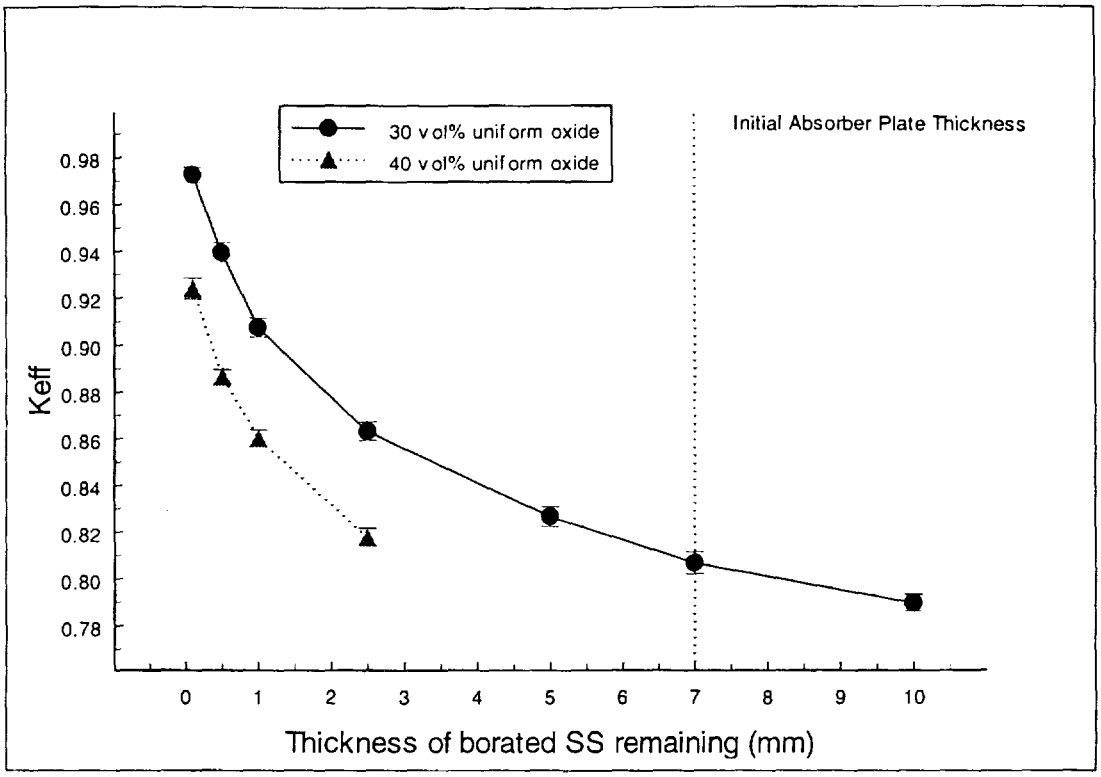

Figure 6.2.1-1. k_{eff} as a function of remaining absorber plate thickness for the 4.9%/34 GWd/MTU fuel at 14k years with 33 vol% uniform oxide

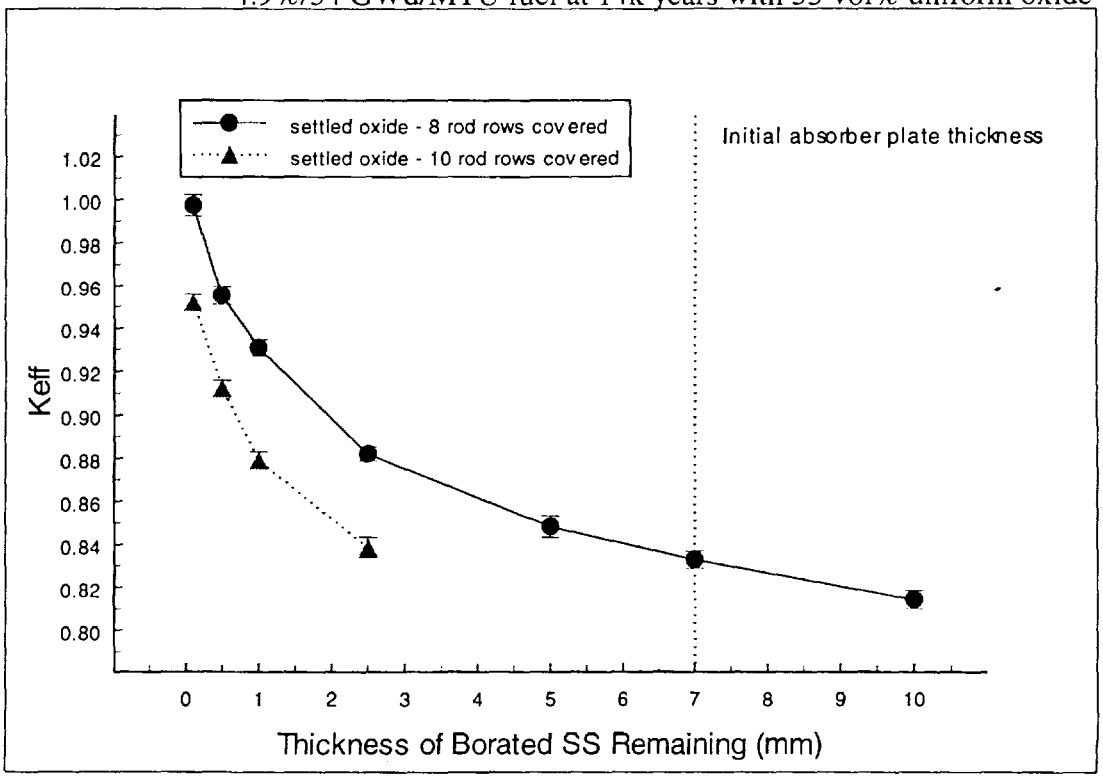

Figure 6.2.1-2. k_{eff} as a function of remaining absorber plate thickness for the 4.9%/34 GWd/MTU fuel at 14k years with 58 vol% settled oxide

6.2.2 Fully Degraded Basket with Intact Fuel

As with the partial basket model, the fully degraded 21 PWR absorber plate waste package was modeled in MCNP by explicitly modeling ¼ of the package and then using two reflective planes to represent the entire package. The composition and dimensions of the containment barriers are modeled explicitly. The details of the outer barrier's skirt were not modeled in detail, since the skirt would not effect the criticality results appreciably (less than the standard deviation in the Monte Carlo method). The fuel assemblies are modeled as part of a lattice array, with the lattice positioned such that it represents a basket structure which has uniformly collapsed towards the bottom of the waste package. The assemblies were not modeled as resting on the bottom of the waste package because some oxide from corrosion of the side guides may be there to support them, and the approximate cylindrical geometry is more reactive than that which would occur if all assemblies were touching the bottom. Each fuel assembly is treated as a heterogeneous system with the fuel rods, control rod guide tubes, and instrument guide tubes modeled explicitly. Fuel rods are conservatively modeled with water in the gap region, and guide and instrument tubes are also filled with water only (no oxide). Figure 8-1 shows an example of the MCNP model for the fully degraded basket with 58 vol% settled oxide configuration.

Results of some of the cases evaluated in Reference 2 are provided in the Figures 6.2.2-1 to 6.2.2-4 to demonstrate the behavior of k_{eff} as a result of varying certain parameters. Figure 6.2.2-1 shows the time effects on k_{eff} for several burnup/enrichment pairs for the 33 vol% base uniform oxide configuration. Figure 6.2.2-2 provides the same information for the 58 vol% settled oxide configuration. In all of the configurations, the peak k_{eff} generally occurs between 10,000 and 35,000 years. One noticeable feature is the increasing prominence of the postclosure peak-and-valley in k_{eff} as burnup increases. This effect primarily results from the decay of ^{241}Pu, ^{240}Pu, and ^{239}Pu isotopes which are present at higher concentrations in higher burnup fuels. Figures 6.2.2-3 and 6.2.2-4 show the effects of varying the amount of iron oxide in the waste package for the 58 vol% settled and uniform oxide configurations, respectively, for two burnup enrichment pairs at the time of peak k_{eff}. As expected, the results show that increased amounts of oxide in both configurations result in reduced k_{eff} due to moderator exclusion and the modest absorption cross section of iron. As discussed in Section 5.1, the amount of oxide resulting from basket degradation covers 3.5 layers of assemblies in the settled configuration, and takes up 33 vol% in the uniform configuration. Reference 2 determined that an addition of 2,659 kg of carbon steel basket material would produce sufficient oxide upon degradation to reduce the peak k_{eff} below 0.91 for both fully degraded configurations. Other general observations from this part of the evaluation were: (1) the settled configuration is more limiting than the uniform, (2) for burnup/enrichment pairs with the same k_∞ per the relationship in Reference 28, the one with the highest burnup will have the highest k_{eff} in the degraded configurations, and (3) the 4.9% enriched, 34 GWd/MTU fuel was bounding for the absorber plate waste package (i.e., highest k_{eff} for fuel with $k_\infty \approx 1.13$) under the current loading scheme defined in Reference 16.

To evaluate the effects of 0.67% boron adsorption onto the iron oxide, both 33 vol% uniform and 58 vol% settled configurations were evaluated for time of peak k_{eff} for several burnup/enrichment pairs. Table 6.2.2-1 presents the k_{eff} and $\Delta k_{eff}/k_{eff}$ results for 0.67% ^{10}B adsorption onto the iron

oxide. The results indicate that boron adsorption provides less than a 1.4% reduction in k_{eff} for the uniform cases, and a 0.2% reduction for the settled cases. Boron adsorption is less effective for the settled configuration because the assemblies contributing to the high k_{eff} are those which are above the level of the oxide, and thus not affected by the boron adsorbed therein. Based on these results, this boron retention mechanism cannot be counted on for significant criticality control for either oxide distribution scenario.

Table 6.2.2-1. Effects on k_{eff} of Peak Boron Adsorption on Iron Oxide

Burnup/ Enrichment Pair	Decay Time (years)	33 vol% Uniform			58 vol% Settled		
		k_{eff}	σ	$\Delta k_{eff}/k_{eff}$	k_{eff}	σ	$\Delta k_{eff}/k_{eff}$
4.9%/34 GWd/MTU	25000	0.96586	0.00175	-0.0139	1.01598	0.00218	-0.0026
3.9%/27 GWd/MTU	35000	0.94447	0.00134	-0.0120	0.99602	0.00188	-0.0016
1.7%/9 GWd/MTU	14000	0.8695	0.00167	-0.0107	0.93223	0.00122	-0.0022

Figure 6.2.2-5 presents the $\Delta k_{eff}/k_{eff}$ results for various concentrations of dissolved ^{10}B in the entire water volume for the 58 vol% settled oxide cases for several burnup/enrichment pairs at the time of peak k_{eff}. Based on the few cases run, it appears that there is a slight trend towards decreasing boron worth with increasing burnup. This is likely the result of the fact that higher burned fuels have higher ^{239}Pu concentrations, and thus a harder spectrum (more epithermal fission) which makes the boron less effective.

Depending on the amount and distribution of holes on the upper surface, the waste package may not be entirely flooded. Figure 6.2.2-6 presents the k_{eff} results for the 4.9%/34 GWd/MTU fuel in the 58 vol% settled oxide configurations at the time of peak k_{eff} for various water levels. The results indicate that, for the settled configuration, uncovering the top layer of assemblies drops k_{eff} below 0.90. Analysis of the 33 vol% uniform configuration for the same burnup/enrichment pair indicates that the water level must drop below the middle of the third layer to achieve the same result. However, this is partially an artifact of maintaining 33 vol% oxide as the water level is reduced. These cases also demonstrate that a fully degraded unflooded absorber plate waste package which contains only a hydrated oxide will not be a criticality concern.

Finally, Table 6.2.2-2 presents k_{eff} results for the two PWR control rod waste package burnup/enrichment pairs (4.3%/3GWd/MTU and 4.7%/13 GWd/MTU) in the 58 vol% settled oxide and 33 vol% uniform oxide configurations. Results are presented with and without the 16 rod DCRAs, indicating that the DCRAs provide an ≈24-25% reduction in k_{eff} for these fuel compositions in the settled configuration, and ≈26-27% reduction for the uniform configuration. k_{eff} results for the bounding burnup/enrichment pair for the absorber plate waste package, 4.9%/34 GWd/MTU, are also shown in Table 6.2.2-2. These results indicate that use of DCRAs eliminates any criticality concern for this fuel in any degraded configuration.

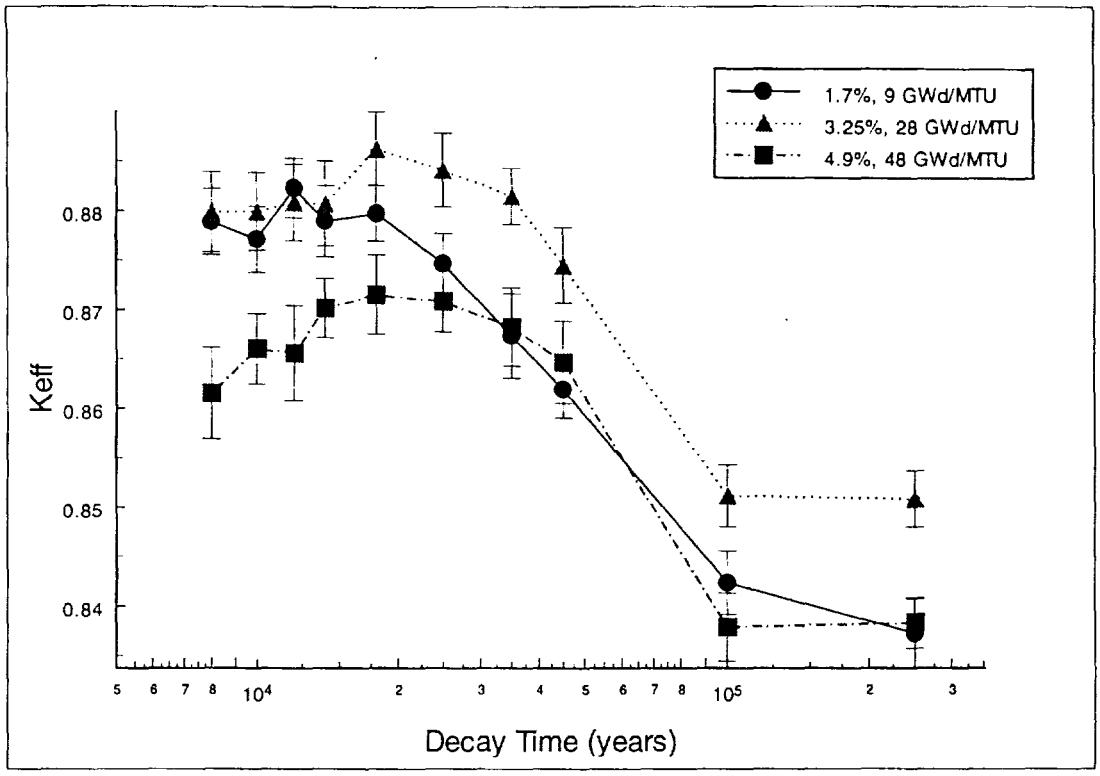

Figure 6.2.2-1. Time dependence on k_{eff} as a function of assembly burnup for the fully degraded basket with 33 vol% uniform oxide distribution.

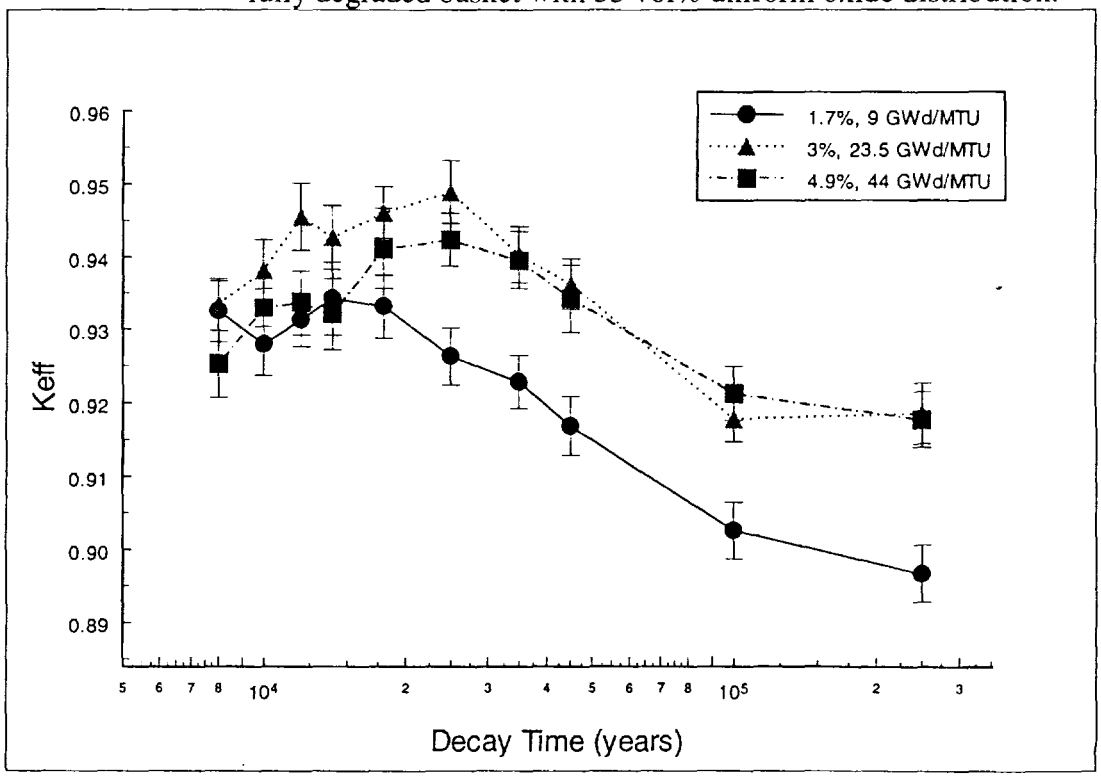

Figure 6.2.2-2. Time dependence on k_{eff} as a function of assembly burnup for the fully degraded basket with 58 vol% settled oxide distribution.

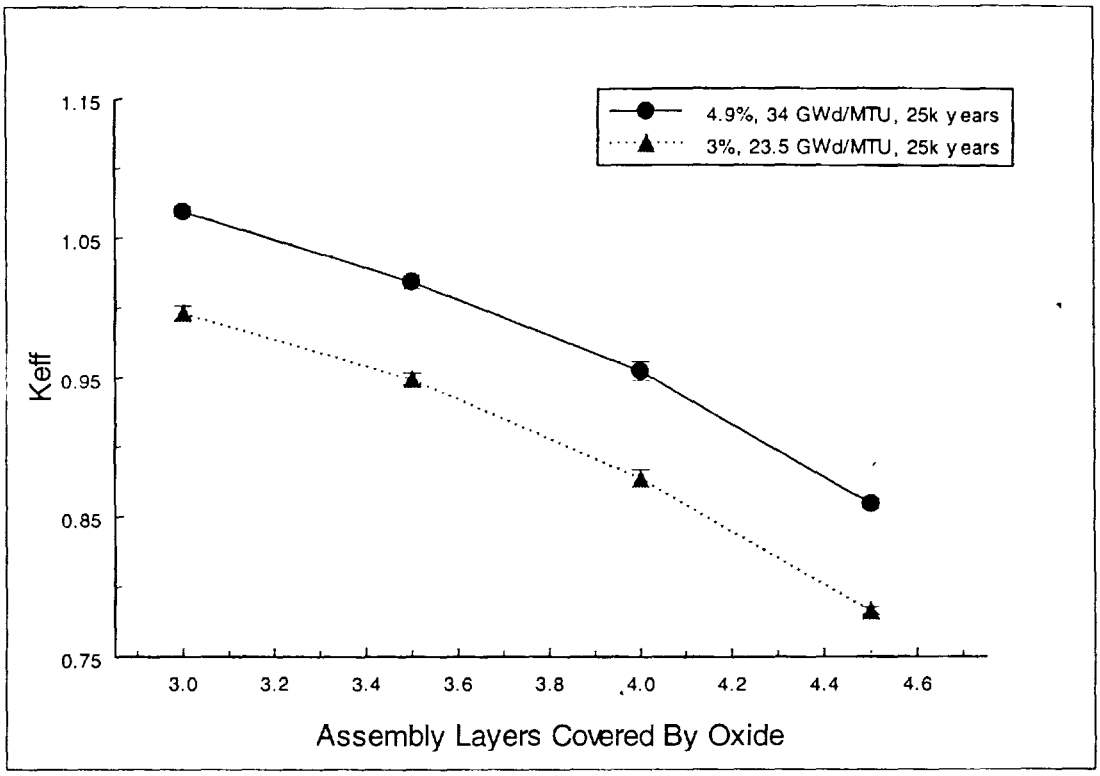

Figure 6.2.2-3. Effects of oxide level on fully degraded basket k_{eff} for 58 vol% settled configuration

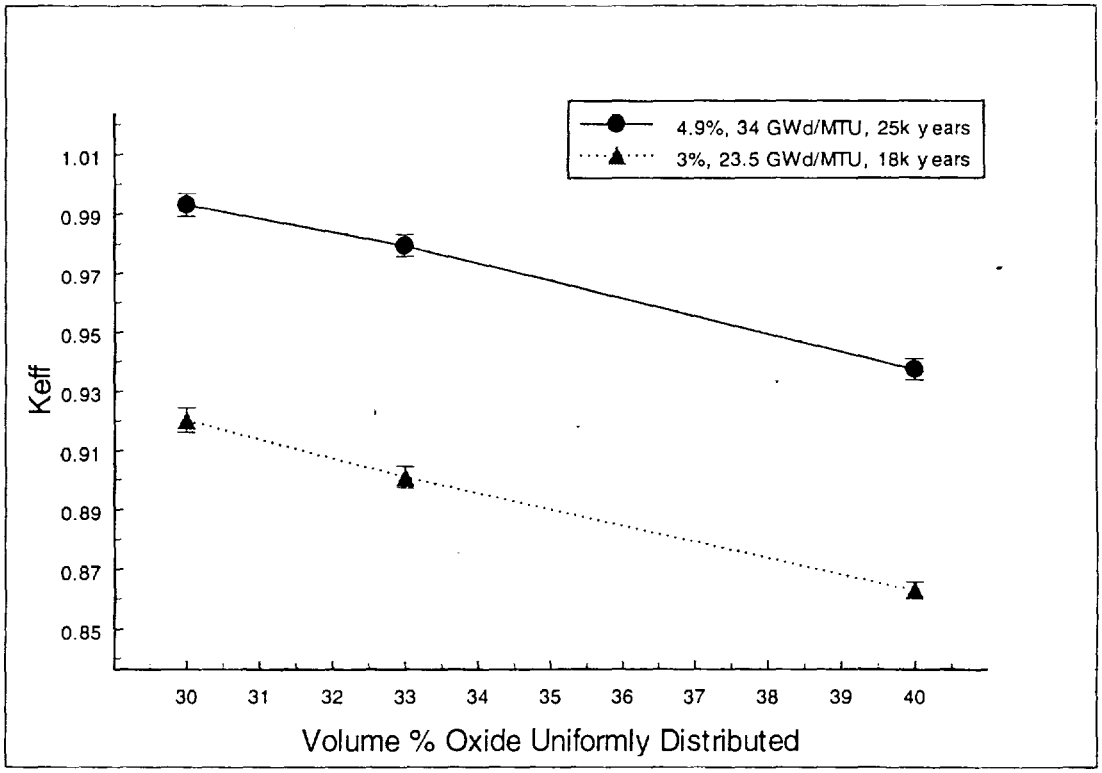

Figure 6.2.2-4. Effects of uniformly distributed oxide vol% on fully degraded basket k_{eff}

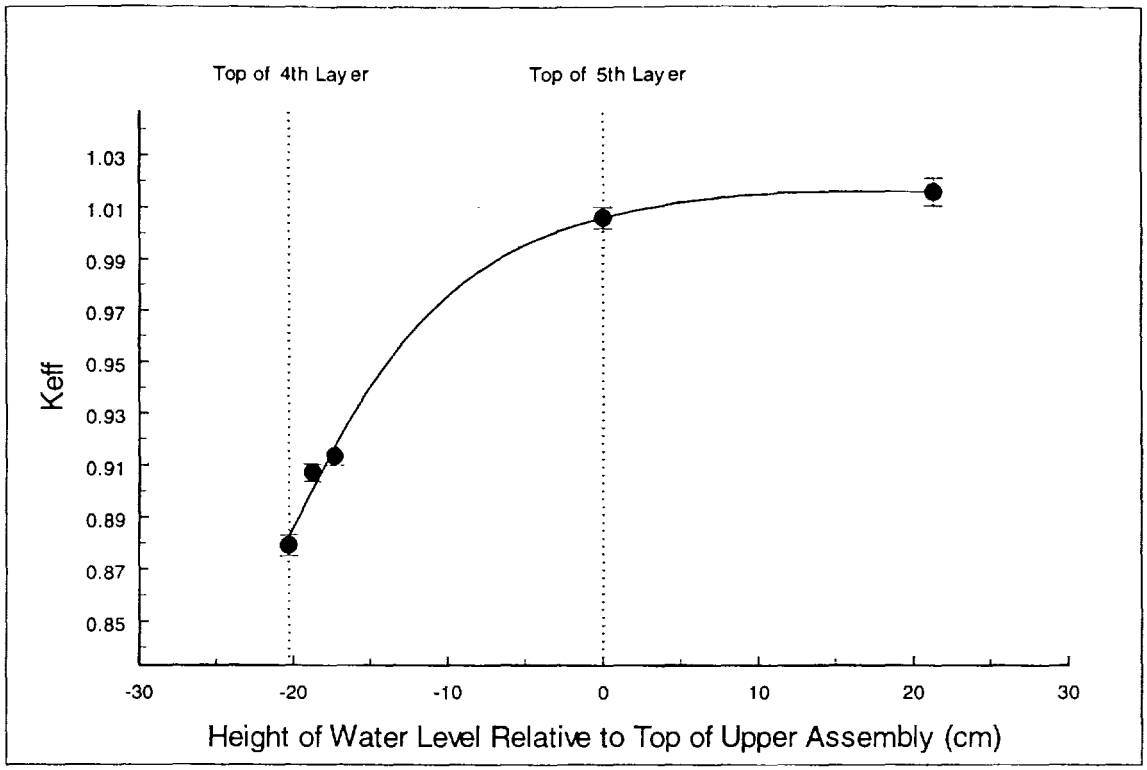

Figure 6.2.2-5. Effects of internal water level on fully degraded basket k_{eff} (4.9% enrichment, 34 GWd/MTU, 35,000 years decay)

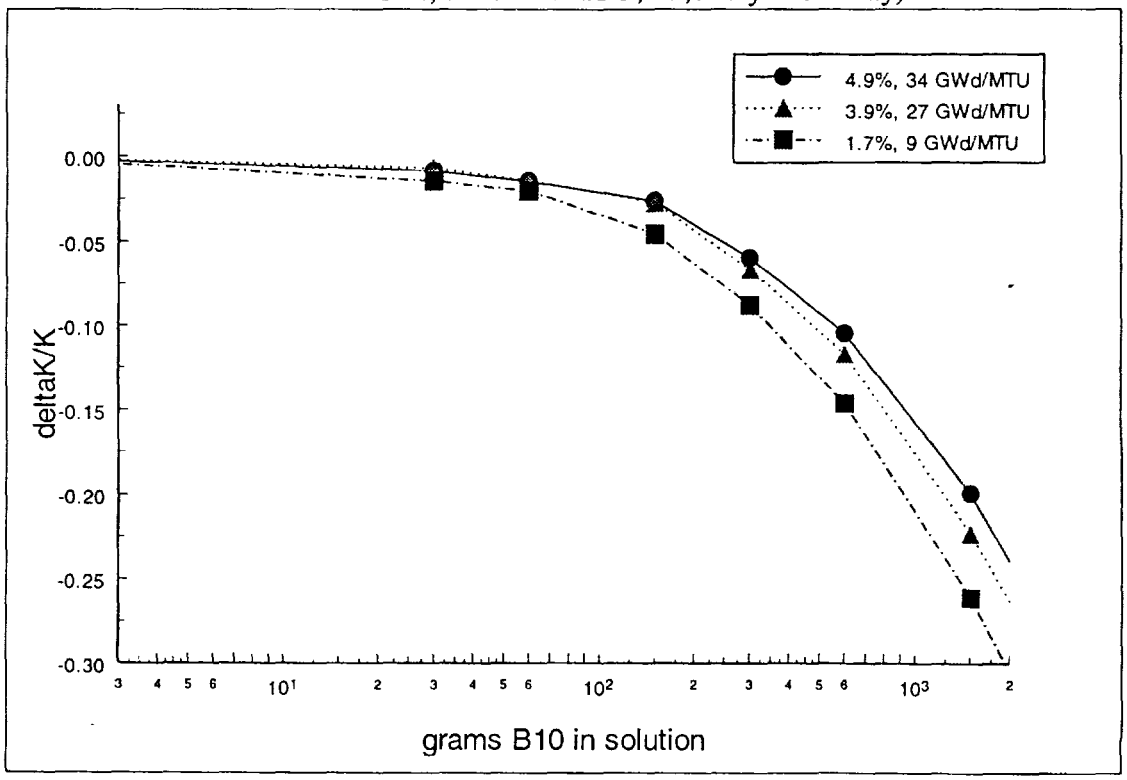

Figure 6.2.2-6. Effects of dissolved ^{10}B on fully degraded basket k_{eff} for the 58 vol% settled oxide configuration

Table 6.2.2-2. k_{eff} Results for with and without 16 Rod DCRAs

Burnup/ Enrichment Pair	58 Vol% Settled				33 Vol% Uniform			
	without DCRAs		with 16 rod DCRAs		w/o DCRAs		with 16 rod DCRAs	
	k_{eff}	2σ	k_{eff}	2σ	k_{eff}	2σ	k_{eff}	2σ
4.3%/3 GWd/MTU	1.21464	0.00410	0.91253	0.00418	1.18004	0.00446	0.86228	0.00494
4.7%/13 GWd/MTU	1.16360	0.00430	0.87859	0.00470	1.12942	0.00484	0.83002	0.00432
4.9%/34 GWd/MTU	1.01860	0.00486	0.7599	0.00448	0.97950	0.00370	0.71312	0.00458

6.2.3 Fully Degraded Basket with Degraded Fuel

This section describes the MCNP evaluations performed for the possible fully degraded basket configurations with degraded fuel assemblies. Only the 33 vol% uniform configuration was evaluated, as consolidation of the fuel rods in the 58 vol% settled case would cause the rods in the top 1.5 assembly rows that are currently in clear water to settle below the oxide layer. Thus, evaluation at 33 vol% uniform is bounding for the settled oxide scenario as well. As this evaluation of sensitivity to consolidation is performed primarily to demonstrate that collapsed assemblies are less reactive than intact assemblies, only the bounding for the absorber plate waste package fuel was evaluated at a decay time of 25,000 years. A rod clearance of 73% corresponds to a 0 cm clearance between guide tubes and adjacent fuel rods. Fuel rod consolidation in only the vertical direction and in both vertical and horizontal directions was evaluated. Variations in spacing of the consolidated assemblies was also performed. The results are provided in Table 6.2.3-1, and as expected, show a decreasing k_{eff} as the rods move closer together.

Table 6.2.3-1. Effects of reduced rod spacing for the 4.9%, 34 GWd/MTU fuel at 25,000 years in the 33 vol% uniform configuration

% Original Fuel Rod Clearance		Assembly Horizontal Spacing	k_{eff}	2σ
Vertical	Horizontal			
100%	100%	0 cm	0.99309	0.00388
73%	100%	0 cm	0.97300	0.00448
73%	73%	1.1 cm*	0.96998	0.00400
73%	73%	0 cm	0.95799	0.00338
0%	100%	0 cm	0.91239	0.00366
0%	0%	4.9 cm*	0.81261	0.00392
0%	0%	2.45 cm	0.85417	0.00338
0%	0%	0 cm	0.79258	0.00342

*Spacing maintains original assembly center-to-center spacing

A final case run with all of the fuel rods touching and completely settled into a cylinder segment at the bottom of the waste package yielded a k_{eff} of 0.65588 ± 0.00394. Based on these results, it is evident that any degradation of the assembly structure, be it by corrosion of the grid spacers or dynamic loading, will result in reduced k_{eff} values.

As the above analyses indicated reduced reactivity with further consolidation, completely degraded fuel with only pellet size and smaller particles of fuel distributed in the oxide was not explicitly evaluated. Previous studies (Ref. 33) of fuel rubble conducted as part of the Three Mile Island Unit 2 defueling examined the k_{eff} of spherical UO_2 particles (evaluated at enrichments of 2.34% and 2.96%) distributed in borated water, and found an optimum particle size of 3.5 cm in diameter and occupying 66% of the total volume. Since a fuel pellet is much smaller than this particle size, an increase in k_{eff} above that shown for fully consolidated rods would not be expected.

6.3 k_{eff} Regressions

Reference 2 (Section 7.6) developed regressions which relate the k_{eff} for a particular class of degraded waste package configurations (e.g., intact fuel with fully degraded basket and oxide settled to bottom of waste package) to various parameters for that class (e.g., time, burnup, enrichment, assemblies covered by oxide, etc.). Since MCNP is a Monte Carlo code, each result is reported as a mean and a standard deviation (σ). For conservatism, the regressions were fit to $k_{eff}+2\sigma$ (upper bound at 95% confidence). The coefficients for the partially degraded basket regressions for both a uniform and settled distribution of oxide corrosion products are provided in Table 6.3-1, and the form of the regression in both cases is as follows:

$$k_{eff}+2\sigma = C_0+C_1b+C_2b^2+C_3a+C_4a^2+C_5Ln(t)+C_6Ln(t)^2+C_7Ln(t)^3+C_8O+C_9T+C_{10}T^2+C_{11}T^3 \qquad (6\text{-}1)$$

where b is burnup in GWd/MTU, and a is initial enrichment in wt%, t is decay time in years, T is thickness of borated stainless steel remaining in mm, and O is either vol% oxide for the uniform oxide configuration, or fuel rod rows covered for the settled cases. Reference 2 indicates that for the uniform case, the vol% of Fe_2O_3 uniformly distributed throughout the waste package void space may be quickly obtained by multiplying the kg of Fe released by basket corrosion by a factor of 4.9998E-3.

Table 6.3-1. Regression Coefficients for Partially Degraded Basket WP $k_{eff}+2\sigma$

Regression Coefficients	Uniform Oxide	Settled Oxide
C_0	2.35498	1.72095
C_1	-6.6737e-03	-6.7237e-03
C_2	-1.8096e-05	-1.6667e-05
C_3	1.4180e-01	1.3348e-01
C_4	-7.1354e-03	-6.0497e-03
C_5	-5.1930e-01	-3.1232e-01
C_6	5.9471e-02	3.7442e-02
C_7	-2.2406e-03	-1.4715e-03
C_8	-5.0889e-03	-1.6797e-02
C_9	-7.4906e-02	-6.6316e-02
C_{10}	1.0646e-02	9.4036e-03
C_{11}	-5.2334e-04	-4.6905e-04

The coefficients for the fully degraded basket regressions for both a uniform and settled distribution of oxide corrosion products are provided in Table 6.3-2, and the form of the regression in both cases is as follows:

$$k_{eff}+2\sigma = C_0+C_1Ln(t)+C_2b+C_3a+C_4Ln(t)^2+C_5Ln(t)^3+C_6b^2+C_7b^3+C_8a^2+C_9a^3+C_{10}Ln(t)b+C_{11}Ln(t)a+C_{12}O \quad (6\text{-}2)$$

where b is burnup in GWd/MTU, a is initial enrichment in wt%, t is decay time, and O is vol% oxide for the uniform oxide configuration and assembly rows covered for the settled cases.

Table 6.3-2. Regression Coefficients for Fully Degraded Basket WP $k_{eff}+2\sigma$

Regression Coefficients	33% Uniform Oxide	58% Settled Oxide
C_0	-5.12955	-1.25161
C_1	1.65615	6.83155e-01
C_2	-8.52852e-03	-6.65133e-03
C_3	2.92660e-01	2.66145e-01
C_4	-1.53971e-01	-6.40282e-02
C_5	4.67070e-03	1.92631e-03
C_6	6.89640e-05	-2.67041e-05
C_7	-1.63227e-07	6.12197e-07
C_8	-6.71372e-02	-6.18276e-02
C_9	5.36083e-03	5.20352e-03
C_{10}	-4.08151e-04	-1.36497e-04
C_{11}	7.23708e-03	5.08490e-03
C_{12}	-5.25978e-03	-1.40918e-01

Reference 2 also developed a multivariate regression for predicting the $\Delta k_{eff}/k_{eff}$ resulting from various amounts of boron remaining in solution for the partially degraded basket with various amounts of iron oxide settled to the bottom of each assembly, and various borated stainless steel plate thickness remaining. While the amount of boron in solution is generally much smaller than in the basket, this correction is justified because it still an effective neutron absorber until it is removed from the waste package. The corrected k_{eff} is obtained using:

$$Corrected\ k_{eff} = k_{eff} + \Delta k_{eff} = k_{eff}\left(1+\frac{\Delta k_{eff}}{k_{eff}}\right) \quad (6\text{-}3)$$

The coefficients of the regression are provided in Table 6.3-3, and the form of the regression is as follows:

$$\Delta k_{eff}/k_{eff} = C_0+C_1\ln(B)+C_2\ln(B)^2+C_3\ln(B)^3+C_4T+C_5O \quad (6\text{-}4)$$

where b is burnup in GWd/MTU, and B is the total grams of ^{10}B in solution in the fully flooded

waste package, T is thickness of borated stainless steel remaining in mm, and O is fuel rod rows covered.

Table 6.3-3. Regression Coefficients for $\Delta k_{eff}/k_{eff}$ as a Function of Dissolved ^{10}B for the 58 vol% Settled Oxide Partially Degraded Basket Configuration

C_0	6.37971e-03
C_1	-6.07375e-02
C_2	2.08433e-02
C_3	-2.21564e-03
C_4	3.59713e-04
C_5	4.23685e-03

Reference 2 also developed a multivariate regression for predicting the $\Delta k_{eff}/k_{eff}$ resulting from various amounts of boron remaining in solution for the fully degraded basket with 58 vol% iron oxide settled to the bottom. The coefficients for this regression are provided in Table 6.3-4, and the form of the regression is as follows:

$$\Delta k_{eff}/k_{eff} = C_0+C_1\ln(B)+C_2\ln(B)^2+C_3\ln(B)^3 \quad (6\text{-}5)$$

where b is burnup in GWd/MTU, and B is the total grams of ^{10}B in solution in the fully flooded waste package.

Table 6.3-4. Regression Coefficients for $\Delta k_{eff}/k_{eff}$ as a Function of Dissolved ^{10}B for the 58 vol% Settled Oxide Fully Degraded Configuration

C_0	2.32558e-02
C_1	-3.56383e-02
C_2	1.42821e-02
C_3	-1.91685e-03

Finally, Reference 2 provided a regression which predicts the peak k_{eff} for the fully degraded basket with settled oxide configuration as a function of fuel assembly burnup and initial enrichment. The regression coefficients are provided in Table 6.3-5, and the form of the regression equation is as follows:

$$Peak\ k_{eff}+2\sigma = C_0+C_1B+C_2E+C_3B^2+C_4E^2+C_5B^3+C_6E^3 \quad (6\text{-}6)$$

where B is burnup in GWd/MTU, and E is initial enrichment in wt%.

Table 6.3-5. Regression Coefficients for 58 Vol% Settled Peak k_{eff} as a Function of Burnup and Enrichment

C_0	6.40653e-01
C_1	-1.02912e-02
C_2	3.00169e-01
C_3	-2.54581e-05
C_4	-4.90929e-02
C_5	9.92035e-07
C_6	3.64521e-03

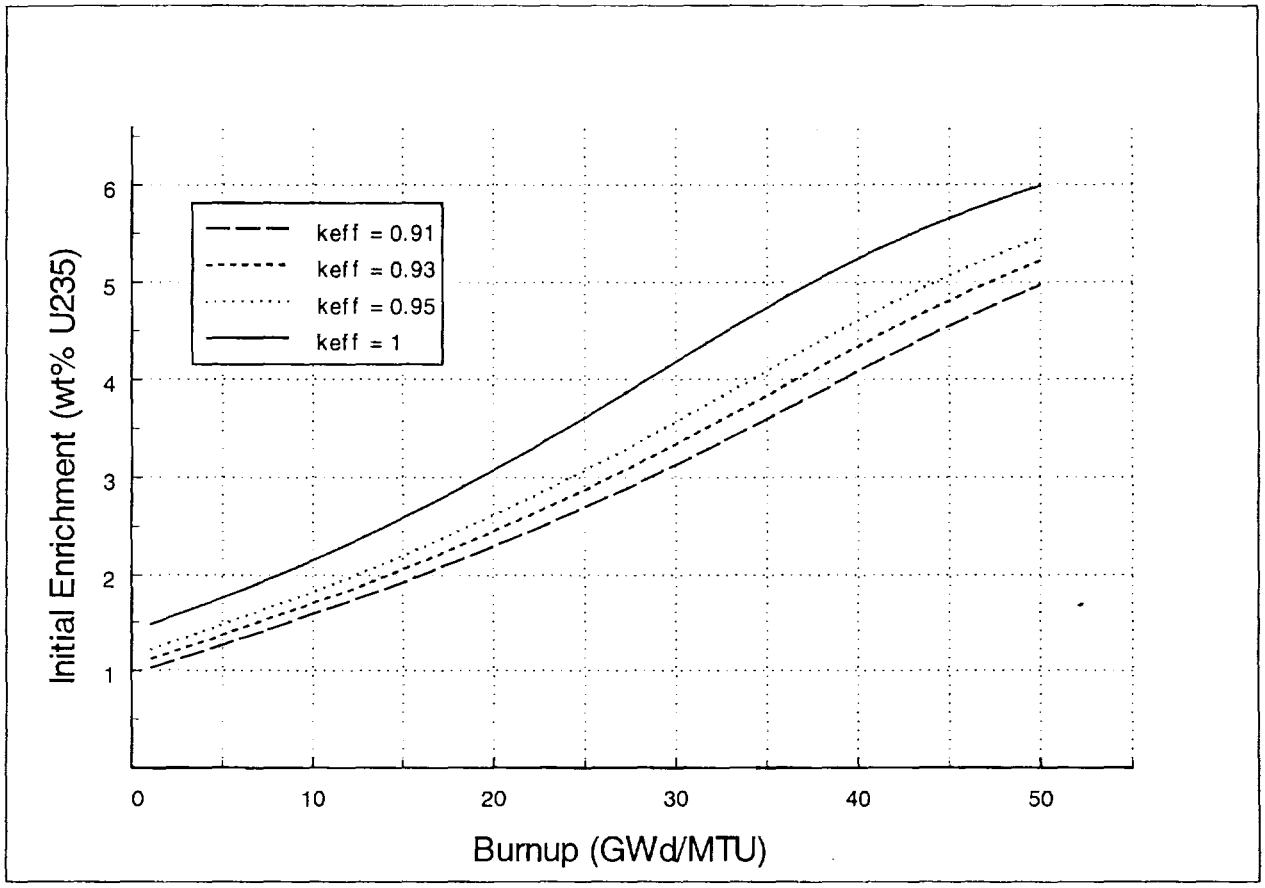

Figure 6.3-1. Peak $k_{eff}+2\sigma$ as a Function of Burnup and Enrichment for the Flooded Fully Degraded WP Basket with 58 Vol% Iron Oxide Settled to the Bottom and No Boron Remaining

7. Probabilistic and Statistical Evaluations

7.1 General Configuration Generator Code

Previous evaluations (Refs. 3, 6, 9, 12) of the possibility of degraded waste package criticality have used computer codes to track the concentrations of fissile and neutron absorber species and estimate k_{eff} for the most likely geometric configurations. Specifically, two general codes were developed: one for commercial SNF in a waste package with partly or completely degraded basket, and the other for degraded immobilized plutonium waste forms (glass or ceramic) with fissile material collected in clay precipitate in the lower portion of the waste package. It is now desired to combine and extend these codes to be able to cover the four general categories of waste form expected at the repository which have significant criticality potential: (1) commercial SNF, (2) DOE owned SNF, (3) immobilized plutonium waste forms, and (4) mixed oxide (MOX) SNF containing plutonium from decommissioned weapons. This program is also intended to be able to track all the successive stages of waste form degradation and the resulting possible criticality locations: internal, near-field external, and far-field external.

For this purpose, the locations are divided into two categories: paths and ponds. Paths represent vertical flow through a geologic layer of the repository. Ponds represent locations where fissile material can be concentrated in a critical mass and where there can be sufficient water as moderator to cause a criticality. The waste package itself is designated as pond number 0, but its concentrations are computed by a unique subroutine, which is initially driven by the dissolution rates of the waste forms and the basket materials, and by the concentrations in the water dripping or infiltrating into the waste package. The other ponds, and all the paths, are driven only by the concentrations in the inflowing water (solution). Ponds are nominally connected by one or more paths (in series), although ponds may be directly linked without any intervening path (e.g., the package outflow feeding a possible pond in the invert). The algorithms used to model these two regime categories are described in the following sections.

The algorithms of this code are constructed to model the physical and chemical processes, which include the following:

- Trace movements of fissile and absorber elements between entities (ponds and paths between) from initial concentrations/locations (which are also entities). For most waste forms there will be no multiple ponds within the waste package, but only the single waste package pond and the possibility of external ponds. The paths will have the capability for retardation of the fissile material, particularly U. Ultimately, retarded fissile material may be remobilized. The relative importance of retardation and remobilization will be determined by whether significant remobilization can occur within the time horizon which could be as high as 1,000,000 years.

- Account for water buildup as a function of time (both to transport key elements and to provide moderator for criticality).

- Determine criticality potential as a function of time at individual locations, which are defined

as either ponds or localized water supersaturations (e.g., moist clay, or porous region in the saturated zone).

- Probability evaluated by the joint occurrence of individual selections.

7.2 Specialized configuration generator

The computer code snfpkg.c is a specialization of the general configuration generator code (generate.c), and all the description of that code in Section 7.1 applies here, except for those features which deal with tracking material outside the waste package. The specialization is to evaluate the entire inventory of commercial PWR SNF expected for emplacement at the repository. For this purpose, the following are additional features provided by this specialized code:

- The k_{eff} regressions developed in Reference 2 are incorporated into the code. There are two basic forms of the regression: partially degraded basket and the fully degraded configuration, which are repeated in this document in Section 6.3 as equations 6-1 and 6-2, with regression coefficients given in Tables 6.3-1 and 6.3-2, respectively. If the infiltration rate is low, the effect of boron in solution may be significant while the borated stainless steel is degrading, and for some time thereafter. This is accounted for by the correction shown in equation 6-3, which uses the regressions of equations 6-4 and 6-5 for the partially degraded basket and the fully degraded configuration, respectively. At the present time, this correction factor has only been developed for the settled oxide distribution. This limitation is acceptable because the uniform oxide distribution is less conservative than the settled distribution, so omitting the correction for boron in solution is conservative.

- The k_{eff} regressions are applied to each batch of commercial SNF assemblies (typically 10 to 20 assemblies having identical in-core histories) as read from the input file "data.in" which is prepared by the Waste Stream Management program (WSM), and which contains upwards of 20,000 individual batch records, approximately 15,000 of which are for PWR SNF. Because of the large amount of computation involved, the k_{eff} calculations are not done at each timestep, but only at intervals specified by the parameter "tabint" which are sufficiently frequent to capture the main features of the time dependent behavior. At each of these tabulation intervals, the result of calculating k_{eff} for all the assembly batches is expressed in terms of the fraction of the assemblies which show k_{eff} to be greater than a threshold value which is generally taken to be significantly less than 1, according to regulatory requirements. This fraction is called the potentially critical fraction (PCF), and the maximum value of this fraction is called the peak potentially critical fraction (PPCF). These acronyms are used throughout the rest of this section.

  It should be noted that Reference 2 states ranges of applicability of the regressions, with respect to SNF and basket characteristics, based on the range of parameters in the cases used to develop the regressions. The range of basket thicknesses used for this study fall within the range specified in Reference 2. A significant fraction of the SNF does, however, fall outside the parameter range for the partial basket regression, both on the more critical and the less

critical side (i.e., parameters which would lead to a higher k_{eff} and a lower k_{eff} than those which would be calculated for parameter values within the specified ranges). For SNF which falls outside on the more critical side, the Reference 2, Table 7.6-3, shows that for typical cases the regression gives a slightly higher k_{eff} than actual MCNP calculations. Therefore, the only possible error in applying the regression to SNF on the more critical side will be conservative, i.e., the k_{eff}, and consequently the PCF, will be overestimated. This conclusion also holds for fuel which falls on the less critical side of the regression parameter range specified in Reference 4, because the only way to misclassify such SNF would be to include it in the PCF.

7.3 Statistical and Probabilistic Analysis

7.3.1 Criticality Control Measure of Effectiveness

The potentially critical fraction of the entire family of commercial PWR SNF is a useful parameter for summarizing the long-term criticality performance capability of the borated stainless steel as the principal criticality control material. This fraction is not a measure of any criticalities which are expected to occur, but rather an indication of the SNF which cannot be emplaced in the absorber plate waste package, and will, therefore, require additional criticality control measures (e.g., zircaloy clad boron carbide control rods, or a much smaller waste package capacity).

Since this package relies primarily on borated stainless steel for criticality control, and since most of the neutron absorbing boron is released from the waste package within a few thousand years of the borated stainless steel corrosion (depending, of course, on the infiltration rate and the exchange fraction), the long-term criticality performance is most sensitive to the rate of corrosion of this material. For this reason most of the results are presented for a range of corrosion rates. It would be expected that the PCF would also be dependent on the thickness of the borated stainless steel plates, so this sensitivity has been considered in Reference 3, Section 7.5.4. The thickness sensitivity turns out not to be as strong as the sensitivity to borated stainless steel corrosion rate.

Sensitivity to exchange fraction (ex) was examined, and the results are detailed in the file ex.sum listed in Attachment II of reference 3. These results are not presented here for the following reasons:

- The results were found to be insensitive to changes over the range chosen (0.1 to 0.5).
- The derivation of the range for exchange rate (Ref. 3) indicates that the exchange rate is strongly correlated with the infiltration rate, so that the sensitivity to decreasing the exchange rate is already represented by decreasing the infiltration rate.
- The omission of this sensitivity analysis is consistent with the uncertainty connected with estimating the exchange fraction.

7.3.2 General time dependent behavior of potentially critical fraction

The general time dependent behavior is summarized in Figures 7.3-1 and 7.3-2: one for the settled oxide distribution, and one for uniform. Each has three graphs: (1) nus (SS corrosion rate

in microns/year) =0.08, dr (drip rate in mm/year) =5, (2) nus=0.40, dr=5, and (3) nus=0.40, dr=50; nominal values are used for all the other parameters. The following are the principal observations from these results:

- Progression from cases 1 to 3 reflects increasing environmental stress (higher dr) and decreasing material performance (higher SS corrosion rate). Going from cases 1 to 2 shifts the PPCF forward drastically in time and increases its value. Going from cases 2 to 3 eliminates the early minimum (because the high infiltration rate reduces the boron in solution to below the threshold of minimum effectiveness, 30 grams, and thus no k_{eff} correction is performed; Ref. 2, Sect. 7.4) and significantly increases the PCF just before the complete basket dissolution (0.0101 versus 0.0145 at 8,000 years which is just before the tbskt=8,646 years).

- Shows fraction of the fuel which should go into packages with greater criticality control (control rods or drastically reduced waste package capacity).

- Comparison between figures shows dominance (conservativeness) of the settled oxide configuration, so it will be used for the sensitivity studies.

- The general time dependence shown in Figures 7.3-1 and 7.3-2 holds for the range of parameters considered in this document, so it will not be repeated in the following presentation of the results of the sensitivity studies and the generated probability distributions. Instead, the following results are presented in terms of the summary statistics, the peak potentially critical fraction (PPCF), and time to peak potentially critical fraction (TPPCF).

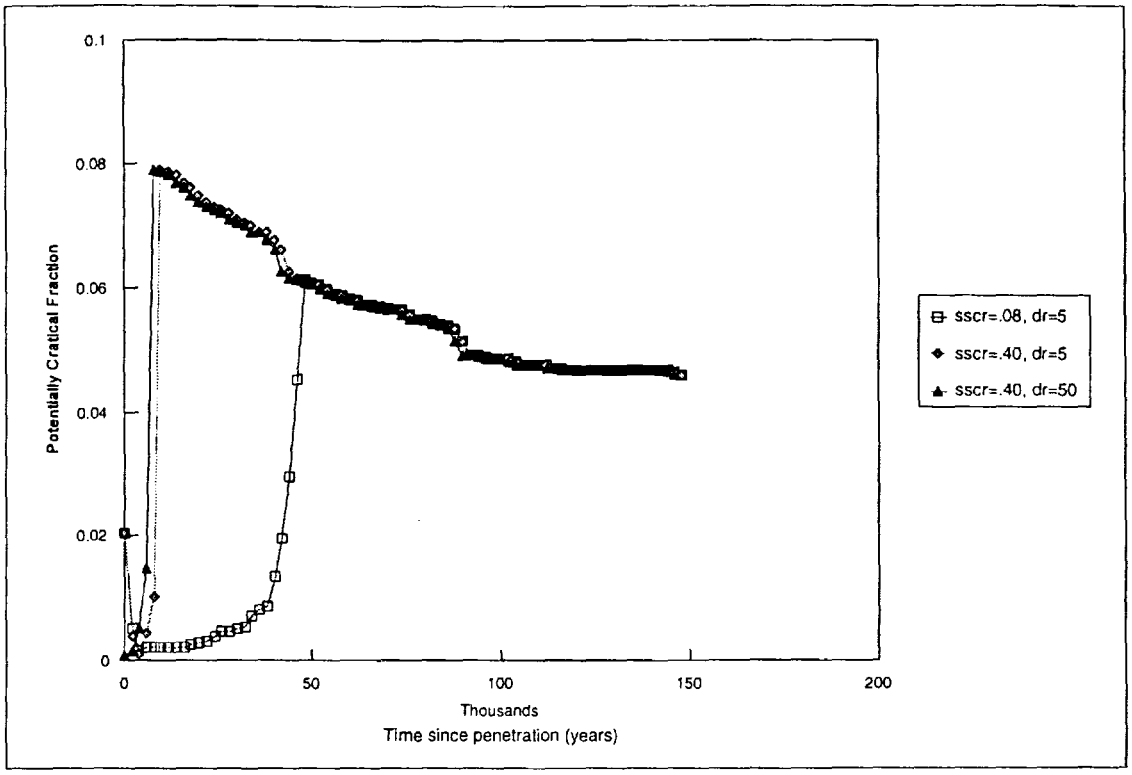

Figure 7.3-1. Time Dependence of Potentially Critical Fraction - Settled Oxide, WP Penetration Time = 3,000 years

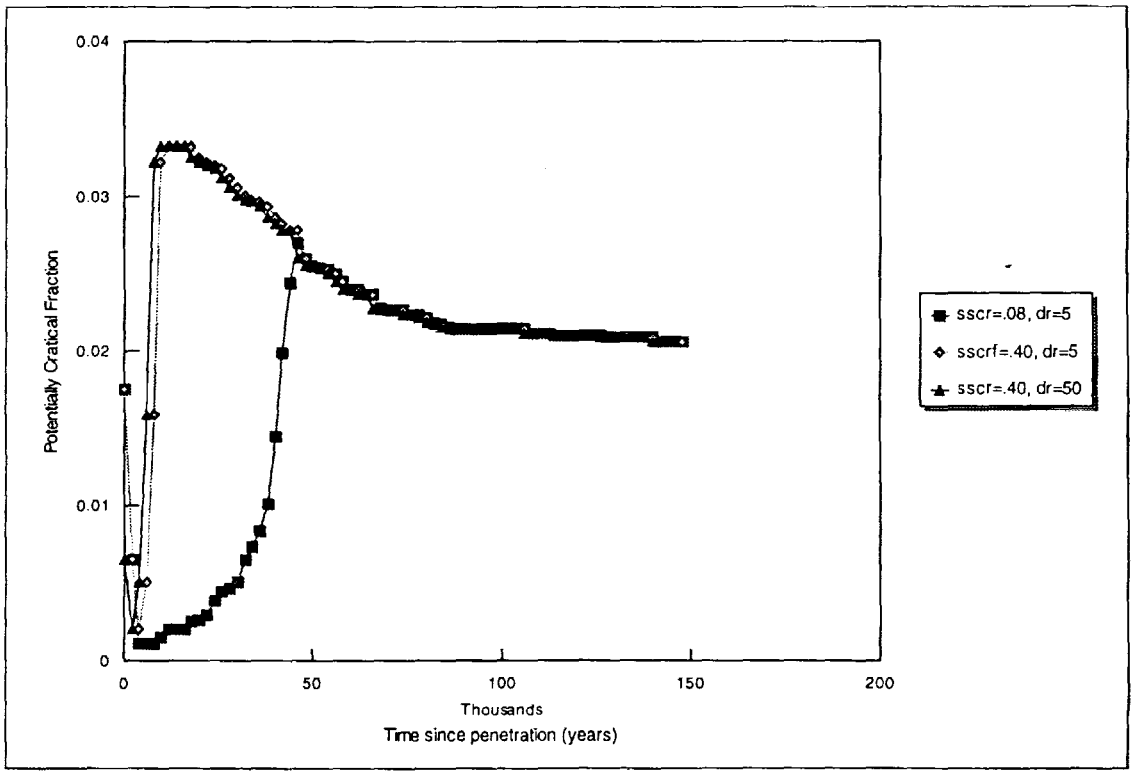

Figure 7.3-2. Time Dependence of Potentially Critical Fraction - Uniform Oxide, WP Penetration Time = 3,000 years

7.3.3 Sensitivity to k_{eff} threshold

The sensitivity of PPCF to threshold k_{eff} is shown in Figure 7.3-3, and the corresponding TPPCF in Figure 7.3-4. These results are for the settled oxide distribution and for the range of borated stainless steel corrosion rates from 0.08 microns/year to 0.40 microns/year. More complete results covering even higher corrosion rates, and also giving corresponding data for the uniform distribution of oxide, are given in reference 3, Table 7.5.2-1, from which the figures are derived. The original data on which the graphs are based are given in the output file keff.sum.

- As would be expected, the PPCF declines with increasing k_{eff} threshold, and also with decreasing corrosion rate of borated stainless steel, as can be seen from Figure 7.3-3.

- It should be noted that the saturation of corrosion rate sensitivity for the uniform oxide distribution shows a similar behavior with two significant differences: (1) the saturation effect for the uniform oxide distribution does not begin until the corrosion rate has reached 2.0 microns/yr; and (2) the TPPCF for the uniform oxide distribution drops to 2,000 years. Both of these differences are artifacts of the condition that the borated stainless steel corrosion time is less than 2,000 years for the corrosion rates of 2.0 and 4.0 microns/yr (1,729 and 864 years, respectively). After the borated stainless steel corrosion time, the basket is considered fully degraded and that regression is applied. However, the smallest time in the dataset used for the fully degraded basket regression in Reference 4 was 8,000 years. This is 3,000 years greater than the 2,000 years plus 3,000 years penetration time, so some anomalous behavior may be expected.

- It should be noted that the data of Figure 7.3-3 can be used as the basis for estimating the cost to the program associated with any criticality threshold below 1.0. The difference between the highest PPCF at threshold = 1.0 (0.018) and the PPCF at a lower threshold, is the fraction of the commercial PWR SNF which will have to be accommodated in a more expensive waste package (e.g., a waste package with control rods as the primary criticality control measure or a greater number of smaller, but not correspondingly cheaper, waste packages).

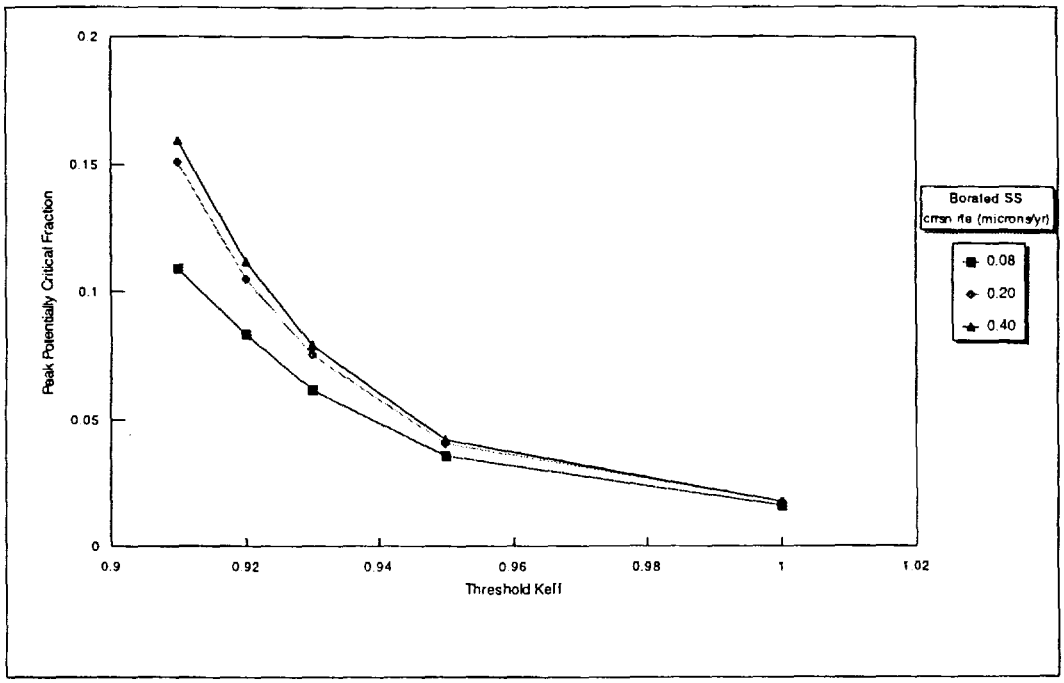

Figure 7.3-3. Effect of Threshold k_{eff} on Peak Potentially Critical Fraction for the Range of Borated Stainless Steel Corrosion Rates

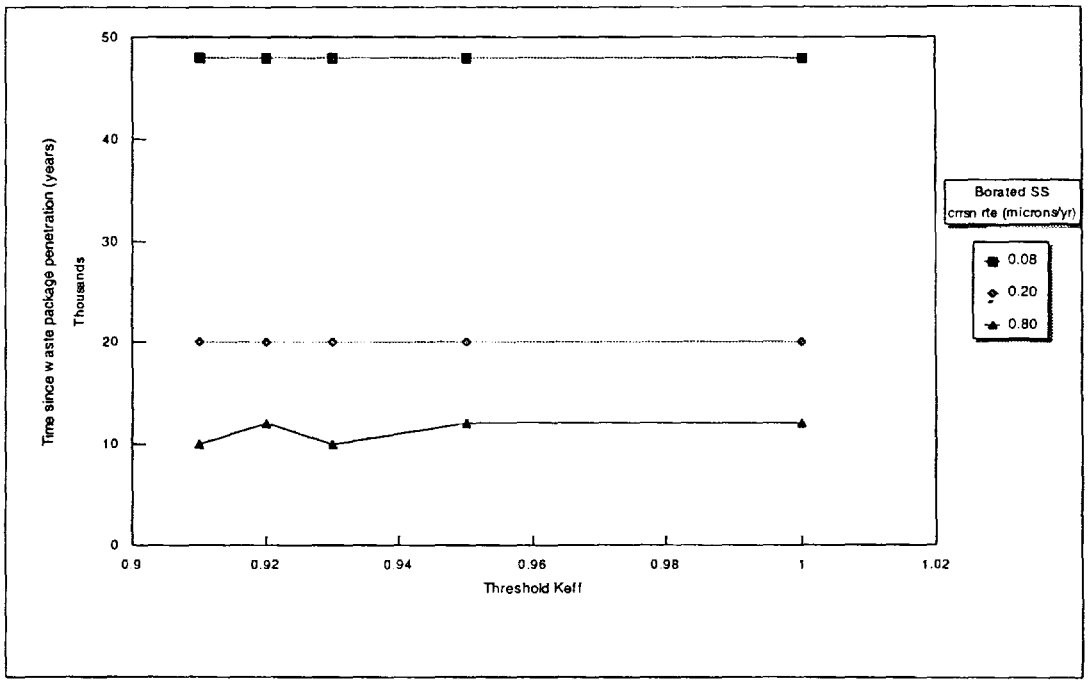

Figure 7.3-4. Effect of Threshold k_{eff} on Time of Peak Potentially Critical Fraction for the Range of Borated Stainless Steel Corrosion Rates

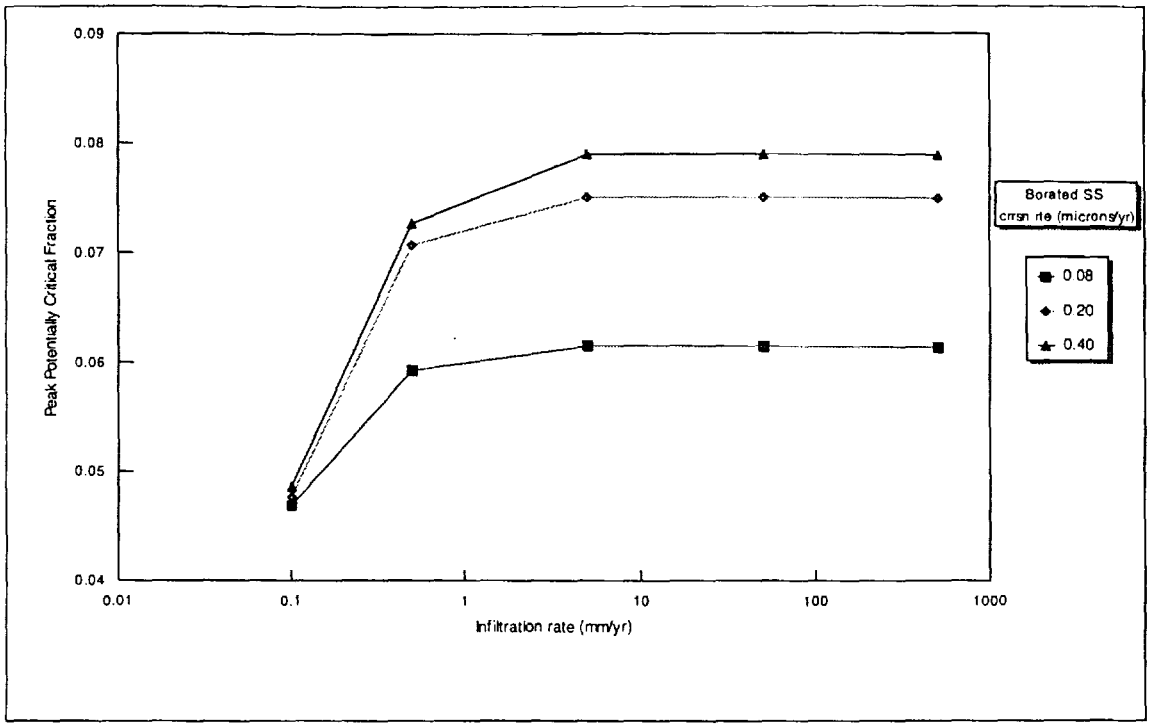

Figure 7.3-5. Peak Potentially Critical Fraction as a Function of Infiltration Rate (for a family of borated stainless steel corrosion rates)

7.3.4 Sensitivity to infiltration rate

A low infiltration rate permits some boron released from the stainless steel corrosion to remain in solution (since the flushing rate is slow), thereby lowering the k_{eff}, particularly since the boron in solution is somewhat more effective at absorbing neutrons than the boron in the spatially limited plates. The resulting reduction in PPCF is shown in Figure 7.3-5.

- The PPCF increases with increasing infiltration rate, but this effect saturates at 10 mm/yr. The TPPCF decreases with increasing infiltration rate, and, as with the PPCF, saturates at 10 mm/yr.

- The low values of PPCF for low values of infiltration rate are due to the fact that the low flushing rate permits the retention of a significant amount of boron in solution for a significant period of time after complete dissolution of the borated stainless steel. This delay results in a longer TPPCF which, in turn, assures a lower PPCF because of the inherent decrease in SNF reactivity with time (beyond the 15,000 - 25,000 year peak, of course).

- As with all the sensitivities, the PPCF decreases with increasing stainless steel corrosion rate, but this effect saturates at 0.4 microns/yr, which is the reason that the curves for higher values are not shown in these figures.

- The usually strong dependence of PPCF and TPPCF on borated stainless steel corrosion rate is weakened for very low infiltration rates. This is because the removal time for boron in solution becomes much longer than the corrosion time itself, so it no longer makes much difference how long the borated stainless steel lasts. It should, however, be noted that this boron retention effect is only significant for infiltration rates of 0.1mm/yr or lower. Unless further infiltration rate investigations show that such low infiltration rates are likely after all, the current high infiltration rates of the CDA will preclude any credit for benefit from potential boron retention after complete corrosion of borated stainless steel.

7.3.5 Sensitivity to thickness of borated stainless steel plates

The principal effect of increasing borated stainless steel thickness is to increase the time to complete dissolution of the borated stainless steel, which increases the TPPCF, and correspondingly decreases the PPCF because of the monotonic decrease in reactivity with time. This effect is shown in Reference 3, Figures 7.5.4-2 and 7.5.4-1, respectively. However, the effect is not as strong as would be expected, particularly for the high borated stainless steel corrosion rates, for the following reasons:

- The variation in borated stainless steel thickness is dominated by the much larger range in corrosion rates (40% versus 400%).

- At the higher corrosion rates, even a 10 mm thickness does not prevent the high corrosion rate from dropping the corrosion time well below the time of the intrinsic k_{eff} peak, 15,000 to 25,000 years.

- At the higher corrosion rates, even a 10 mm thickness does not prevent the high corrosion rate from dropping the corrosion time well below the time of the intrinsic k_{eff} peak, 15,000 to 25,000 years.

7.3.6 Sensitivity to time of package barrier penetration

A major goal of waste package design is to increase the penetration time (time to waste package breach by aqueous corrosion of the barriers). It is, therefore, useful to test the sensitivity of criticality performance to penetration time. The detailed results are given in Reference 3, Figures 7.5.5-1 and 7.5.5-2. The following items are of interest:

- There is a small decrease in PPCF with increasing penetration time which reflects the decrease of reactivity with time (already discussed above).

- The TPPCF measured from the time of penetration changes very little with penetration time. If this time were measured from emplacement, it would, obviously, show an increase approximately equal to the increase in penetration time. Hence increasing penetration time does have a significant benefit with respect criticality performance.

7.4 Probability distributions of potentially critical fraction

The greatest uncertainty in the long-term criticality evaluation is associated with three parameters which cannot even be modeled quantitatively at this time: (1) the length of time for which there will be standing water in the waste package, (2) the number of assembly layers covered by such standing water, and (3) the distribution of iron oxide within the waste package (which can't even be modeled by a single parameter). It is expected that some quantitative modeling of these parameters will be developed to secure Nuclear Regulatory Commission (NRC) approval for any probabilistic criticality evaluation, and certainly for the license application. In the meantime, the probabilistic methodology will be applied to the three input parameters having the next greatest degree of uncertainty: infiltration rate, borated stainless steel corrosion rate, and waste package penetration time. For this purpose, appropriate ranges of these parameters were developed in Reference 3, and represented by the following discrete distributions:

- Stainless steel corrosion rate (microns/yr): 4 value, probability pairs: 0.08,0.25; 0.2,0.25; 0.4,0.25; 0.8,0.25.
- Infiltration rate (mm/yr): 3 value, probability pairs: 0.5,0.3; 5.0,0.4; 50.0,0.3
- Penetration time (yrs): 3 value, probability pairs: 3000,0.4; 5000,0.4; 7000,0.2

These distributions were used to generate 36 combinations of the three parameters. These 36 combinations were input as cases to the specialized configuration generator, snfpkg.c, together with the associated probabilities. The resulting probability distributions for PPCF and TPPCF are shown in Figures 7.4-1, and 7.4-2, respectively.

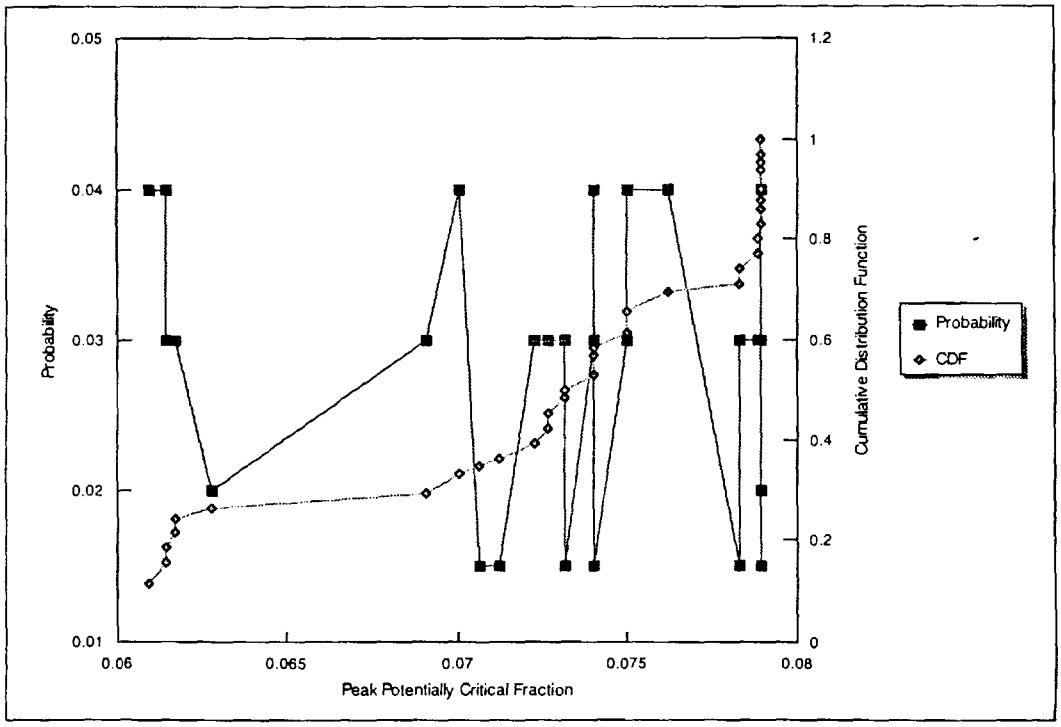

Figure 7.4-1. Probability Distribution of Peak Potentially Critical Fraction

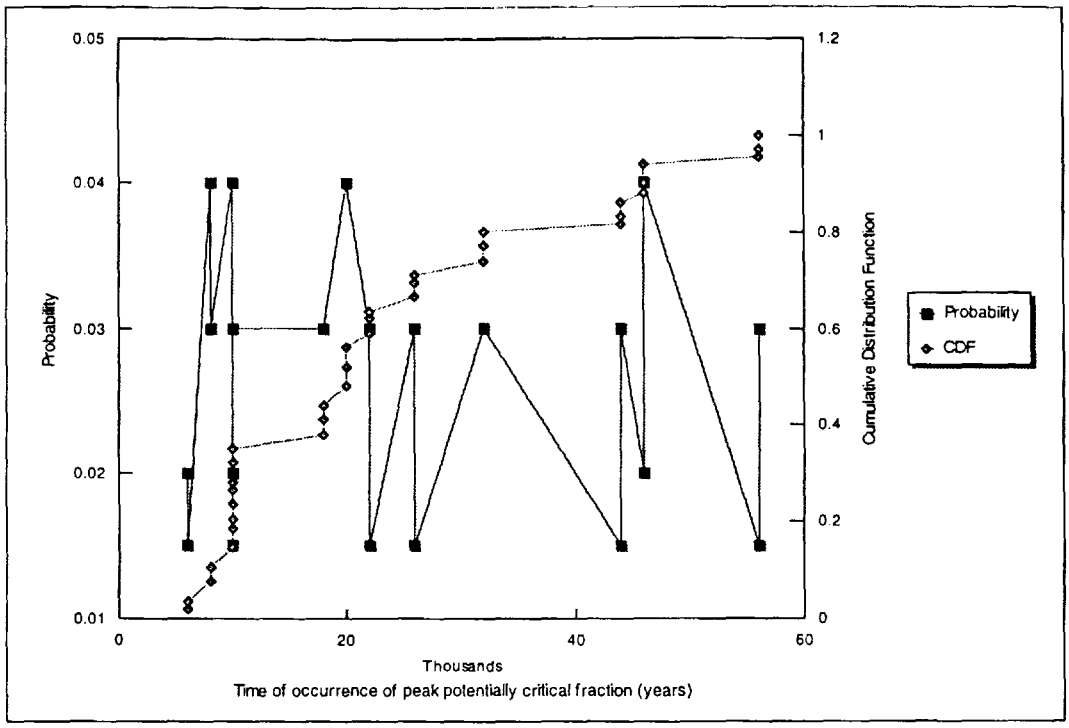

Figure 7.4-2. Probability Distribution for Time of Occurrence of Peak Potentially Critical Fraction Assuming Iron Oxide has Settled to the Bottom of the Waste Package

The following features of these figures should be noted:

- The probability functions (which can be interpreted as similar to the probability density function of a continuous distribution) show considerable fluctuation, reflecting the variations in probability within two of the three individual parameter distributions.

- The cumulative distribution function (CDF) in Figure 7.4-1 shows major jumps, or steps, at PPCF=0.061, 0.074, 0.078, which correspond to the PPCF levels for the borated stainless steel corrosion rates=0.08, 0.20 and 0.40 microns/yr illustrated in Figure 7.3-5 for the nominal parameter values infiltration rate = 5 mm/yr and borated stainless steel plate thickness = 7 mm.

7.5 Implementation of loading strategy

The results of this study will be used to establish preliminary rules for selecting the appropriate emplacement package for each batch of PWR SNF, and for determining the fraction of fuel which will have to be emplaced in the more expensive package with the greater criticality control. In particular, the results presented in Figure 7.5-1 show the fractions requiring the greater criticality control waste package for the range of stainless steel corrosion rates, with the nominal assumptions for the other parameter values.

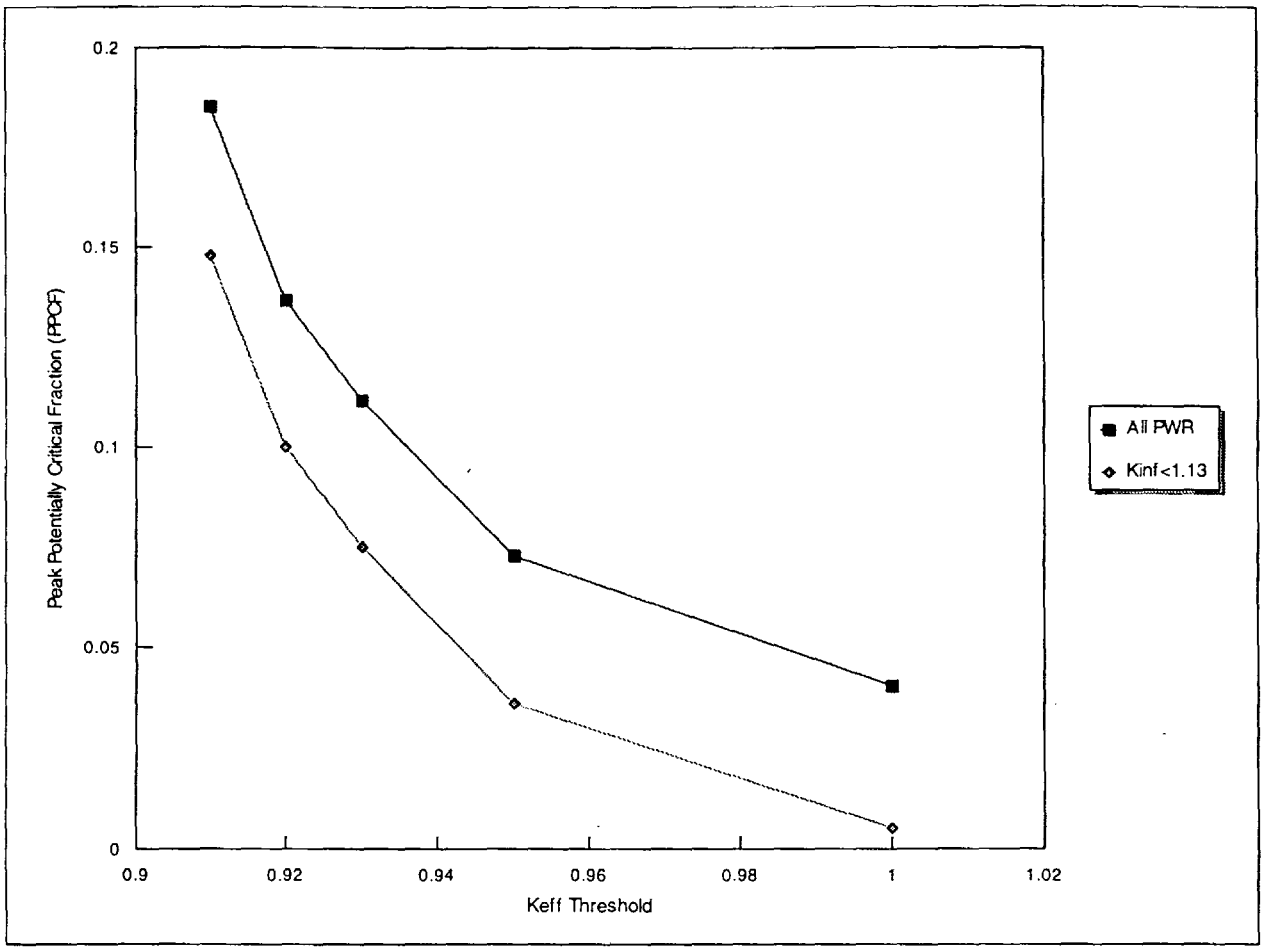

Figure 7.5-1. PPCF Before and After k_∞ Screening

A more conservative approximation of peak potentially critical fraction can be developed from a worst case, time independent regression developed in Reference 4 (repeated as equation 6-6 herein). That regression represents the peak k_{eff} values which would generally occur at the time of the intrinsic peak k_{eff}, between 15,000 and 25,000 years after discharge. In many cases, the borated stainless steel dissolution required to permit this k_{eff} would not be achieved within 15,000 to 25,000 years. If this conservative k_{eff} regression is applied to the range of characteristics of commercial PWR SNF, the results are as shown in Figure 7.5-1.

Also shown in Figure 7.5-1 is the application of this conservative regression to the fraction of the commercial PWR SNF which has burnup and enrichment which would satisfy the criticality control threshold used in Reference 16 (k_∞<1.13). The degree to which the values of this second graph are all above zero, indicates the inadequacy of k_∞ as an effective parameter for measuring the amount of fuel which would require the greater criticality control waste package.

8. Evaluation of Criticality Consequences

As described in Section 4.1.1, the effects on k_{eff} of fuel burnup, enrichment, and decay time, as well as degradation of basket components, were investigated. The most reactive fuel/ waste package configuration combination identified was in the 21 PWR absorber plate waste package. The analysis of the absorber plate waste package identified SNF with an enrichment of 4.9%, with a burnup of 34 GWd/MTU, and a flooded fuel-clad gap, as most reactive. The most reactive configuration occurs with the basket fully degraded, the boron removed, the PWR assemblies stacked together, and accumulated iron oxide from the basket materials at it highest reasonable density of 58% (packed sand, Ref. 2), leaving one and a half rows of assemblies at the top of the stack immersed in water only and free of oxidation products. This configuration is illustrated in Figure 8-1.

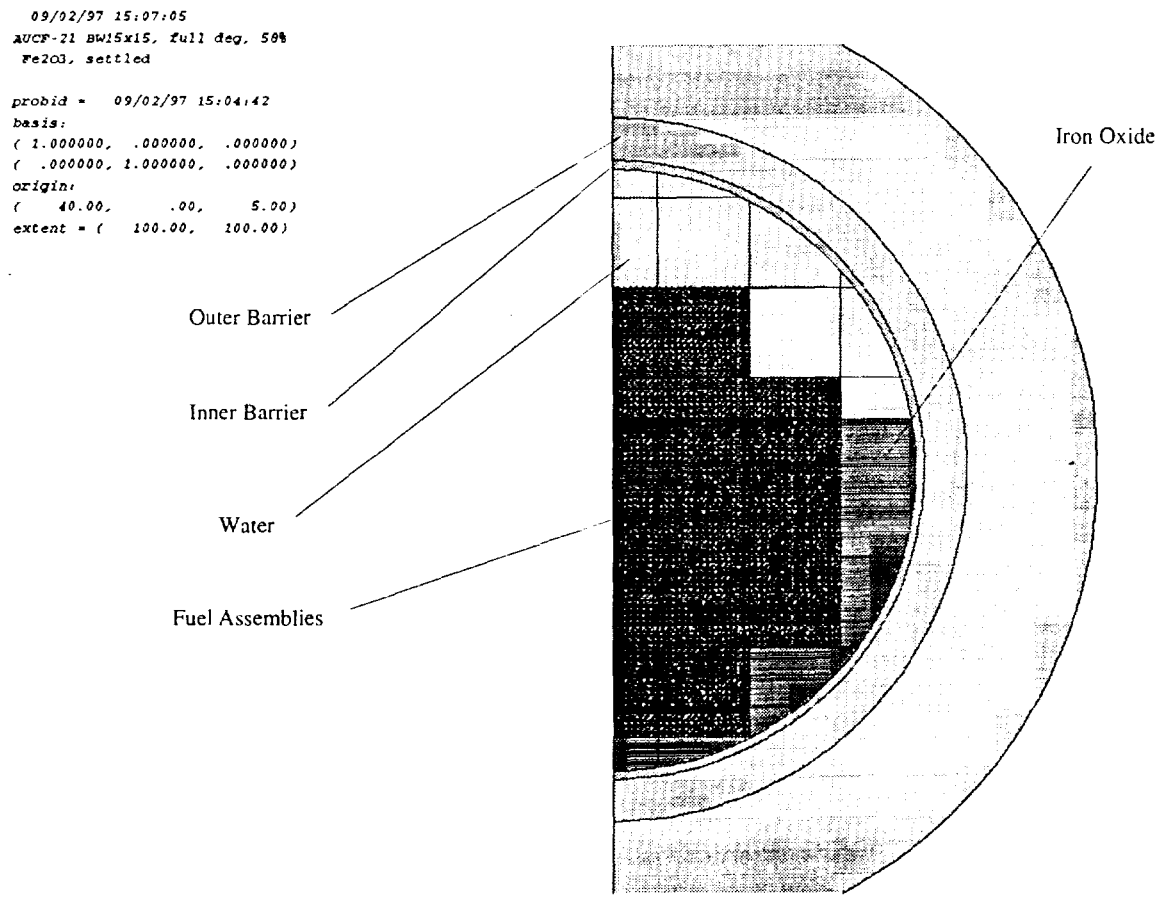

Figure 8-1. Base Configuration for Consequence Analysis - Stratified Degraded Waste Package

8.1 RELAP5 Model Description

The purpose of this section is to describe the RELAP5 model used for the coupled neutronic-thermal-hydraulic analyses of a criticality event in a waste package where the integrity of the outer barrier has been compromised leading to a fully degraded basket assembly. The spatial orientation of the waste package is such that the cylindrical waste package axis long fuel assembly dimension are in the horizontal plane. Figure 8-1 depicts an idealized configuration of the fully degraded waste package system viewed parallel to the waste package axis. The heavily shaded rectangular areas in the figure represent the SNF assemblies, the intermediate shaded areas represent the iron oxide-water mixture, and the lightly shaded areas represent water only. The iron oxide was assumed to have settled to the bottom of the waste package covering the lower 3.5 rows of assemblies. The presence of oxide material was included in the development of the reactivity parameters but not specifically included in the hydrodynamic or thermodynamic modeling.

The RELAP5 code is designed for use with fundamentally one-dimensional hydraulic systems but does include models simulating multi-dimensional flow under restricted conditions (Ref. 21). In the fully degraded condition used for the waste package internal structure in this analysis (Ref. 2), the SNF assemblies are in an open lattice arrangement, allowing cross flow among them. The RELAP5 model of the idealized configuration (Figure 8-1) is quasi-two dimensional, containing flow connections in the two directions normal to the waste package cylindrical axis but not parallel to the axis. Because the model is quasi-two dimensional, the waste package and SNF assemblies are modeled at one-fifth their actual length with adjustments to the appropriate model parameters. The principal components of the RELAP5 model are control volumes where the fluid properties are defined, junctions where momentum properties are defined, and heat conductors where energy transport can occur (other than through the fluid motion).

The RELAP5 model (Ref. 5) of the degraded waste package, illustrated as a block diagram in Figure 8.1-1, consists of 27 control volumes, 43 junctions, and 35 heat conductors. The diagram displayed in Figure 8.1-1, while not to scale, shows the relative control volume and junction arrangement with minimal identifier (ID) numbers. The model represents one half of the waste package cross sectional area since the system has left-right symmetry. Control volumes are represented in Figure 8.1-1 by the rectangles labeled with the volume ID and junctions by labeled arrows indicating the direction (arbitrary) of positive mass flow. Numbers on the left of the figure show the change in vertical elevation for each row of control volumes. The metal portions of SNF assembly cross sectional areas are represented by heat conductors, not shown in Figure 8.1-1, and the fluid portions of these areas, as well as non-fueled areas, by control volumes. Two time-dependent control volumes representing the external boundary waste package environment complete the RELAP5 geometry setup. Note that control volumes and/or junctions whose thermodynamic states are a priori specified, i.e., time-dependent entities, serve as boundary conditions, either as sources or sinks for the fluid inventory. The total volume contained in the control volumes is 0.4545 m^3 resulting in an initial inventory of 450.04 kg of water. The fluid inventory in the waste package control volumes is initialized at 323.16 K and 1.013e+05 Pa (liquid water).

Junctions define the cross sectional area between two control volumes available for fluid transport. This area must intersect both volumes. In the RELAP5 model of the waste package, vertical junctions and areas normal to the long fuel rod dimension define the "normal" flow paths (normal with reference to the one-dimensional hydraulic characteristic of the RELAP5 code) and horizontal junctions and areas (likewise normal to the long fuel pin dimension) define cross flow paths. Physical constraints on flow paths in the waste package are incorporated into the junction flow areas and frictional loss coefficients. Initial conditions for all junctions except the in-flow junction (J370-1 in Figure 8.1-1) are zero mass flow rate. In-flow from the drift is conservatively modeled as 20 m^3 per year (time dependent volume, or TDV, 360).

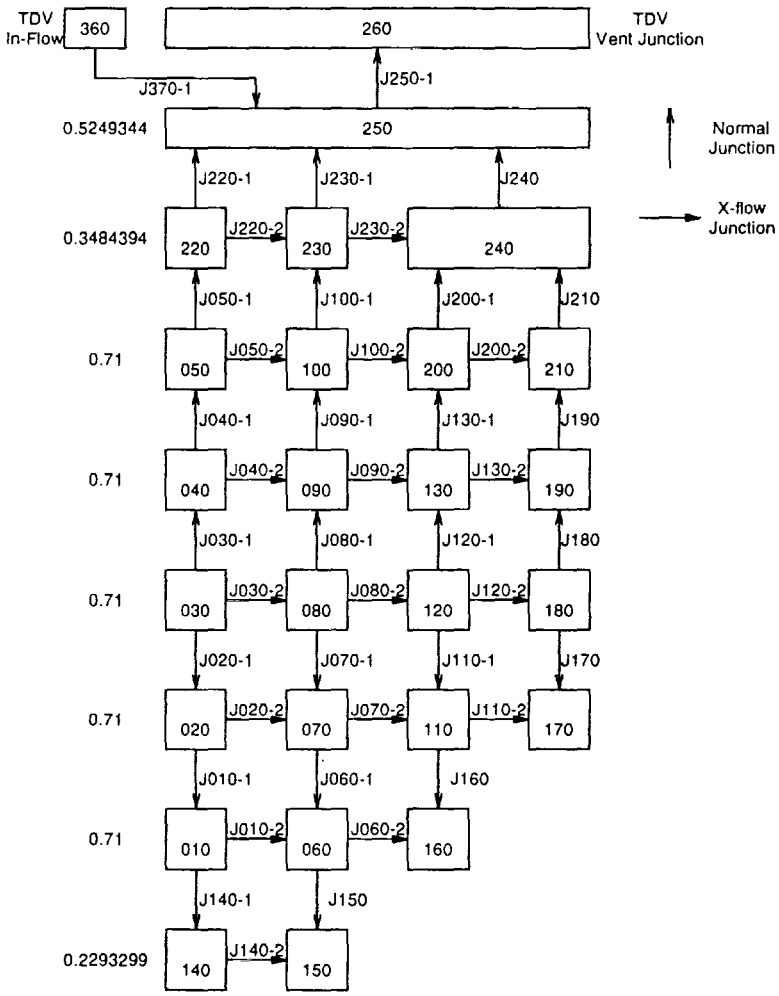

Figure 8.1-1. Block Diagram of RELAP5 Model

The SNF fuel pins in an assembly and waste package exterior barrier are represented in the RELAP5 model as heat conductors; the UO_2 pellets in the fuel rods as one conductor per assembly, the zircaloy cladding and guide tubes as a second conductor per assembly. The fuel rods were modeled with independent pellet and clad conductors to simulate the loss of fuel pin

integrity with water in direct contact with the UO_2. In this model, the fuel rod cladding was disassociated from the fuel pellet-to-water heat conduction path placing the pellets directly in contact with the control volume water mass. The cladding and guide tubes were in turn heated from secondary contact with the control volume water mass. The heat conductors representing fuel assemblies were modeled geometrically as a single fuel pin to maintain proper thermal response characteristics with the heat transfer area scaled up to the surface areas of full assemblies. The waste package outer shell was modeled as large carbon steel heat sinks connected to the non-assembly filled peripheral control volumes. Initial conditions for all heat conductors were 323.16 K.

8.2 Feedback Mechanisms

The effects on reactivity due to changes in the system are separated into leakage effects and material effects. Leakage effects are primarily dependant on boundary conditions such as water level in the waste package and must be calculated using two- or three-dimensional waste package models. Material effects such as changes to fuel temperature, moderator temperature, or moderator density are primarily localized and can be approximated using one-dimensional assembly-cell models with a constant buckling (leakage) term.

Reactivity is defined as (Ref. 20, p. 222):

$$\rho = \frac{k_{eff} - 1.0}{k_{eff}}$$

and a change in reactivity ($\Delta\rho$) is defined as (Ref. 20, p. 222):

$$\Delta\rho = \rho_{Change} - \rho_{Base} = \frac{1}{k_{eff\ -\ Base}} - \frac{1}{k_{eff\ -\ Change}}$$

Thus, a positive reactivity change results when ρ_{Change} is greater than ρ_{Base}. In the RELAP5 input, ρ and $\Delta\rho$ are noted in terms of dollars ($) which is defined as (Ref. 20, p. 246):

$$\rho(\$) = \frac{\rho}{\beta_{eff}} \quad and \quad \Delta\rho(\$) = \frac{\Delta\rho}{\beta_{eff}}$$

where β_{eff} is the effective delayed neutron fraction and is equal to 0.005.

The feedback reactivity in the RELAP5 point kinetics model can be specified as direct time dependent tables (labeled as scram tables), weighted tables of fluid density versus reactivity, or through control system variables. The control system allows reactivity values to be more generally specified as functions of model variables.

The RELAP5 reactivity changes for fuel and moderator temperature effects were calculated to be entered as weighted tables and are shown in Tables 8.2-1 and 8.2-2. The SCALE4.3 with its SAS2H sequence (XSDRNPM), and an associated cross section library with sufficient temperature dependant data was, used to calculate the reactivity changes required for the consequence analysis, because MCNP4A does not have the required temperature dependent data. A one-dimensional SAS2H model was developed based on comparison to baseline three-dimensional MCNP cases. SAS2H was demonstrated to provide matching results for the baseline degraded configuration with appropriate material and buckling (leakage) adjustments.

Table 8.2-1. Average Fuel Temperature versus Reactivity

Fuel Temperature (K/°F)	Δρ($)
273 / 32.0	+0.1719079
300 / 80.33	+0.1719079
323 / 122.0	+0.0
373 / 212.0	-0.3488604
433 / 320.0	-0.7295469
543 / 518.0	-1.3918144
813 / 1004.0	-2.8696928

During the development of the model, it was noted that the reactivity was remaining high during the transient when the water level was decreasing down through the upper row of assemblies. Based on the results from the analysis investigating k_{eff} as a function of water level in the waste package (Ref. 2, Table 7.4-10), this was a very large negative effect that needs to be included. The control system input option was used to incorporate the results in Table 8.2-3 into the RELAP5 model. A control block was added to the input file to compute an average liquid level in the top row of fuel assemblies and adjacent fluid volumes having the same elevation. Δρs for lower water levels are not required because the negative effect of dropping the water level to the bottom of the upper row is great enough to overwhelm the insertion postulated in Section 8.3. The inclusion of the control block for water level necessitated that the moderator density table be overridden. Note that this is conservative since the drop in moderator density is shown in Table 8.2-2 to always result in a negative change in reactivity.

Table 8.2-2. Moderator Density versus Reactivity

Density (lb_m/ft^3)	Density (g/cm^3)	Δρ($)	Fuel Temperature (K/°F)
43.6995724	0.700	- 22.8341124	813 / 1004
45.2602714	0.725	-20.0375898	813 / 1004
46.8209705	0.750	-17.4413905	813 / 1004
48.3816695	0.775	-15.0255317	813 / 1004
49.9423685	0.800	-12.7766726	813 / 1004
51.5030675	0.825	-10.6782739	813 / 1004
53.0637665	0.850	-8.7187079	813 / 1004
54.6244655	0.875	-6.8856192	813 / 1004
56.1851645	0.900	-5.1688975	543 / 518
57.4337238	0.920	-3.9010990	543 / 518
58.6822830	0.940	-3.9010990	543 / 518
59.8121897	0.958	-1.6592902	543 / 518
60.7424057	0.973	-0.8234196	373 / 212
61.6903146	0.988	0.00	323 / 122
62.4279606	1.000	+0.6225345	323 / 122
65.0000000	1.041	+0.6225345	300 / 80.33

Table 8.2-3. RELAP5 Reactivity Table for WP Water Level

Water Level Relative to Assembly Top (cm) - MCNP	$ = Δρ/β
0	0.0
-12.98	-12.911
-14.43	-14.959
-15.87	-16.660
-20.30	-30.902
-21.64	-30.902

8.3 Reactivity Insertion Scenarios

In the degraded state where a waste package has been breached by water and where the iron oxide has settled in the bottom of the waste package occupying 58 vol% of the space, the MCNP k_{eff} is 1.0186 with a standard deviation of $\pm$ 0.0049 (Ref. 2, Table 7.4-7). This is the most reactive reasonable configuration possible in the absorber plate waste package. If the critical point is designated as a k_{eff} of 0.95, the maximum reactivity insertion possible is:

$$\frac{\Delta\rho}{\beta_{eff}} = \left[\frac{1}{0.95} - \frac{1}{1.0186}\right] \times \frac{1}{0.005} = 14.18\$.$$

A change in reactivity value of this magnitude roughly corresponds to an insertion scenario involving the transition from a homogeneous distribution of iron oxide within the waste package to the stratified base configuration described above (Ref. 2, Table 7.4-9) or an increase in water level (Ref. 2, Table 7.4-10) for an SNF configuration not already completely submerged.

The negative reactivity effects of reduced water level in the package, increased fuel temperature and increased water temperature (decreased density) will eventually overwhelm any conceivable reactivity insertion mechanism. A significant transient criticality event can occur only when the balance of reactivity insertion and these negative counterbalancing effects exceed +1.0$ (prompt critical). If the insertion rate is sufficiently fast, the power level could be increasing by a factor of 2.7 (exponential period) on a time scale of a millisecond or less while the thermal changes are occurring on a time scale of a second or longer (Ref. 20, pp. 233-277). The greater the balance exceeds 1.0$ and the longer the duration, the greater will be the significance of the transient event in terms of the energy generated and its associated phenomena. This translates into a requirement for a relatively short insertion time (seconds) in order to achieve a prompt critical situation. The transition from a homogeneous to a stratified distribution of iron oxide within the waste package would, in general, be a slow process taking many days, months, or years. Low probability events which conceivably could result in an insertion rate on a time scale of a second or minute would include:

(1) Increasing ambient episodic focused flow of water of 20 m^3 to 100 m^3 in one week (Ref. 16, CDA Assumption TDSS 026),

(2) Earthquake resulting in shaking of waste package and redistribution of iron oxide, and

(3) Rock fall resulting in shaking of waste package and redistribution of iron oxide.

The water level scenario (1) could insert reactivity on a minute time scale and the particle redistribution scenarios (2 and 3) could insert reactivity on a second or minute time scale depending on average particle size. Attachment III of Reference 5 contains idealized terminal velocity (free fall, no impediment from other obstacles) calculations for particles sizes of 0.010

mm and 0.063 mm, which would take approximately 1 and 40 minutes, respectively, to fall to the bottom of the waste package. The typical crud particle size from metal oxidation is in the range of 0.0001 to 0.01 mm (Ref. 5, Section 7.2.3).

Based on these considerations, insertion times of 30 seconds and 3,600 seconds were chosen for the RELAP5 calculations in order to demonstrate transient behavior for the criticality event.

8.4 Results of RELAP5 Analysis

All results in this section from RELAP5 calculations are TBV because the RELAP5/MOD3 code has not been qualified according QAP-SI-0.

The consequences of a large reactivity insertion in the waste package, one where the insertion rate was on the order of minutes and the second where the rate was on the order hours, were investigated with the RELAP5 model (Ref. 5). In particular, the scenarios investigated were a positive reactivity insertion of 14.18$ at a constant rate over 30 seconds and over 3,600 seconds. The short term (initial power excursion) transient responses in both cases were qualitatively similar, being dominated by the positive ramp reactivity insertion and negative Doppler feedback reactivity which terminated the initial power rise in each case prior to the introduction of significant negative void reactivity. Note that the fuel temperature, and thus Doppler reactivity, tracks the power closely during the initial excursion phase. Void reactivity responds much more slowly since surface heat transfer is required to generate the voids.

The transient response of the waste package system following termination of the initial power rise was controlled by the rate of energy addition affecting the rate and magnitude of the void formation and thus the time evolution of the void reactivity component. Ultimately, sufficient fluid inventory was lost from the waste package (> 225 kg in either case) to sustain a large negative void reactivity component, keeping the system in a subcritical condition. A major factor contributing to differences in the two scenario responses was the magnitude of the net reactivity; with a maximum value of 1.15$ during the 30 second scenario exceeding prompt critical (1.0$) and remaining below prompt critical during the 3600 second scenario. Once the net reactivity reaches or exceeds the prompt critical point, the fission power level is rising rapidly. In addition, more negative (Doppler) reactivity is required to terminate the power excursion which translates into high peak power levels. During the 3600 second scenario, the net reactivity did not exceed 0.77$. The thermo-hydraulic response times in this scenario are closer to the neutron response time, permitting a quasi-balance during the period between 200 and 600 seconds between reactivity insertion and compensating mechanisms.

Maximum pressures in the waste package system remained below 2.55e+05 Pa and maximum center line fuel rod temperatures remained below 570 K. Sufficient fluid inventory remained in the waste package at the problem termination to redistribute the energy in the system and to reduce the fuel rod temperatures to less than 373 K. Values of key parameters from the RELAP5 analyses (Ref. 5) are summarized in Table 8.4-1. Relative locations of volume and junction components with their IDs are shown in Figure 8.1-1.

Table 8.4-1. Summary of 14.18$ Ramp Reactivity Insertion Cases

Variable	30 second reactivity insertion	3600 second reactivity insertion
Peak fission power/assembly	9.47e+07 watts	8.76e+05 watts
Time of peak fission power	2.52 seconds	176.0 seconds
Total fission and decay heat power per assembly at time of fission power maximum	9.48e+07 watts	9.00e+05 watts
Total energy into WP/assembly at termination time	5.16e+07 joules	8.15e+07 joules
Maximum volume pressure	2.544e+05 Pa	2.258e+05 Pa
Control volume where maximum pressure monitored	150*	150
Peak mean fuel rod temperature	497.5 K	438.4 K
Time of peak rod temperature	4.18 seconds	633 seconds
Water inventory - Initial	450.04 kg	450.04 kg
Water inventory - Final	209.02 kg	219.29 kg
Incremental burnup	1.6e-03 MWd/MTU	1.8 MWd/MTU
Termination time	1200 seconds	1800 seconds

* Control volume ID in Figure 8.1-1.

The consequences of each reactivity insertion scenario were directly related in severity to the reactivity insertion rate in the flooded waste package which is typical of transient reactivity events analyzed in reactor systems such as during Anticipated Transients Without Scram (ATWS) (Ref. 19). The total energy generated may be larger for slower insertion rate events as shown in Table 8.4-1, but is distributed over longer time periods than the more rapid insertion rate events. Within an essentially closed system such as the waste package being analyzed, the energy generation can be considered as an adiabatic process since the time scales are too short for significant amounts of energy to be transferred into the waste package barriers as heat sinks. Thus, although the detailed histories differ markedly, preliminary analysis indicates that the final state of the system is, at most, only weakly dependent upon reactivity insertion rate since the fission reaction terminates as soon as the waste package is sufficiently voided. In this state, sufficient fluid inventory has been converted to steam (or a two-phase fluid) and expelled from the waste package to preclude any short term return to criticality.

The time evolution of key parameters from the 30 second ramp scenario are shown in Figures 8.4-1 through 8.4-8 for: assembly power, reactivity components, control volume pressures, waste package fluid inventory, junction flow rates, and average fuel temperature. The total assembly power shown in Figures 8.4-1 and 8.4-2 is comprised of the two components: the direct fission component and the longer lived component from the decay of fission products.

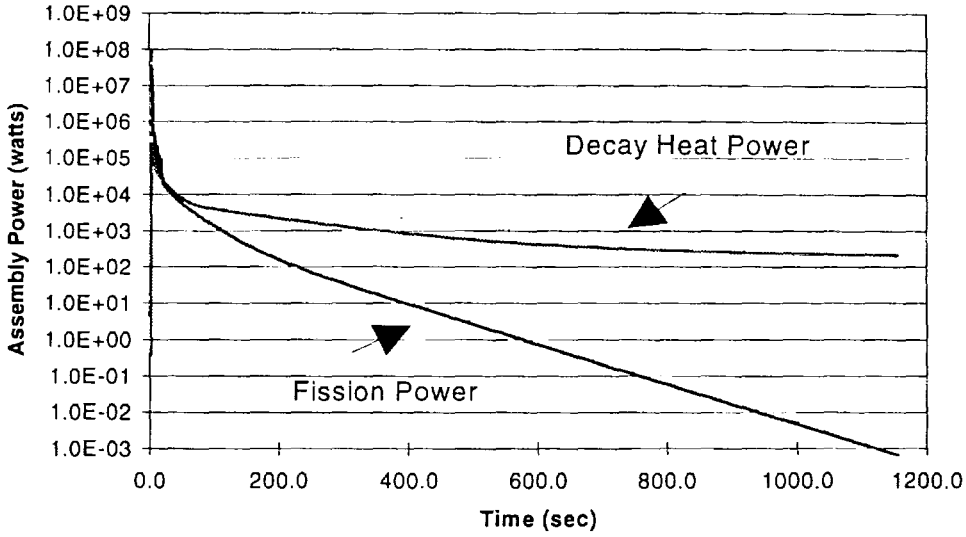

Figure 8.4-1. Assembly Power - 30 second Reactivity Insertion Scenario

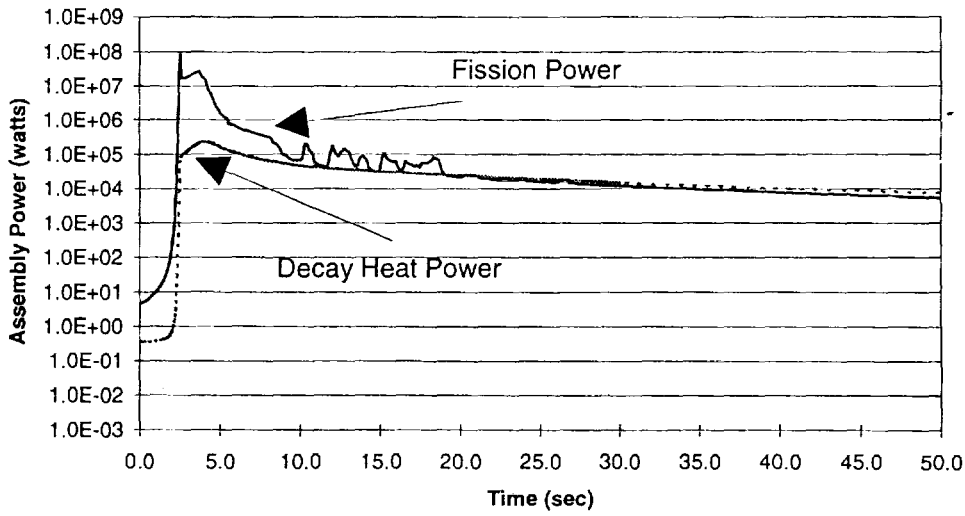

Figure 8.4-2. Assembly Power - 30 second Reactivity Insertion Scenario

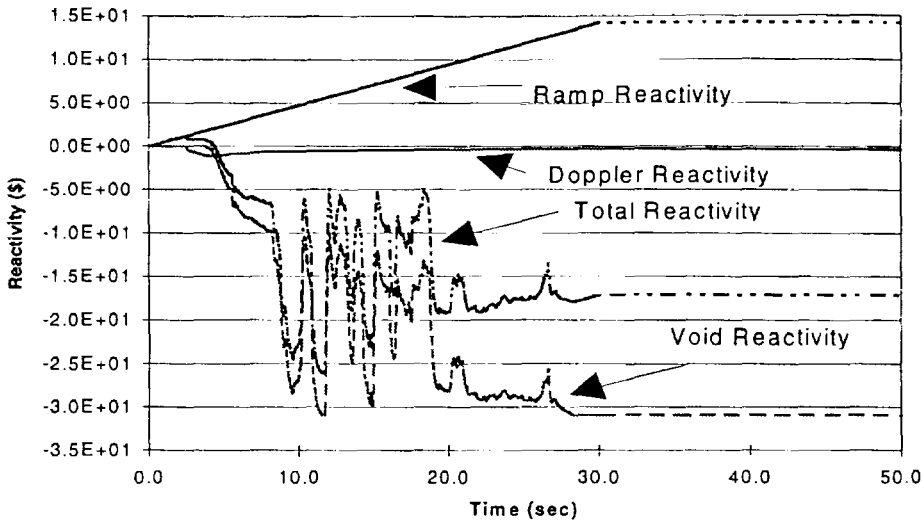

Figure 8.4-3. Reactivity Components - 30 second Reactivity Insertion Scenario

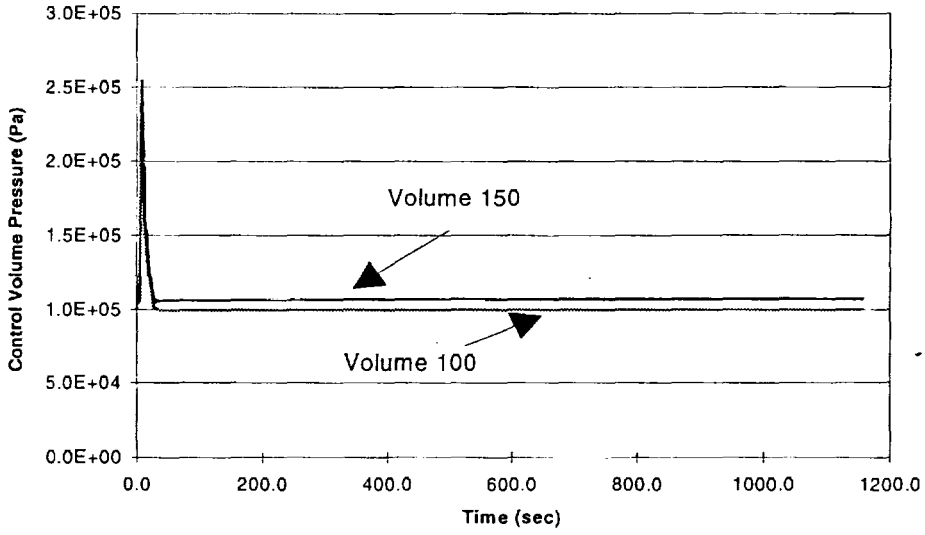

Figure 8.4-4. Volume Pressures - 30 second Reactivity Insertion Scenario

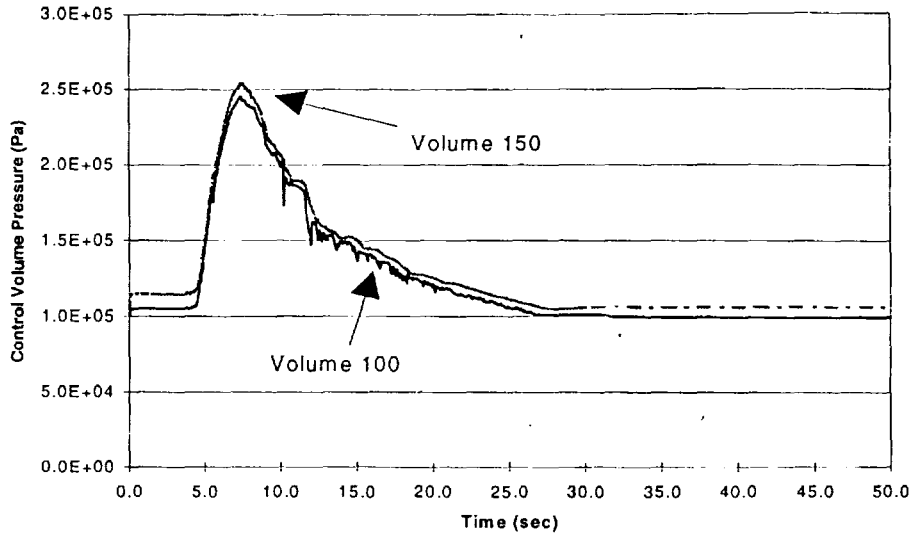

Figure 8.4-5. Volume Pressures - 30 second Reactivity Insertion Scenario

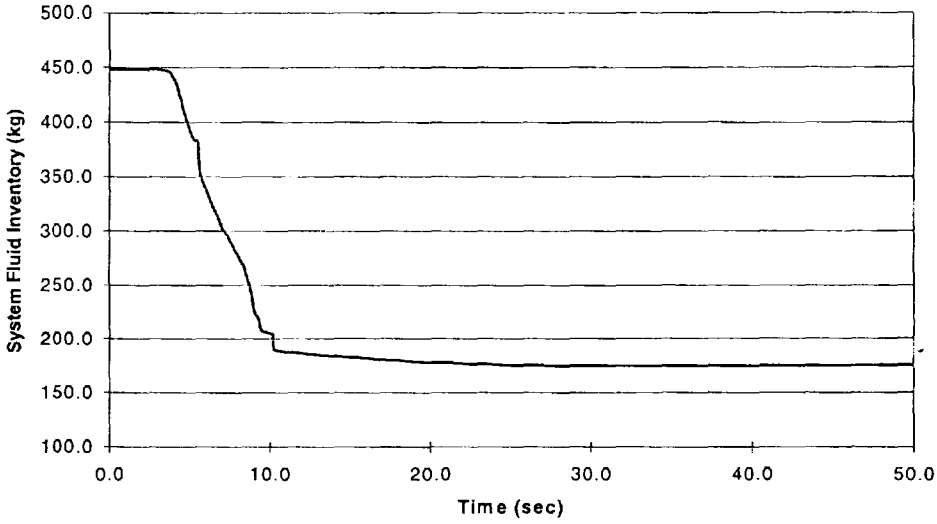

Figure 8.4-6. Waste Package Fluid Inventory - 30 second Reactivity Insertion Scenario

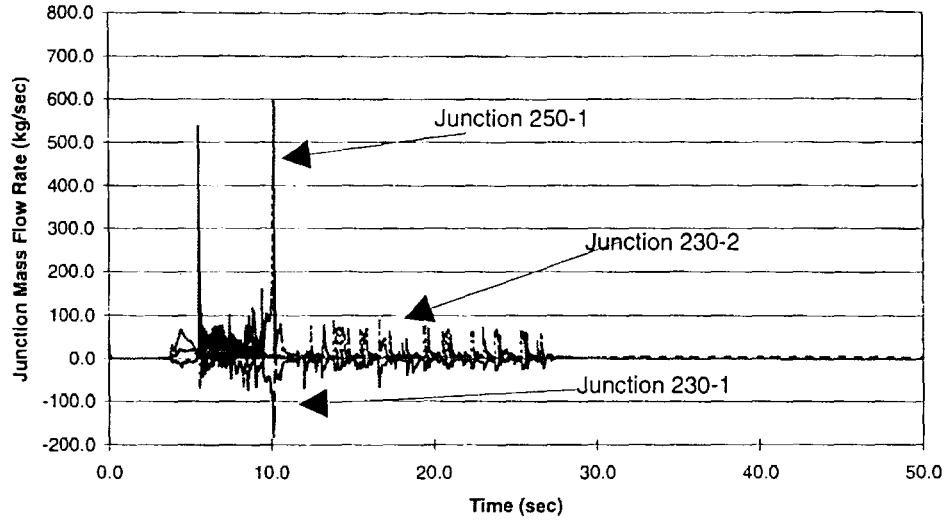

Figure 8.4-7. Junction Flow Rates - 30 second Reactivity Insertion Scenario

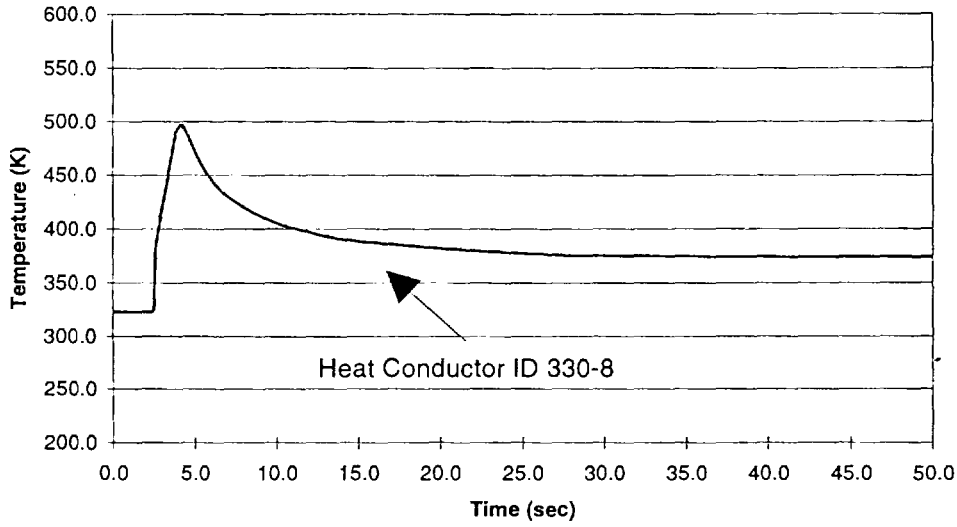

Figure 8.4-8. Average Metal Temperature* - 30 second Reactivity Insertion Scenario

* Heat conductor 330-8 connected to control volume 080.

Two ranges are shown for several of the parameters, one showing a panoramic view of the parameter value over the total time period, and the second providing details at higher resolution over a limited time scale. In the 30 second scenario, the energy generation rate (sum of fission and decay heat contributions) was sufficiently rapid during the initial power excursion to raise fuel temperatures (Figure 8.4-8) well into the range where void formation occurs generating the sharp pressure rise (Figure 8.4-4 and Figure 8.4-5) and inventory loss (Figure 8.4-6). As shown in Figure 8.4-3, the large negative void reactivity component generated by the steam formation and inventory loss at this point in the scenario prevented any possible return to criticality in the waste package system and the fission power level (Figure 8.4-1) asymptotically approaches the characteristic 79 second decay period of the longest lived delayed neutron precursor group (standard 6-group delayed neutron model).

The total system reactivity and its three components (positive ramp insertion, negative Doppler and void feedback) are given in Figure 8.4-3. This figure shows the early Doppler feedback reactivity which terminated the initial power excursion, followed by the larger negative void reactivity which ultimately terminates the event. All values of the reactivity components have reached their asymptotic values by 30 seconds.

Maximum pressures in the waste package system reach approximately 2.5e+05 Pa during the initial phases of the event as shown in Figure 8.4-4 and 8.4-5, then return to near initial values. The lower final values reflect the gravity head from the reduced final fluid inventory as shown in Figure 8.4-6.

The flow rates in the exit junction to the drift environment and for two internal junctions are shown in Figure 8.4-7 over the initial phase of the event. Flow rates return to near zero values as pressures in the system return to near ambient values. Choking in the exit junction limits the junction flow rate which controls the rate of inventory loss and pressure relief. The direction of flow for the exit junction is predominately outward (inventory loss) with very low reverse mass flow rates since the external environment was modeled as water vapor. Interior junctions, as shown in these figures, may experience either positive or negative flow rates as the pressure distribution dictates. As stated previously, the system returns to a stable sub-critical configuration following the initial activity.

The much lower reactivity insertion rate in the 3,600 second reactivity insertion scenario, and thus the energy generation rate, resulted in a less severe transient response than for the 30 second reactivity insertion scenario as shown in Table 8.4-1. The time evolution of key parameters from this scenario are shown in Figures 8.4-9 through 8.4-17 for assembly power, reactivity components, control volume pressures, waste package fluid inventory, junction flow rates, and average fuel temperature, respectively. As with the previous scenario, two ranges are shown for several of the parameters, one showing a panoramic view of the parameter value over the total time period, and the second providing details at higher resolution over a limited time scale. In the 3,600 second reactivity insertion scenario, the power excursion is terminated by the negative Doppler reactivity (Figure 8.4-11) with fuel pin metal temperatures (Figure 8.4-17) at values where subcooled boiling can be initiated. The initial vapor generation was coincident with the

initial waste package inventory loss (Figure 8.4-12) but did not result in a prominent pressure surge as shown in Figure 8.4-13 and Figure 8.4-14. During the 200-600 second time period in the scenario,

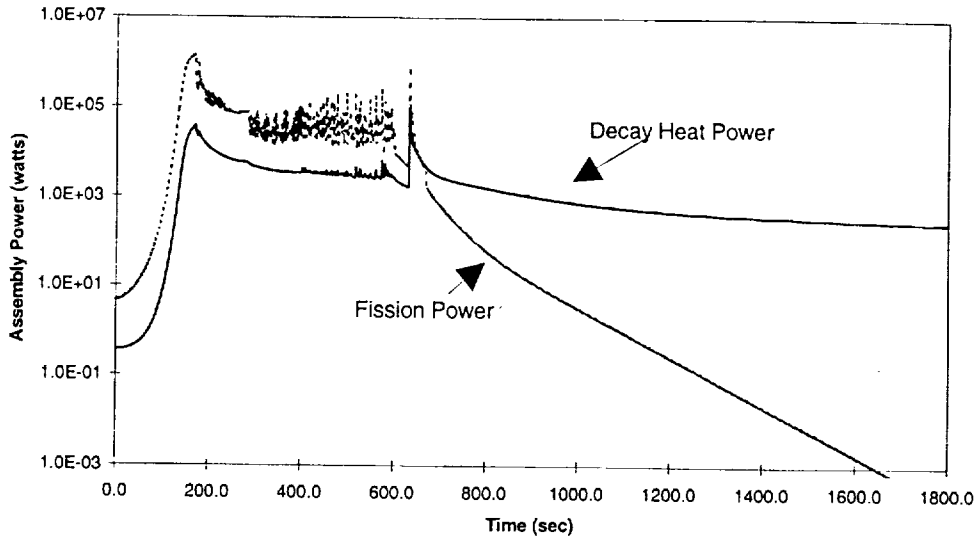

Figure 8.4-9. Assembly Power - 3,600 second Reactivity Insertion Scenario

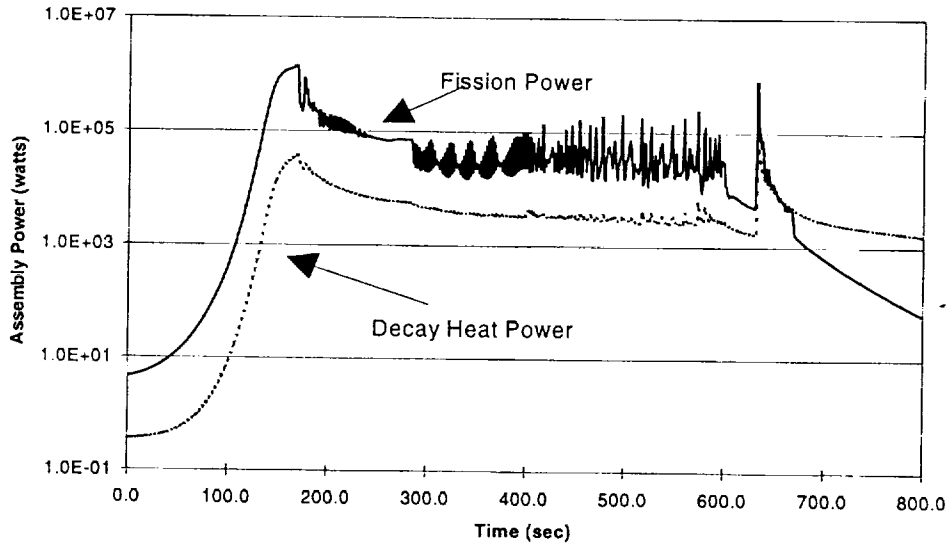

Figure 8.4-10. Assembly Power - 3,600 second Reactivity Insertion Scenario

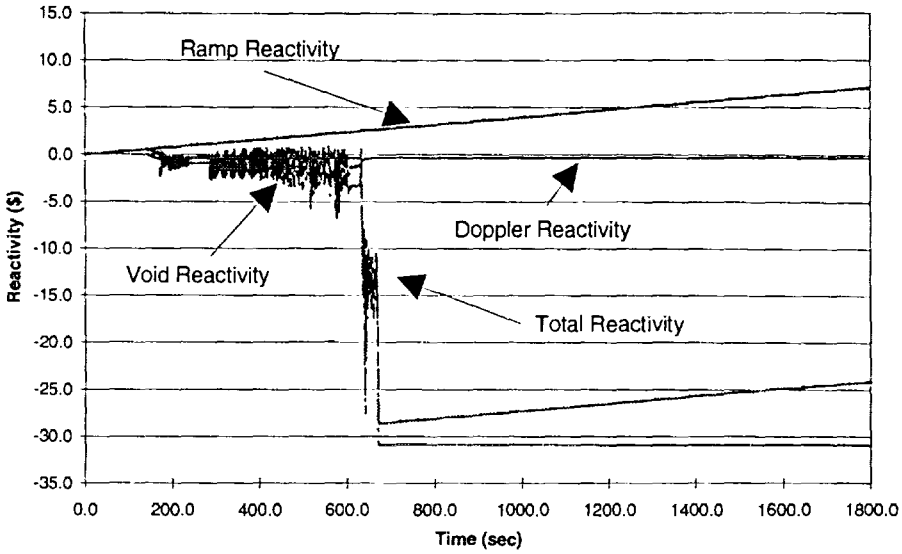

Figure 8.4-11. Component Reactivity - 3,600 second Reactivity Insertion Scenario

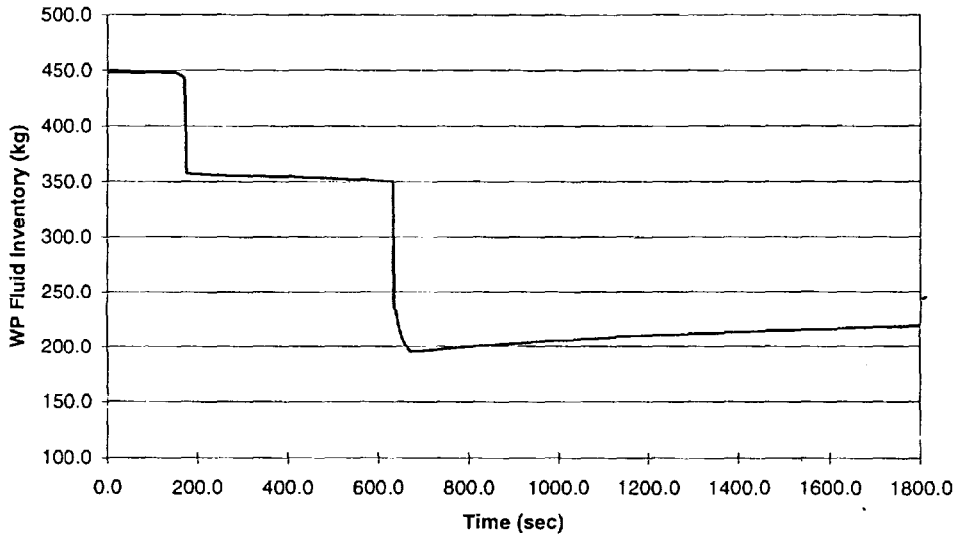

Figure 8.4-12. Waste Package Fluid Inventory - 3,600 second Reactivity Insertion Scenario

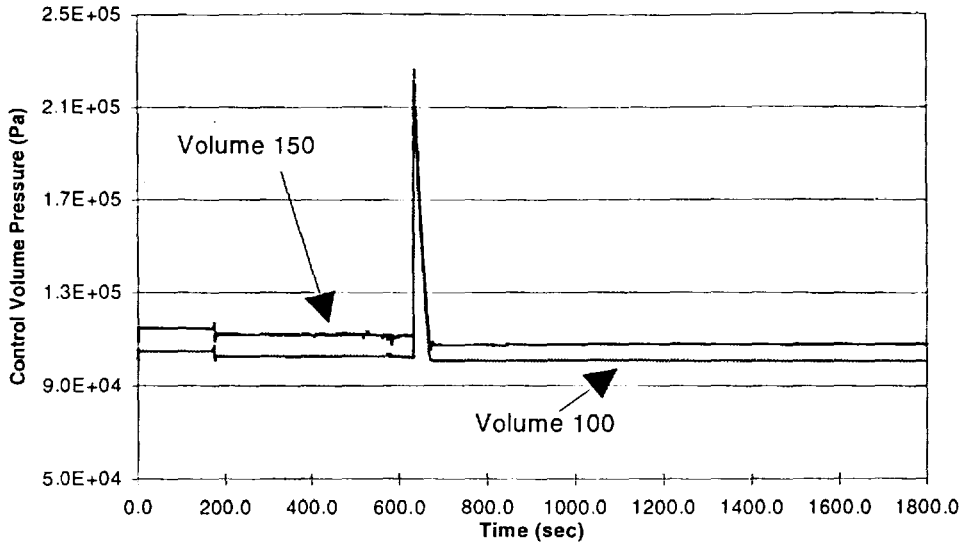

Figure 8.4-13. Volume Pressures - 3,600 second Reactivity Insertion Scenario

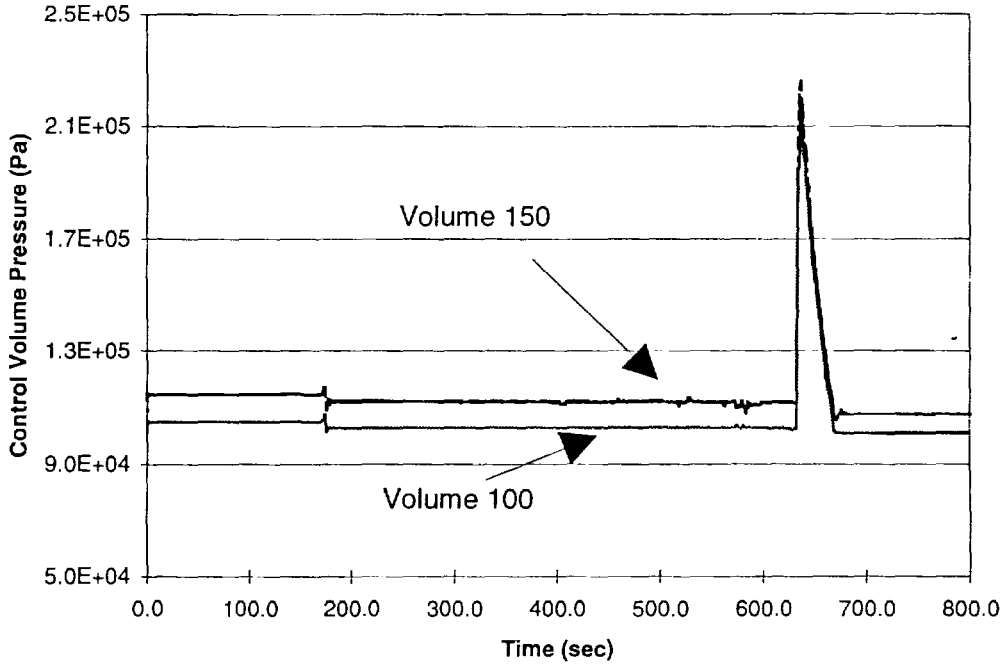

Figure 8.4-14. Volume Pressures - 3,600 second Reactivity Insertion Scenario

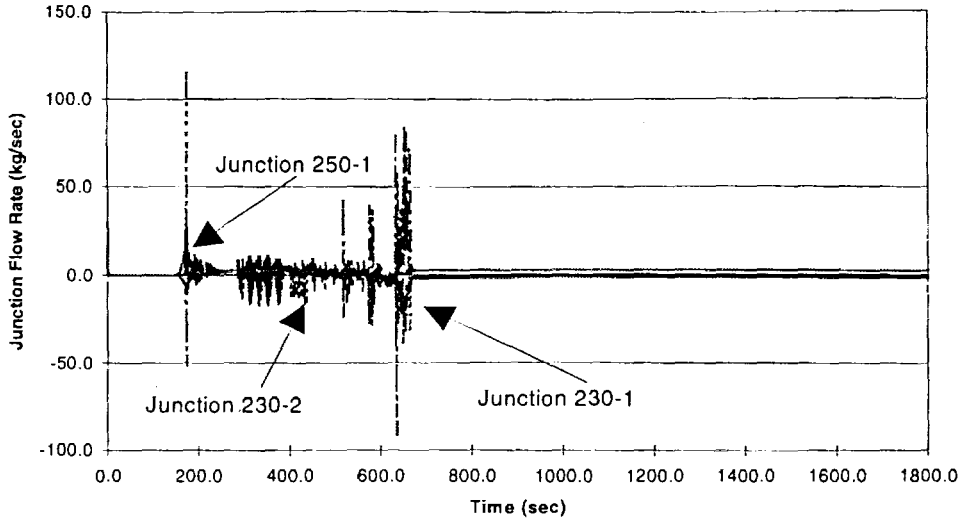

Figure 8.4-15. Junction Flow Rates - 3,600 second Reactivity Insertion Scenario

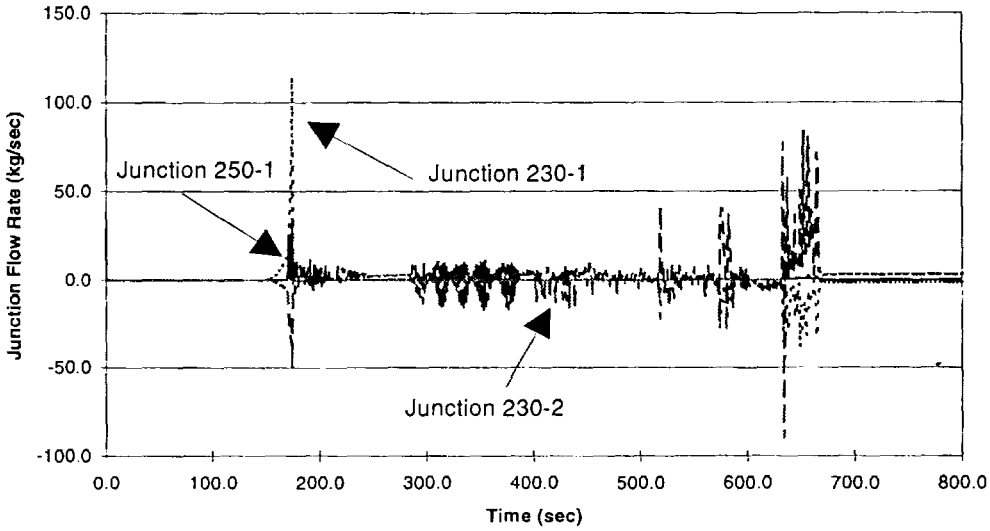

Figure 8.4-16. Junction Flow Rates - 3,600 second Reactivity Insertion Scenario

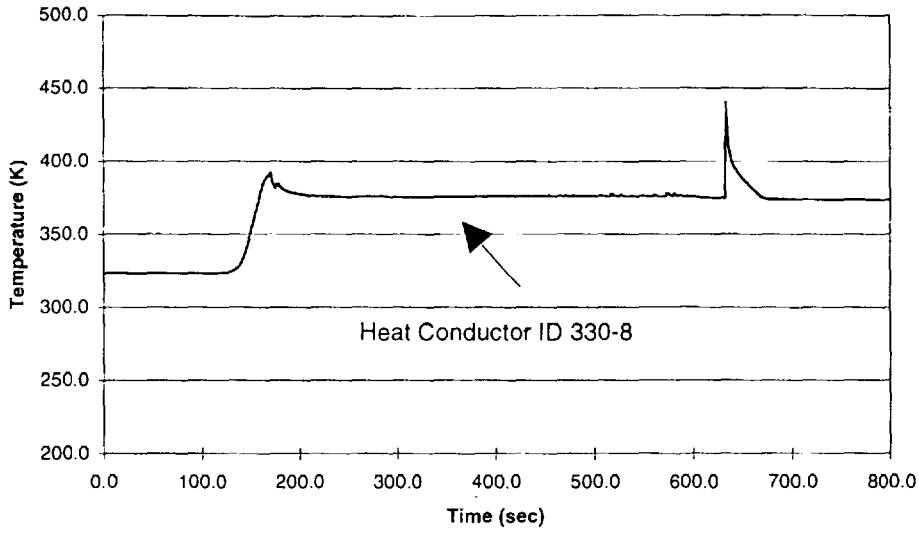

Figure 8.4-17. Average Metal Temperature* - 3,600 second Reactivity Insertion Scenario

* Heat conductor 330-8 is connected to control volume 080.

negative reactivity from the void and Doppler effects was nearly equal to the positive ramp insertion reactivity, maintaining the fission power at an elevated level (Figure 8.4-10). The rising moderator enthalpy resulted in an increase in the vapor generation rate around 600 seconds into the scenario generating a pressure surge (Figure 8.4-13) and further inventory loss. As shown in Figure 8.4-11, the large negative void reactivity component at this point in the scenario prevents any possible return to criticality in the waste package system and the fission power level (Figure 8.4-9) asymptotically approaches the characteristic 79 second decay profile. The inventory loss at this point is sufficient to prevent any possible return to critical conditions until the waste package refills with water which has a time scale of years.

8.5 Changes to the Radionuclide Inventory Due to Transient Criticality Event

To evaluate the effects of a criticality on the radionuclide inventory of a waste package, the code sequence SAS2H was run using the PWR criticality design basis fuel, power histories from the RELAP5 analyses, and a decay period of one year. The maximum decay period of one year was based on the short operating time of the criticality event which precludes formation of significant inventories of long lived isotopes. The transient fission power history and fuel temperature from each reactivity insertion scenario was approximated by a histograms for the SAS2H input. The burnup calculated from these histograms are only 1.6E-3 MWd/MTU and 1.8E-3 MWd/MTU for the short and the long cases, respectively. The change in isotopic inventories due to such low burnups would be expected to be insignificant and this is validated by the SAS2H results. The radionuclide inventories in curies after a one year decay for the 30 second and 3,600 second reactivity insertion scenarios (Ref. 5), respectively, are compared in Table 8.5-1 to the initial radionuclide inventory for a base 25,000 year decay period (Ref. 2). For this analysis, only those

isotopes whose inventories after one year decay differed from the original values by a minimum cutoff value (~10^{-20}) are listed. As shown, small differences appear in the fission product activity, but the principal radioactivity is due to the actinide decay which is not significantly altered by the criticality events.

Table 8.5-1. Radionuclide Inventory after One Year Decay Period (TSPA-95 isotopes only)

Isotope	Initial Activity (Ci) (Ref. 2)	30 second Reactivity Scenario (short.out) Increase (Ci)	3,600 sec Reactivity Scenario (long.out) Increase (Ci)
Actinides	-	-	-
th229	3.71e-02	5.63e-06	5.63e-06
th230	2.60e-01	1.17e-05	1.17e-05
pa231	9.01e-03	5.20e-07	5.20e-07
u233	6.20e-02	-	-
u234	1.23e+00	-	-
u235	2.33e-02	-	-
u236	2.25e-01	-	-
u238	1.45e-01	-	-
np237	6.10e-01	-	-
pu238	0.00e+00	5.65e-04	6.27e-04
pu239	9.74e+01	-	-
pu240	1.56e+01	-	-
pu241	5.72e-03	-	-
pu242	5.57e-01	-	-
am241	5.95e-03	-	-
am243	5.59e-01	-	-
cm244	0.00e+00	1.22e-05	1.34e-05
Fission Products	-	-	-
tc99	6.02e+00	1.34e-02*	1.34e-02*
sm151	0.00e+00	1.22e-04	1.36e-04

* These values may be significantly overestimated as a result of roundoff to 3 digits in SAS2H.

9. Conclusions

9.1 Potential for Critical Near-Field Accumulations

Extensive simulations of the range of physically possible dissolution/transport/deposition scenarios, using the geochemical code package EQ3/6 have shown very little capability for the accumulation of potentially critical amounts of fissile material in the repository near-field (drift invert) for the following reasons:

- Significant deposition requires a high pH (both to carry a significant concentration of fissile in the fluid and to support a sufficiently strong deposition reaction) which only lasts for a few hundred years (or a few thousand years at most).
- Void space is largely filled with competing precipitates which have higher concentrations in solution and stronger reactions with the rock (Section 5.2 and Reference 4).

9.2 Potential for Far-Field Accumulations

The evaluation of natural uranium deposits with respect to Yucca Mountain geology has shown that there is very little likelihood for neutronicly significant accumulations of uranium in the repository far-field for two fundamental reasons: (1) there has to be a reducing agent (one strong enough to resist the invasion of oxidizing solutions) or a source of vanadium within the host rock; and (2) precipitation conditions must be persistent over the geologic time scale required to accumulate the significant amounts, otherwise there will only be short term accumulation followed by remobilization. The specific conditions which would be required for (1) are listed in Table 5.3-1. The reasons why these conditions are unlikely at Yucca Mountain are summarized in Reference 4, Section 7.3.7.

9.3 Waste Package Criticality Control Effectiveness

The worst case degraded configuration was identified in Section 6.2 as a flooded absorber plate WP with a fully degraded basket, no boron remaining, and all oxide corrosion products settled to the bottom of the WP (settled oxide k_{eff} values are ≈4% higher than uniform oxide for fully degraded basket with the same amount of oxide). The 4.9% enriched, 34 GWd/MTU fuel was bounding for the absorber plate waste package (i.e., highest k_{eff} for fuel with $k_\infty \approx 1.13$) under the current loading scheme defined in Reference 16. The worst projected fuel for the absorber rod WP never exceeded a k_{eff} of 0.92 in the same configuration when 16 rod natural B_4C DCRAs were used. Furthermore, water level evaluations demonstrated that k_{eff} is significantly reduced once the top layer of assemblies is uncovered, and thus degraded configurations involving unflooded WPs with only hydrated oxide settled to the bottom are not a criticality concern. It was also shown that the maximum amount of boron adsorption possible on iron oxide provided, at best, only a 1.4% reduction in k_{eff}. Finally, it was shown that mechanisms which result in collapse of the fuel spacer grids and consolidation of the fuel rods, such as dynamic loading (e.g., rockfall) or spacer grid corrosion, will reduce k_{eff} by 2% to 20% depending on the amount of consolidation.

Section 6.3 discussed the multivariate nonlinear regressions, developed using the MCNP results, which relate the k_{eff} for a particular class of configurations (e.g., intact fuel with fully degraded basket and oxide settled to bottom of WP) to various parameters for that class (e.g., time, burnup, enrichment, assemblies covered by oxide, etc...). For the settled oxide configurations, regressions were also developed which provide the $\Delta k_{eff}/k_{eff}$ resulting from various amounts of boron in solution (which would be present in a flooded WP during corrosion of the borated stainless steel).

Potential options were also identified for reducing the peak postclosure k_{eff} of the absorber plate WP. The first option involves adding sufficient carbon steel (2,659 kg) to the intact basket to reduce the k_{eff} to below 0.91 for all fuels currently planned to be loaded into the absorber plate WP ($1.0 \leq k_\infty < 1.13$; see Ref. 16). This carbon steel has the effect of providing additional iron oxide when it corrodes, which is insoluble, occupies a greater volume than the undegraded steel (e.g., excludes moderator), and is a fair neutron absorber. The second option does not require any change to the WP designs, but requires abandoning the use of k_∞ as a means for binning fuel assemblies into one WP type or another, and results in a greater number of absorber rod WPs. Section 6.3 provides a regression which gives the peak k_{eff} of the worst degraded configuration for the absorber plate WP as a function of the burnup and enrichment of the fuel assemblies, and can be used to determine which fuel should be placed in the absorber rod WP from the standpoint of degraded mode criticality.

9.4 Statistical/Probabilistic Analysis

The degraded mode criticality performance results are rather insensitive to changes of infiltration rate above 5 mm/yr (the nominal value used in this study) to as high as 500 mm/yr. Therefore, if the long-term average infiltration turns out to be closer to the CDA predictions of 50 mm/yr (CDA fully mediated case) or even 100 mm/yr (the average between the fully mediated, 0.5 m^3/yr and the steady focused or episodic focused, 20 m^3/yr, which are projected to occur 0.025% of the years) the analyses presented here will still be valid. (Section 7.3.4)

The k_{eff} regressions given in Section 6.3 are suitable for selecting between the borated stainless steel waste package and the control rod waste package when loading individual assemblies. In particular, the PPCF gives the fraction of the PWR SNF which will require the control rod waste package. There is a range of values expected for PPCF, depending on the values of the various uncertain input parameters. The use of k_{eff} based selection criteria is expected to be much more accurate than the use of k_∞ based criteria, and certainly more conservative. The latter fact is clearly demonstrated by estimating the PPCF for the set of PWR SNF which has already passed a k_∞ screening criterion, as shown in Figure 7.5-1.

9.5 Consequence Analysis Conclusions

All conclusions in this section from RELAP5 calculations are TBV because the RELAP5/MOD3 code has not been qualified according QAP-SI-0, as was indicated in Section 6.

The criticality consequence analyses performed for the fully degraded 21 PWR assembly waste package loaded with 15X15 B&W SNF demonstrated that, based upon conservative assumptions, the system remains in a safe configuration following scenarios where 14.18$ of positive reactivity is added to the waste package system over time scales of 30 to 3600 seconds. The 14.18$ reactivity value represents the maximum possible reactivity attainable in the waste package designs as discussed in Section 8.3. The probability of these criticality scenarios will be addressed in the future. The results of the consequence analysis show that the 21 PWR SNF waste package system returns to a subcritical configuration, with the fuel rod temperatures and waste package internal pressures remaining well below levels which could melt fuel or generate more than minor effects on adjacent waste package systems, i.e., humidity levels will increase temporarily in the drift environment. The results discussed in Section 7.4 also show that consequences of a reactivity insertion event decrease in severity as the insertion rate decreases. However, the final state of the system, where sufficient water is lost from the waste package to maintain a subcritical state, depends primarily on the energy generated rather than the rate, since steam formation is the primary energy dissipation mechanism in the waste package.

Consequently, criticality events in a waste package will be restricted to localized incidents and not involve additional WPs or compromise the natural repository barriers. The principal impact on the environment external to the waste package experiencing a criticality event is the return of water in vapor form to the drift environment, thereby increasing the ambient humidity. This should not significantly impact the waste package environment in an adverse manner since the presence of water in the environment is assumed initially. Although not considered in the RELAP5 model, condensation of the ejected water vapor will prevent any significant over-pressurization of adjacent waste package modules since the drift environment is assumed to be at 326.2 K. The criticality analysis of the waste package (Ref. 2) showed that the system is subcritical unless the SNF in the waste package is submerged in water. This criticality consequence analysis shows that sufficient water inventory is expelled from the waste package to preclude any immediate return to a critical configuration. Flooding the waste package to levels where criticality is again possible would require several years even at the most conservative flow rates forecast for the drift region.

The SAS2H analysis of the transient reactivity scenarios showed that the radionuclide inventories had a negligible change after a one year decay period for less than 2.0e-03 MWd/MTU burnup from either scenario.

Based on the calculated transient response and insignificant increase in radionuclide inventories, the consequences of such a criticality (if it were to occur) would be so small as to be unnoticeable from outside the repository

10. References

1. *Degraded Waste Package Criticality: Summary Report of Evaluations Through 1996*, Document Identifier Number (DI#): BBA000000-01717-5705-00012 REV 00, CRWMS Management and Operating Contractor (M&O).

2. *Criticality Evaluation of Degraded Internal Configurations for the PWR AUCF Waste Package Designs*, DI#: BBA000000-01717-0200-00056 REV 00, CRWMS M&O.

3. *3rd Waste Package Probabilistic Criticality Analysis: Methodology for Basket Degradation with Application to Commercial Spent Nuclear Fuel*, DI#: BBA000000-01717-0200-00049 REV 00, CRWMS M&O.

4. *Evaluation of the Potential for Deposition of Uranium/Plutionium from Repository Waste Packages,* DI#: BBA000000-01717-0200-00050 REV 00, CRWMS M&O.

5. *Criticality Consequence Analysis Involving Intact PWR SNF in a Degraded 21 PWR Assembly Waste Package,* DI#: BBA000000-01717-0200-00057 REV 00, CRWMS M&O.

6. *Degraded Mode Criticality Analysis of Immobilized Plutonium Waste Forms in a Geologic Repository*, DI#: A00000000-01717-5705-00014 REV 01, CRWMS M&O.

7. *Report on Evaluation of MOX Spent Fuel from Exxisting Reactors for Repository Disposal*, DI#: A00000000-01717-5705-00012 REV 01, CRWMS M&O.

8. *Initial Waste Package Probabilistic Criticality Analysis: Uncanistered Fuel*, DI#: B00000000-01717-2200-00079 REV 01, CRWMS M&O.

9. *Second Waste Package Probabilistic Criticality Analysis: Generation and Evaluation of Internal Criticality Configurations*, DI#: BBA000000-01717-2200-00005 REV 00, CRWMS M&O.

10. *Probabilistic External Criticality Evaluation*, DI#: BB0000000-01717-2200-00037 REV 00, CRWMS M&O.

11. *Probabilistic Criticality Consequence Evaluation*, DI#: BBA000000-01717-0200-00021 REV 00, CRWMS M&O.

12. *Disposal Criticality Analysis Methodology Technical Report*, DI#: B00000000-01717-5705-00020 REV 00, CRWMS M&O.

13. *Controlled Design Assumptions Document*, DI#: B00000000-01717-4600-0032 REV 04, ICN 02, CRWMS M&O.

14. *Total System Performance Assessment 1995: An Evaluation of the Potential Yucca Mountain Repository*, DI#: B00000000-01717-2200-00136 REV 01, CRWMS M&O.

15. *Waste Package Materials Selection Analysis,* DI#: BBA000000-01717-0200-00020 REV 00, CRWMS M&O.

16. *Determination of WP Design Configurations*, Document Identifier Number (DI#): BBAA00000-01717-0200-00017 REV 00,CRWMS M&O.

17. *Software Qualification Report for MCNP4A*, CSCI: 30006 V4A, DI#: 30006-2003 REV 02, CRWMS M&O.

18. *Software Qualification Report for The SCALE Modular Code System Version 4.3*, CSCI: 30011 V4.3, DI#: 30011-2002 REV 01, CRWMS M&O.

19. Jensen, Peter J., et al, *Anticipated Transients Without Scram Analysis for the River Bend Station*, Proceedings: Fourth International RETRAN Conference, EPRI NP-4558-SR, p. 23-1, May 1986.

20. Duderstadt, James J., Hamilton, Louis J., *Nuclear Reactor Analysis*, John Wiley & Sons, New York, 1976.

21. *RELAP5/MOD3 Code Manual*, NUREG/CR-5535, INEL-95/0174, Prepared by Idaho National Engineering Laboratory for the U.S. Nuclear Regulatory Commission, August 1995.

22. *Technical Document Preparation Plan for the Supporting Analysis Results Summary Reports for the Disposal Criticality Analysis Methodolgy Reports*, DI#: B00000000-01717-4600-00087 REV 00, CRWMS M&O.

23. *Perform Probabilistic Waste Package Design Analyses*, QAP 2-0 Activity Evaluation WP-25, 8/3/97, CRWMS M&O.

24. *Quality Assurance Requirements and Description*, DOE/RW-0333P, REV 7, Department of Energy Office of Civilian Radioactive Waste Management.

25. *10 CFR Part 60; Disposal of High-Level Radioactive Wastes in Geologic Repositories; Design Basis Events; Final Rule*, U.S. Nuclear Regulatory Commission, Federal Register, Volume 61, Number 234, pp. 64257-64270, December 4, 1996.

26. Flint, A. L., Hevesi, J. A., Flint L. E., *Conceptual and Numerical Model of Infiltration for the Yucca Mountain Area*, U. S. Geological Survey, 3GUT623M, September 20, 1996.

27. *Input Files and Models Used in the Waste Quantity, Mix and Throughput Study,* Interoffice Correspondence (IOC) #: VA.SAI.MF.03/97.007, CRWMS M&O, March 21, 1997.

28. *Reactivity and Isotopic Composition of Spent PWR Fuel as a Function of Initial Enrichment, Burnup, and Cooling Time*, ORNL/CSD/TM-244, Oak Ridge National Laboratory, October 1987.

29. *SAS2H Generated Isotopic Concentrations for B&W 15x15 PWR Assembly,* DI#: BBA000000-01717-0200-00012 REV 01, CRWMS M&O.

30. *Mined Geologic Disposal System Advanced Conceptual Design Report,* DI#: B00000000-01717-5705-00027 REV 00, CRWMS M&O.

31. Knief, R. A., *Nuclear Criticality Safety - Theory and Practice*, American Nuclear Society, La Grange Park, IL, 1993.

32. Goldberg, S., Glaubig, R. A., "Boron Adsorption on Aluminum and Iron Oxide Minerals", *Soil Sciences Society of America Journal,* Volume 49, pp. 1374-1379, 1985.

33. *TMI-2 Criticality Studies: Lower-Vessel Rubble and Analytical Benchmarking*, ORNL/CSD/TM-222, Oak Ridge National Laboratory, December 1985.

34. Myers, W., Rojas S., Kimpland, R., Jaegers, P., Sanchez, R., Hayes, D., Paternoster, R., Anderson, R., Stratton, W., *Dynamic Characteristics of Mixtures of Plutonium, Nevada Tuff, and Water,* Draft Report, Los Alamos National Laboratory, 1997.

35. *Q-List*, YMP/90-55Q, REV 4, Yucca Mountain Site Characterization Project.